Assessing and Reducing the Uncertainty in Regional Wave and Coupled Wave-Atmosphere Models during Extreme Events

Dissertation

zur Erlangung des Doktorgrades der Naturwissenschaften

an der Fakultät für Mathematik, Informatik und Naturwissenschaften

Fachbereich Geowissenschaften der Universität Hamburg

vorgelegt von

Anne Jasmin Wiese

aus Lübeck

Hamburg, 2020

Als Dissertation angenommen am Fachbereich Geowissenschaften

Tag der Disputation:	09.12.2020
Gutachter/Gutachterinnen:	Dr. Joanna Staneva Prof. Dr. Corinna Schrum
Vorsitzender des Fachpromotionsausschusses Geowissenschaften:	Prof. Dr. Dirk Gajewski
Dekan der Fakultät MIN:	Prof. Dr. Heinrich Graener

Abstract

Large waves during heavy weather can threaten the safety of vessels out on the ocean, therefore, for all activities conducted at sea, good knowledge about weather and wave conditions is inevitable for the safety of humans at sea. However, the uncertainties in atmosphere and wave models are large during those extreme events. This study discloses possible paths for operational forecast but also for hindcast and climate studies to improve and reduce uncertainties.

The thesis starts with showing the importance of high-quality and high temporal resolved wind forcing to the wave model. When using the wave model on the regional scale in the North Sea, hourly wind forcing is necessary for the wave model in order to have a chance to properly depict the extreme events. With the coarser temporal resolution of six hours of the wind forcing, the peak in wind speed can be missed, since the peak can occur in between update times. This circumstance leads to underestimation of the significant wave height of the wave model with the majority of the wind forcing data. Thus, an hourly temporal resolution proved to be a key factor for simulating extreme events with the wave model in this study. Furthermore, the quality of the newly available Sentinel-3A satellite data is assessed in comparison with older satellite missions, namely Jason-2 and CryoSat-2. The focus is on the coastal zone, where the data quality of satellites tends to change for the worse. The data quality has been improved for Sentinel-3A compared to the other two, especially in the coastal zone. Still the data quality is not accurate enough compared to in situ observations to strictly force the wave model to the data measured by Sentinel-3A, but the data can be used to guide the model towards an improved best-guess wave field.

This is then followed by studies about the impacts waves can have on the atmosphere in a coupled wave-atmosphere model. The results support the finding of an underestimation of the roughness length over the ocean by the atmospheric model compared to the one calculated by the wave model. The enhanced roughness results in a reduction of 10 m wind speed and significant wave height, leading to better agreement with observational data. Also it is shown, that the differences between the coupled simulation, in which the roughness length is calculated by the wave model, and the reference simulation, in which the roughness length is calculated within the atmospheric model, can spread within the planetary boundary layer.

The question of uncertainties of coupled and reference simulations as well as the significance of differences between them is then examined in the third part of the thesis using ensemble simulations. The analysis conducted in this thesis shows that the differences between coupled and reference ensemble are significant during the majority of the time. Large differences in 10 m wind speed and significant wave height occur at the same time as peaks in 10 m wind speed, hence during extreme events. For the majority of these events the differences are larger than the internal variability and, therefore, can be clearly differentiated from one another. Furthermore, it is shown that the internal variability in the atmospheric model can be reduced when coupling the wave model to it. When using spectral nudging or different boundary conditions in the atmospheric model, the differences between coupled and reference ensemble in 10 m wind speed and significant wave height are very similar, while the differences in mean sea level pressure are more sensitive and can show some deviations from one another.

Thus, this thesis exposes possible paths to reduce the uncertainty in wave and atmosphere model results. First, the necessity of high-quality and high temporal resolved wind fields for the regional wave model during extreme events is shown. Second, the coupling between the wave and atmosphere model reduces the uncertainty in both models and enhances the accordance with observational data.

Zusammenfassung

Hohe Wellen bei schwerem Wetter gefährden die Sicherheit von Schiffen auf See maßgeblich. Daher ist für alle Aktivitäten auf dem Wasser eine gute Kenntnis der Wetter- und Wellenbedingungen für die Sicherheit der Menschen auf See unumgänglich. Die Unsicherheiten in den Atmosphären- und Wellenmodellen sind jedoch bei Extremereignissen ausgeprägt. Diese Studie zeigt mögliche Wege für die Reduktion der Unsicherheiten und die Verbesserung operationeller Vorhersagen, aber auch von Hindcast- und Klimastudien, auf.

Zu Beginn dieser Arbeit wird die Wichtigkeit von qualitativ hohem und zeitlich hoch aufgelöstem Windantrieb für das regionale Wellenmodell gezeigt. Bei der Nutzung des Wellenmodells auf der regionalen Skala in der Nordsee sind stündliche Windfelder nötig, damit das Wellenmodell die Möglichkeit hat, Extremereignisse korrekt abzubilden. Mit einer gröberen zeitlichen Auflösung des Windes von sechs Stunden kann es sein, dass das Maximum in der Windgeschwindigkeit zwischen den Aktualisierungszeitpunkten liegt und somit nicht abgebildet wird. Dies führt mit der Mehrzahl der Winddaten zu einer Unterschätzung der signifikanten Wellenhöhe in dem Wellenmodell. Somit erweist sich in dieser Studie eine stündliche zeitliche Auflösung als ein Schlüsselfaktor für die Simulation von Extremereignissen mit dem Wellenmodell. Darüber hinaus wird die Qualität der neu verfügbaren Sentinel-3A-Satellitendaten im Vergleich zu älteren Satellitenmissionen wie Jason-2 und CryoSat-2 bewertet. Der Schwerpunkt liegt dabei auf dem Küstenbereich, in dem sich die Datenqualität der Satelliten tendenziell verschlechtert. Es konnte gezeigt werden, dass die Qualität der Daten von Sentinel-3A verglichen mit den beiden älteren Satelliten verbessert wurde. Dies trifft insbesondere auf den Küstenbereich zu. Die Datenqualität ist im Vergleich zu in-situ-Messungen allerdings immer noch nicht genau genug, um das Wellenmodell strikt an die von Sentinel-3A gemessenen Daten zu zwingen. Die Daten sind dennoch nützlich, um das Best-Guess-Wellenfeld an in-situ-Daten anzunähern.

Im nächsten Schritt folgen Studien über die Auswirkungen, die die Wellen in einem gekoppelten Wellen-Atmosphären-Modell auf die Atmosphäre haben können. Die Ergebnisse unterstützen die Erkenntnis einer Unterschätzung der Rauhigkeitslänge über dem Ozean durch das Atmosphärenmodell im Vergleich zu der durch das Wellenmodell berechneten. Diese erhöhte Rauigkeit führt zu einer Verringerung der 10 m Windgeschwindigkeit und

der signifikanten Wellenhöhe, wodurch eine verbesserte Übereinstimmung mit Beobachtungsdaten erzielt wird. Außerdem wird gezeigt, dass sich die Unterschiede zwischen der gekoppelten Simulation, bei der die Rauhigkeitslänge durch das Wellenmodell berechnet wird, und der Referenzsimulation, bei der die Rauhigkeitslänge innerhalb des atmosphärischen Modells berechnet wird, in der planetaren Grenzschicht ausbreiten können.

In dem dritten Teil der Arbeit wird die Frage der Unsicherheiten von und der Signifikanz der Unterschiede zwischen gekoppelten und Referenzsimulationen anhand von Ensemblesimulationen untersucht. Die in dieser Arbeit durchgeführte Analyse zeigt, dass die Unterschiede zwischen gekoppeltem und Referenzensemble die meiste Zeit über signifikant sind. Große Unterschiede in der 10 m Windgeschwindigkeit und der signifikanten Wellenhöhe treten zur gleichen Zeit wie Spitzen in der 10 m Windgeschwindigkeit und somit bei Extremereignissen auf. Die Unterschiede sind bei der Mehrheit dieser Ereignisse größer als die interne Variabilität und somit klar voneinander unterscheidbar. Darüber hinaus wird gezeigt, dass die interne Variabilität in dem Atmosphärenmodell reduziert werden kann, wenn dieses mit dem Wellenmodell gekoppelt wird. Selbst wenn spektrales Nudging oder unterschiedliche Randbedingungen in dem atmosphärischen Modell verwendet werden, sind die Unterschiede zwischen dem gekoppelten und dem Referenzensemble in der 10 m Windgeschwindigkeit und der signifikanten Wellenhöhe sehr ähnlich. Die Unterschiede in dem Luftdruck hingegen können voneinander abweichen.

Diese Dissertation zeigt daher Möglichkeiten auf, wie die Unsicherheit in den Ergebnissen von Wellen- und Atmosphärenmodellen reduziert werden kann. Erstens wird die Bedeutung von qualitativ hohen und zeitlich hoch aufgelösten Windfeldern für das regionale Wellenmodell bei Extremereignissen dargestellt. Zweitens reduziert die Kopplung zwischen dem Wellen- und Atmosphärenmodell die Unsicherheit in beiden Modellen und verbessert die Übereinstimmung mit Beobachtungsdaten.

Publications related to this dissertation

Research article 1 in Appendix A:
Wiese, A., Staneva, J., Schulz-Stellenfleth, J., Behrens, A., Fenoglio-Marc, L., & Bidlot, J.-R. (2018). Synergy of wind wave model simulations and satellite observations during extreme events. Ocean Science, 14(6), 1503-1521, https://doi.org/10.5194/os-14-1503-2018.

Research article 2 in Appendix B:
Wiese, A., Stanev, E., Koch, W., Behrens, A., Geyer, B., & Staneva, J. (2019). The Impact of the Two-Way Coupling between Wind Wave and Atmospheric Models on the Lower Atmosphere over the North Sea. Atmosphere, 10(7), 386, https://doi.org/10.3390/atmos10070386.

Research article 3 in Appendix C:
Wiese, A., Staneva, J., Ho-Hagemann, H.T.M., Grayek, S., Koch, W., & Schrum, C. (2020). Internal Model Variability of Ensemble Simulations With a Regional Coupled Wave-Atmosphere Model GCOAST. Frontiers in Marine Science. Accepted.

Contents

1 Introduction

Wind-generated waves are present at nearly all times on the ocean surface. Especially high waves can be a risk for the safety of humans at sea. Therefore, a good knowledge of the wind-generated waves, hereafter called waves, is important for all operations at sea.

The requirement to provide ship's captains with weather information is written down in the International Convention for the Safety of Life at Sea (SOLAS) by the International Maritime Organization (IMO) (SOLAS, 1974, as amended). To incorporate weather information into the ship's navigation is particularly important to avoid heavy weather threatening the safety of the vessel, but can also minimize the fuel consumption of the vessels. This saves costs for shipping companies and reduces the impact on the climate (Pacheco and Guedes Soares, 2007; Avgouleas and Sclavounos, 2014). Hence, high forecast quality is an essential prerequisite for efficient route planning. Also, for search and rescue operations precise weather and wave along with current information are key for the success of the search (Breivik and Allen, 2008; Breivik et al., 2013).

Moreover, the renewable energy sector is moving more and more offshore. Vessels going out to the platforms usually have strict regulations about maximum wind and waves that they are allowed to operate under (Gintautas et al., 2016), which makes precise forecasts inevitable. For the energy sector also precise hindcast and climate studies with low uncertainties are of great relevance, when planning new sites and estimating the weather and wave conditions at the intended location (Larsén et al., 2019). Furthermore, for the wind power forecast, low uncertainties in the model providing wind data are required, as wind turbines have exact limits for storm events when to go from full power production to zero (Cutululis et al., 2011). Another sector requiring precise forecasts, hindcasts and climate studies of weather and waves is the coastal protection, including dykes and harbour activities (Staneva et al., 2014; Gautier and Caires, 2015).

These sectors of navigation, offshore energy and coastal protection have the need for accurate forecasts but also hindcast and climate studies with low uncertainties regarding weather and waves on the ocean (Staneva et al., 2014). However, there are limitations in the model systems due to uncertainties in initial conditions and necessary approximations in the models (Ehrendorfer, 1997; ECMWF, 2020). For the sectors mentioned above, these limitations become visible especially during extreme events with high wind speeds and large waves.

Historically, the need for wave forecasts became evident also for naval operations and landings (Ardhuin and Orfila, 2018). Sverdrup and Munk (1947) made considerable contributions to the fundamentals of understanding waves at the ocean surface and their forecast. Due to swell being dispersive, with long periods propagating faster than shorter periods, the spectral modelling of the surface waves seemed natural. For that, the surface elevations are depicted by the sum of many sinusoidal waves with various wavelengths and periods (Ardhuin and Orfila, 2018). The first wave models postulated that the waves suddenly stop growing, when they reach an universal saturation level, based on the saturation spectrum by Phillips (1958) (ECMWF, 2019). These first generation wave models, though, overestimated the wind input and non-linear transfer was not considered. This essential process of the non-linear wave-wave interaction in generating the wave spectra, where energy is transported from the shorter waves to the longer waves (Ardhuin and Orfila, 2018), was theoretically shown by Hasselmann (1962) and experimentally verified 11 years later by Hasselmann et al. (1973). Hasselmann et al. (1973) findings along with direct measurements of the wind input to the waves (Snyder et al., 1981; Hasselmann et al., 1986) resulted in the development of the second generation wave models (ECMWF, 2019). These models, though, had deficits with the treatment of wind sea and swell, especially during rapidly changing wind fields. Aiming at improving the wave models the WAM Group was formed (WAMDI Group, 1988) and developed the third generation wave model WAM, which has advanced since then and is still in use today. Through integration of the energy balance equation the wave spectrum is calculated. The source terms of the energy balance equation consist of the wind input source function, which contains the wave growth by the wind, the non-linear wave-wave interaction term, where the energy is transferred from shorter to longer waves, and the dissipation due to whitecapping and in shallow areas also due to bottom friction (Komen et al., 1994; ECMWF, 2019).

Third generation wave models, like WAM, have been used and are still used for forecasting (e.g. ECMWF, 2019; DWD, 2020). Additionally, a variety of scientific research about improving the wave forecasts (e.g. Bidlot et al., 2002; Aouf et al., 2018; Janssen and Bidlot, 2018) but also wave hindcasts (e.g. Romeiser, 1993; Weisse et al., 2002; de León and Soares, 2008; Reistad et al., 2011) and wave climate studies (e.g. Günther et al., 1997; Weisse et al., 2009; Dobrynin et al., 2012; Bonaduce et al., 2019) have been conducted.

The quality of the wind input data was identified as a major source of uncertainty for the wave model (Cavaleri and Bertotti, 2003b; Cavaleri et al., 2007; Thomas and Dwarakish, 2015; Van Vledder and Akpınar, 2015; Janssen and Bidlot, 2018). Especially in coastal

areas, where the fetch is limited and the wind is disturbed by the coast, wind fields used to have weaknesses due to coarse resolution of the wind data (Cavaleri and Bertotti, 2003b). Cavaleri and Bertotti (2004) have shown that a higher spatial resolution of the wind field results in an outcome of the wave model closer to observations. The available wind forcing data have improved over the last years. However, still today, the wave model output can only be as accurate as the applied wind forcing data (Nose et al., 2018). While the spatial resolution has improved over the past years, the temporal resolution of reanalysis data remained low, with only the most recent product increasing the temporal resolution to an hourly resolution (Copernicus Climate Change Service (C3S), 2017; Hersbach et al., 2020). Particularly when depicting extreme events the uncertainty in wave model output might be reducible with this higher temporal resolution of the wind field.

Assimilating wave measurements into the model is an additional way of reducing the uncertainty of wave model simulations (Lionello et al., 1992). This assimilation delivers good results and is routinely used for the open ocean due to the fact that satellite data are of good quality and swells can persist for a long time (Lionello et al., 1992; Janssen et al., 1997; ECMWF, 2019). In the regional and coastal ocean, however, the quality of the satellite data tend to deteriorate, resulting in systematic flagging of up to a few tens of kilometres from the coast (Cipollini et al., 2010; Vignudelli et al., 2011; Fenoglio-Marc et al., 2015). The deterioration is usually caused by land contamination in the footprint of the altimeter, leading to incorrect waveform interpretations and, hence, an incorrect significant wave height estimation. For new satellite missions, like Sentinel-3A, the error due to land contaminations should be reduced by increasing the footprint resolution supposedly resulting in improved data quality closer to the coast (Beneviste and Vignudelli, 2009; Vignudelli et al., 2011). Hence, using Sentinel-3A might lead to possibilities for improving best-guess wave fields. However, this assumption had not been tested, since the start of the satellite mission was only one year prior to the start of this study.

Stand-alone models for waves or the atmosphere have conceptual limitations, since they parameterise processes that would interact with another part of the earth's system. The waves are right at the interface between the ocean and the atmosphere. Consequently, the waves determine the exchange of energy, mass, heat and momentum between the two mediums, resulting in non-linear feedback to the waves as well as the atmosphere and the ocean (Cavaleri et al., 2012b; Staneva et al., 2014). Therefore, the path for the future is to incorporate waves into coupled ocean-atmosphere models (Cavaleri et al., 2012b; Staneva

et al., 2014; Schrum, 2017). Before using fully coupled earth system models, it is important to understand the processes between each component of the system, such as waves and atmosphere individually. The uncertainty of the model system needs to be estimated and potentially reduced in order to improve the forecast and hindcast quality. Major sources of uncertainty in regional models are internal model variability, here called internal variability, model uncertainty and forcing uncertainty. The internal variability stems from the ambiguity in initial conditions of the model (Laprise et al., 2012; Sieck, 2013; Sanchez-Gomez and Somot, 2018; Ho-Hagemann et al., 2020). Parameterisations in the model contribute to the model uncertainty (ECMWF, 2016; Ho-Hagemann et al., 2020). The forcing uncertainty is introduced to the regional model through the boundary forcing driven by global simulations (Sieck, 2013; Ho-Hagemann et al., 2020). Hence, the model uncertainty could be reducible by coupling wave and atmosphere components, expressed in the model being less sensitive towards initial conditions. For ocean-atmosphere coupling the stabilising effect of the coupling has already been shown (Ho-Hagemann et al., 2020).

The idea of coupling the wave model to an atmospheric model is almost as old, as the wave model itself, as the wind induced waves affect the overlying atmosphere (Janssen, 1989). In the free atmosphere, the flow of air is determined by the balance between pressure gradient and Coriolis force. Within the planetary boundary layer (PBL) friction at the earth's surface affects the flow of air, leading to cross-isobar flows. The higher the friction is the more the wind direction is changed into the low pressure systems, resulting in faster filling of them. The roughness of the ocean strongly depends on the waves (Janssen, 2004). In many atmospheric models the roughness length over water surfaces is estimated using the Charnock parameterisation, which calculates the roughness length dependent on the wind speed (Charnock, 1955; Doms et al., 2013). However, this parameterisation does not take the wave age or swell travelling into the area into account. Especially young sea states are associated with high friction (Donelan et al., 1993; Janssen, 2004), resulting in large changes in surface roughness (Katsafados et al., 2016; Wu et al., 2017). This increased friction then leads to more direct flow into the low pressure system resulting in a weaker pressure gradient. Enhanced friction, on the other hand, also leads to an enhanced heat flux, which tends to deepen low pressure systems (Janssen, 2004). Therefore, the effect waves can have on the atmosphere are oppositional. The dominant process, through which the system develops, determines the effect waves have on the low pressure system. While for lows in the extratropics the momentum flux plays the major role, leading to less intense cyclones (Doyle, 1995; Lionello et al., 1998; Janssen et al., 2002; Janssen, 2004), for hurricanes the temperature gradient between the water surface and the atmosphere

can become large. Hence, the heat flux can play a role as well, leading to a deeper hurricane due to coupling wave and atmospheric models (Bao et al., 2000; Janssen, 2004). Therefore, for the area of interest, namely northern Europe, the major effects can be expected in a weakening of low pressure systems. There are already a couple of studies, where differences in surface parameters are analysed (e.g. Doyle, 1995; Lionello et al., 1998; Bao et al., 2000; Wahle et al., 2017), but only very few of them look at differences that might occur within the atmosphere (e.g. Janssen and Viterbo, 1996; Katsafados et al., 2016; Janssen and Bidlot, 2018; Varlas et al., 2018).

The coupling of waves and atmosphere was introduced into the operational forecast of the European-Centre for Medium-Range Weather Forecasts (ECMWF) in 1998. The coupling leads to substantial improvements in various surface parameters, such as 10 m wind speed and significant wave height and has modest impact on the 1000 hPa and 500 hPa geopotential height (Janssen et al., 2002; Janssen, 2004). When analysing the results of global ensemble simulations, the effect of the waves proved to be significant in the storm track area in both hemispheres (Janssen and Viterbo, 1996; Janssen et al., 2002). For regional simulations, though, the impacts of coupling on the atmosphere have been stated to be insignificant, since large differences are in the same range as the internal variability (Weisse et al., 2000; Weisse and Schneggenburger, 2002). One reason for that might be the spatial resolution of the models. Janssen and Viterbo (1996) and Wu et al. (2017) found the spatial resolution of the models to be a crucial factor for the impacts of waves on the atmosphere. They stated that the spatial resolution of the atmospheric model plays a major role in the magnitude of the impacts of ocean waves on the atmosphere. Since the early 2000s the spatial resolution of regional atmospheric models has increased and the models developed further. However, the significance of the impacts of waves on the atmosphere using ensemble simulations has not been reassessed using state-of-the-art high resolution regional models.

This dissertation aims at improving the depiction of extreme events in waves and atmospheric models and lowering the uncertainty in model results. For the stand-alone wave model the focus is on the effect of wind input resolution on the uncertainty of the wave model during extreme events. Furthermore, the data quality of the satellite Sentinel-3A is investigated and compared to older satellite missions. This is followed by an analysis, whether Sentinel-3A data can enhance the quality of the wave model results. With moving to a coupled wave-atmosphere model, the effects of the coupling on both models can be explored. The analyses include differences in parameters at the surface and within the

planetary boundary layer in the atmospheric model. In the next step, the significance of the impacts of the waves on the atmosphere compared to the internal variability in the atmospheric model is investigated. Moreover, the impact of the coupling on the uncertainties stemming from initial conditions in the atmospheric model is examined. These questions are elaborated in the course of three papers, tackling first the wave model as a stand-alone model and then the coupled system of waves and atmosphere. In the following, an overview over the three research articles is illustrated. Therein, the specific research questions contributing to the overall aim of the thesis are formulated and answered. Ultimately, conclusions and an outlook are provided, emphasising the application of the findings and suggesting topics for further research. The complete research articles are provided in the Appendices A, B and C.

2 Uncertainties in wave and atmosphere models during extreme events

The research in the course of this thesis is divided into several specific research questions. In the following these research questions along with the answers leading to the aim of improving the depiction of extreme events in wave and atmospheric models and lowering the uncertainty in model results are presented. The first paper evaluates the synergy of wave modelling and satellite observations and is published in late 2018 in the journal of "Ocean Science" (Wiese et al., 2018). The second paper published in mid 2019 in the journal of "Atmosphere" examines the impacts of the two-way coupling between the wave model and the atmospheric model on the lower atmosphere over the North Sea (Wiese et al., 2019). The third paper assesses the internal model variability of ensemble simulations with a regional coupled wave-atmosphere model and is accepted for publication in the journal of "Frontiers in Marine Science" (Wiese et al., 2020).

2.1 Temporal resolution of wind forcing and satellite data quality

The meteorological conditions have been found to be crucial for conducting a good wave forecast in previous studies (Cavaleri and Bertotti, 2003b; Cavaleri et al., 2007; Thomas and Dwarakish, 2015; Van Vledder and Akpınar, 2015). Especially, on the regional scale

accurate wind forcing data play an important role (Cavaleri and Bertotti, 2006; Van Vledder and Akpınar, 2015). This is already known since more than 20 years, when Cavaleri and Bertotti (1997) suggested that the general performance of the wave model and its performance during extreme events can be improved with a better resolution of the wind field. Since then, a couple of studies assessed the influence mostly of spatial but also temporal resolution of wind forcing on the wave model for different regions such as the coastal areas around the Mediterranean Sea (Cavaleri and Bertotti, 2003a, 2004; Signell et al., 2005; Cavaleri and Bertotti, 2006; Bolaños-Sanchez et al., 2007; de León and Soares, 2008; de León et al., 2012), the Caribbean Sea and the Gulf of Mexico (Appendini et al., 2013), the Black Sea (Van Vledder and Akpınar, 2015) and the Beaufort Sea (Nose et al., 2018) but also on the global ocean (Feng et al., 2006). However, for the area of interest in this study, namely the North and Baltic Seas, no such analysis was found with the wind data available at present. Therefore, the first research question addressed is:

1. Are the wave model results sensitive to wind forcing with different temporal and spatial resolutions and is the resolution important in the depiction of extreme events?

Besides increasing the spatial or temporal resolution of the wind input data, another way of potentially enhancing the accuracy of a wave model is through data assimilation of remote sensing estimates of significant wave height into a best-guess wave field (Lionello et al., 1992; Thomas and Dwarakish, 2015). While this works well on the open ocean, the quality of remote sensing data tends to deteriorate closer to the coast. Hence, the satellite data are discarded up to a few tens of kilometres from the coast (Cipollini et al., 2010; Vignudelli et al., 2011; Fenoglio-Marc et al., 2015). In February 2016 the new satellite Sentinel-3A was launched. The difficulties in taking satellite measurements close to the coast, like retracking at a land-sea interface, are supposed to be reduced by Sentinel-3A (Beneviste and Vignudelli, 2009). Therefore, the two following research questions arise:

2. Is the data quality of the newly available Sentinel-3A satellite improved compared to older satellite missions, especially close to the coast?
3. Can these satellite data be used to increase the accuracy of the best-guess wave field of the wave model?

These three questions have been answered in the paper Wiese et al. (2018) provided in Appendix A. For the first research question on the sensitivity of the wave model towards

the resolution of the wind forcing it can be stated that, especially for the depiction of extreme events, a high temporal resolution of the wind forcing is a key factor. The spatial resolution of the wind forcing seems to be less important for the North Sea and the tested wind input data.

To come to the above conclusion the wind wave model WAM (WAMDI Group, 1988; ECMWF, 2019) is forced with different wind data sets. The reanalysis ERA-Interim (Berrisford et al., 2009; Dee et al., 2011), ERA5 (ECMWF, 2017b; Copernicus Climate Change Service (C3S), 2017) and coastDat-3 (HZG, 2017), as well as the ECMWF operational analysis/forecast (ECMWF, 2017a) and the German Weather Service (Deutscher Wetterdienst, DWD) forecast (Reinert et al., 2018) are used as meteorological input data. While ERA-Interim has a six hourly resolution, its successor ERA5, coastDat-3 and the DWD forecast have hourly resolutions. The ECMWF operational analysis is done six hourly but the dataset has been added with the ECMWF forecast to an hourly resolution as well. To compare better between the temporal resolutions, ERA5, the DWD forecast and the ECMWF operational analysis are used to force the model every six hours.

To evaluate the model performance with the different wind input fields the model output is compared with in situ observations. In general, all simulations compare fairly similar to the observations. The simulations with hourly wind forcing, however, have slightly better statistical values than simulations with corresponding six hourly wind input data. Under normal conditions, the model simulations with all eight wind forcings produce quite similar results. For larger waves differences between the simulations are found.

One extreme event which occurs during the six-month study period is analysed in more detail. The location and strength of the peak in significant wave height differ between model simulations with different wind input data. The maximum of the peak is shifted by around 290 km further to the east and has lower maximum significant wave heights in model simulations forced with six hourly wind input than in corresponding simulations with hourly wind input. The average difference between the maximum significant wave heights in associated simulations with hourly and six hourly wind forcings is around 0.5 m, which corresponds to 10 % of the measured significant wave height for the extreme event analysed here.

The analysis of time series extracted from the measurements in the northern part of the North Sea compared with the model data at the collocated locations reveals the major drawback of too coarse temporal resolution of the wind forcing. When using six hourly

wind input data, the peak in wind speed can just simply be missed, since one update time is prior to the wind peak and the next after the peak. This leads to an underestimation of significant wave height by the wave model in the majority of the cases. Also the opposite can happen, when the update time is at the same time as the peak in wind speed. Then, since the wind speed is kept constant the six hours around the update time, the wind is already that high three hours prior and after the actual peak. In that case, the significant wave height is overestimated by the simulations with six hourly wind forcing. This illustrates the importance of hourly wind input data for the wave model in the depiction of extreme events. However, even for simulations with hourly wind forcing, there are a number of other factors that might play a role in the depiction of extreme events with the wave model. These factors could be swells travelling from other parts of the model domain into the area of the peak, the tuning of the wave model and the depiction of the peak in wind speed in the wind data, which should match the observations reasonably well.

The wave model produces the best and quite similar results with ERA5 and the ECMWF operational analysis/forecast as wind forcing data, although the spatial resolution of the ECMWF operational analysis/forecast is much higher than of ERA5, and the DWD forecast and coastDat-3 have higher spatial resolution than both ECMWF products. Consequently, the temporal resolution of the wind input data seems to be more important than the spatial resolution of the wind forcing for the area of interest. However, the differing spatial resolutions result from different atmospheric models or model set-ups. Hence, the differences between simulations with different wind input data cannot only be traced back to the spatial resolution.

From the analyses above, for the first research question, it is concluded that during extreme events, the wave model results are quite sensitive to the wind forcing. Hence, high-quality and high temporal resolved wind data are needed to improve the ability to depict the sea state during extreme events. Furthermore, the temporal resolution seems to be more important than the spatial resolution.

In this study the emphasis is put on the impact of the temporal resolution of the wind forcing data on the wave model results. Previous studies concentrated on the spatial resolution of the wind, showing that the wave model output improves, when using a higher spatial resolution in the wind field (Cavaleri and Bertotti, 2004, 2006). Van Vledder and Akpınar (2015) stated that the wave model is critically sensitive to the spatial resolution

of the wind input data and less sensitive to the temporal resolution for the Black Sea. One reason for the diverging conclusion compared to this study might be differing methodology applied. Another reason could be that the importance of high spatial or high temporal resolution can vary between regions.

For the general assessment of the data quality of the newly available Sentinel-3A satellite compared to older satellite missions, the data of Sentinel-3A, CryoSat-2 and Jason-2 are compared to in situ observations. Over the whole study area the general performance of all satellite products is good and very similar. However, the satellites tend to slightly overestimate the significant wave heights measured at the in situ stations. To further estimate the quality of Sentinel-3A, the satellite data are compared to the model simulation from the first part of the study, which is closest to the observational data, during both, normal and extreme conditions. The differences of data quality between Jason-2 and Sentinel-3A become visible through calculations of the Scatter Index (SI) along the satellite tracks within the wave models grid boxes. On the open ocean both perform very well, having a low SI. Closer to the coast, especially in the northern part of the Baltic Sea, the Danish Straits and the coastal areas of the southern North Sea, the SI of Sentinel-3A is better compared to the SI of Jason-2. This finding becomes even more evident by an analysis of the statistical values of the satellite data compared to the wave model within the first 10 km of the coast. In that area, the root mean square error (RMSE) and SI could be reduced by around 10 cm and 17 %, respectively. The correlation could be increased by 5-10 %. Furthermore, the statistical values within 10 km from the coast are closer to the ones for the whole study area.

Hence, for the second research question, it can be concluded that the quality of the newly available Sentinel-3A satellite data has substantially improved compared to older satellite missions in coastal areas. Furthermore, no substantial differences in the Sentinel-3A data quality for different crossing directions of the coast, fetch conditions and relative wind and flight directions are found.

Due to that result, the third research question is raised, to check whether the satellite data of Sentinel-3A can be used to increase the accuracy of the model's best-guess wave field. Empirical orthogonal functions (EOFs) (Björnsson and Venegas, 1997) are used to combine the ensemble of wave model outputs applied in the first part of the paper with the satellite measurements for the extreme event analysed. The agreement of the model ensemble with the in situ observations is already quite good, therefore, the satellite data

could not be taken as is to incorporate them with the model results. Instead, a bias correction of the satellite data is carried out, as well as a rather high value of observation error is assumed. With these two adaptions the best-guess wave field comes closer to the in situ observations than the ensemble mean. The reduction in RMSE is from 0.56 m to 0.54 m and in bias from 0.11 m to 0.06 m, the SI stays at 0.14.

Hence, for the third research question it can be concluded that the Sentinel-3A data can be used to guide the wave model towards a better solution. However, the quality of the satellite data is still not accurate enough, compared to in situ observations, to strictly force the already quite good wave model towards the satellite observations.

Thus, the first part of the thesis shows that high-quality and high temporal resolved wind fields enhance the depiction of significant wave height during extreme events in the wave model. Also, the improvement of data quality of Sentinel-3A compared to older satellite missions in the coastal areas is illustrated. However, further improvement of Sentinel-3A data quality is needed, for being able to strictly force the wave model to the satellite observations.

2.2 Impact of coupling between wave and atmospheric model on the lower atmosphere

Having shown that high-quality and high temporal resolved wind fields are essential for the wave model (Wiese et al., 2018), next the effects of coupling waves and atmosphere are investigated. The wind induced waves at the surface of the ocean affect the overlying atmosphere (e.g. Janssen, 1989, 1992; Doyle, 1995; Lionello et al., 1998; Bao et al., 2000; Janssen et al., 2002; Janssen, 2004; Katsafados et al., 2016; Wahle et al., 2017). One widely used approach for the investigation of these effects is to compare a coupled with a reference simulation (e.g. Doyle, 1995; Katsafados et al., 2016; Wahle et al., 2017; Wu et al., 2017; Varlas et al., 2018). In the coupled simulation the atmospheric model receives roughness length information from the wave model. In the reference simulation the atmospheric model uses its own parameterisation to estimate the roughness length over the ocean surfaces. However, the majority of the studies focus on the impact of the coupling on the surface parameters and only very few studies also consider impacts on the higher atmosphere (Janssen and Viterbo, 1996; Katsafados et al., 2016; Janssen and Bidlot, 2018; Varlas et al., 2018). Therefore, the following research question is raised:

4. Can differences between coupled and reference simulations still be detected within and at the height of the atmospheric planetary boundary layer (PBL) within the North Sea area?

This question is answered in the paper available in Appendix B by Wiese et al. (2019). The conclusion is that differences between the coupled and reference simulation can be detected within the PBL. For the analysis, a coupled system consisting of an atmospheric model and a wave model is used. The atmopsheric model used is the Consortium for Small-Scale Modelling (COSMO)- in Climate Mode (CLM) (COSMO-CLM), which is the community model of the German regional climate research community (Rockel et al., 2008; Doms and Baldauf, 2013). As the wave model the wind wave model WAM is used (WAMDI Group, 1988; ECMWF, 2019). The atmospheric model sends the 10 m wind fields to the wave model in the coupled and reference simulation. The atmospheric model receives the roughness length from the wave model only in the coupled simulation and uses the Charnock parameterisation in the reference simulation.

The comparison of roughness lengths coming from the wave and atmospheric models clearly shows that the atmospheric model underestimates the roughness length over the ocean compared to the estimation by the wave model. Especially, for wind speeds exceeding 10 m/s, the roughness length of the wave model becomes larger than the ones calculated by the atmospheric model. This enhancement in roughness length leads to a reduction in wind speed and, thus, to a reduction in significant wave height. The results of the coupled simulation in wind speed and significant wave height compare better to satellite and in situ observations than the reference simulation's results. Particularly during extreme events the coupled simulation matches the observations better than the reference simulation, indicating an enhancement of the ability to depict extreme events in the coupled simulation. Similar results of the coupling enhancing the agreement with observations have also been found by Janssen et al. (2002), Wahle et al. (2017) and Varlas et al. (2020). Also the reduction in pressure gradient found by Janssen (2004) is present in the results of this study.

Differences between the coupled and reference model simulation above the surface are detected by analysing Hovmöller-diagrams in the centre of the North Sea. In the Hovmöller-diagrams a vertical spreading of the differences between coupled and reference simulation within the atmosphere can be seen. In the event analysed, these differences are associated

with steep gradients and slight variations of the exact timing and location of the gradients, like fronts in wind speed or temperature. The vertical spreading of the differences within the atmosphere have also been found by Varlas et al. (2018) for a cyclone in the Mediterranean Sea.

Answering research question four it can be concluded that differences between the coupled and reference simulation are visible within and at the height of the PBL and not solely in surface parameters in the North Sea area.

The approach of comparing reference and coupled simulation is widely used to asses the impacts of the coupling (e.g. Doyle, 1995; Katsafados et al., 2016; Wahle et al., 2017; Wu et al., 2017). However, during the course of the study presented here, the question about uncertainties in coupled and reference model simulations with respect to small variations in initial conditions arose. This question led to the motivation of the studies presented in the third part of the thesis.

2.3 Internal model variability of a regional coupled wave-atmosphere model using ensemble simulations

The question about the significance of the impacts of the coupling compared to the internal model variability, here called internal variability, of the atmospheric model resulting from slightly disturbed initial conditions is discussed differently in the literature. Weisse et al. (2000) and Weisse and Schneggenburger (2002) found that the impacts of coupling are insignificant, pointing out that large differences due to coupling are in the same range as the internal variability. Janssen and Viterbo (1996) stated a significant impact of the sea-state dependent momentum exchange in their ensemble mean of a global model. They suggested that the model resolution is crucial for studying the significant consequences of waves on the atmosphere. Since the studies of Weisse et al. (2000) and Weisse and Schneggenburger (2002) the resolution of the regional atmospheric models has improved, leaving the following research question open:

5. How do the differences between the coupled and reference ensemble compare to the internal variability using a state-of-the-art high resolution regional coupled wave and atmosphere model?

Another point left open, when comparing ensemble simulations of coupled and reference

model systems, is the comparison of the internal variability between the two ensembles. For coupled ocean-atmosphere models a stabilising effect reducing the internal variability of the atmospheric model in coupled simulations can be found (Ho-Hagemann et al., 2020). For coupled wave-atmosphere models the effect of coupling on the internal variability is still open for investigation. Therefore, the next research question is:

6. What is the effect of the coupling between waves and atmosphere on the internal variability of the atmospheric model?

One way of reducing the internal variability in atmospheric models is the use of spectral nudging (von Storch et al., 2000; Weisse and Feser, 2003). By applying this method, the large-scale atmospheric state is kept close to the forcing data, while the regional-scales can develop. This, though, might reduce the effects of coupling between different models (Ho-Hagemann et al., 2020). This leads to the following research question:

7. Are the effects of coupling between waves and atmosphere sensitive to the use of spectral nudging in the atmospheric model?

Furthermore, regional atmospheric models need boundary conditions at their lateral boundaries. These are usually taken from global model simulations. That the boundary conditions can have an impact on the solution found by the regional model is already known (Meißner, 2008; Meissner et al., 2009). However, whether the boundary conditions have an impact on the effects of the coupling is still a topic that needs further investigation. This phrases the following question:

8. Are the effects of coupling between waves and atmosphere sensitive to the choice of boundary conditions?

These four questions have been answered in Wiese et al. (2020) provided in Appendix C. Ensemble simulations with a coupled regional high resolution atmosphere-wave model consisting of COSMO-CLM and WAM are performed. Each ensemble consists of 10 members initialised with slightly differing initial conditions of the atmospheric model covering January till March 2017. These months are chosen for this study, since the effects of coupling on a regional scale are larger during high wind events, which are usually present during this time of the year (Wahle et al., 2017; Wu et al., 2017; Wiese et al., 2019; Varlas et al., 2020).

The analysis shows an enhancement of roughness length within the coupled model area in the ensemble means in the mean over the three months. This enhancement leads to a reduction in wind speed and significant wave height as well as to a reduction in pressure gradient. These effects are also present in previous studies (e.g. Lionello et al., 1998; Janssen et al., 2002). Additionally, this study assesses the significance of the impacts of the coupling on the atmosphere compared to the internal variability. The differences due to the coupling proved to be significant during the majority of the time. The differences between the coupled and reference ensemble of the roughness length are significant during 89 % of the study period. The differences in wind speed showed to be significant in 71 % of the time, while the differences in significant wave height are significant even around 93 % of the time. For these variables the changes due to coupling are mostly limited to the area coupled, while differences in MSLP spread over the whole area. The differences in MSLP are significant in 75 % of the time, reducing to 73 % and 71 % for differences in geopotential at 850 hPa and 500 hPa, respectively. Hence, the differences between coupled and reference ensemble are still significant at higher layers of the atmosphere. These values are the mean over the coupled area. They can vary for different locations. Larger numbers are found in the North Sea area and smaller values in the Baltic Sea area. The differences between coupled and reference simulations prove to be especially large when high wind speeds are present. Usually the internal variability stays low during these events, with the differences being larger than the internal variability. Thus, the effects of the coupling can be differentiated from the internal variability of the model during extreme events. Occasionally events occur, where the internal variability increases, which might lead to larger internal variability than differences, but these events are outnumbered by events with large differences between coupled and reference ensemble and low internal variability.

Therefore, for the fifth research question it is concluded that the differences between coupled and reference ensemble can be stated significant during the majority of the time, with large differences usually being larger than the internal variability. Furthermore, the realism of the system consisting of waves and atmosphere is enhanced compared to the stand-alone models, since again the results of the coupled system are closer to observational data than results from the reference ensemble. This improvement is particularly visible for extremes.

Answering the sixth research question, the analysis shows that the internal variability in the atmospheric model is reduced in the coupled ensemble compared to the reference ensemble. The reduction in internal variability indicates a reduction in model uncertainty

via the replacement of the wind dependent roughness length with the estimation of the ocean surface roughness through wave parameters. This reduction can be detected in the mean internal variability of the atmospheric model but becomes more evident during events with large internal variability. The maximum in internal variability in wind speed is reduced by 23 % and the 99th percentile by 11 %. In significant wave height the spread of the ensemble is introduced through the uncertainty in wind conditions. The maximum spread in significant wave height is reduced by 36 % and even 39 % for the 99th percentile. The mean internal variability in wind speed and the mean spread in significant wave height can be reduced by 7 % and 26 %, respectively.

Next, the sensitivity of coupling to the application of spectral nudging in the atmospheric model is evaluated. For the seventh research question it can be concluded that the differences in 10 m wind speed and significant wave height show very little changes in the ensemble with spectral nudging compared to the one without spectral nudging. Since the internal variability is reduced by the spectral nudging, the number of times with significant differences between coupled and reference simulation increase. However, the differences in MSLP are sensitive towards the application of spectral nudging. For MSLP, the differences between coupled and reference ensemble tend more towards a reduction of MSLP rather than a reduction of pressure gradient as found for the ensemble not using spectral nudging. Also in simulations with spectral nudging the realism of the system is enhanced by the coupling between the wave and the atmospheric models showing results closer to observational data.

Another set of ensembles is conducted using different boundary conditions in order to asses the sensitivity of the influences of coupling to boundary conditions answering research question eight. These simulations have been done without spectral nudging again. The results show that the general impact of the coupling is not sensitive towards the choice of boundary conditions. When analysing the temporal evolution or single events, the differences in 10 m wind speed still appear to be only little effected, while the differences in MSLP can show some deviations, which seems to be caused by the different distribution of MSLP due to differing boundary conditions. Nevertheless, the conclusions answering research questions five and six are proven robust to the application of different sets of reanalysis data at the lateral boundaries of the atmospheric model.

Thus, this study shows the possible positive effects of the wave model on the atmospheric model. The coupled ensemble is closer to observations of 10 m wind speed and significant wave height than the reference ensemble. Furthermore, the internal variability in the

atmospheric model is reduced considerably. Additionally, the differences between coupled and reference ensemble are significant most of the time, with large differences during events with high wind speed. Significant impacts of the coupling have also been found in the storm track area of both hemispheres by Janssen and Viterbo (1996). Weisse et al. (2000) and Weisse and Schneggenburger (2002), however, stated that the waves impact on the atmosphere on the regional scale is about the same magnitude as the internal variability when large differences between coupled and reference simulation are present. These results are contradictory to the findings in this thesis, as the large impacts of the coupling proved to be larger than the internal variability of the atmospheric model most of the time. One possible reason for the contradictory outcome of the studies might be the differing spatial resolution of the models. In this thesis a finer horizontal resolution is used compared to the one of Weisse et al. (2000) and Weisse and Schneggenburger (2002). As Janssen and Viterbo (1996) and Wu et al. (2017) stated, the horizontal resolution is very crucial for the magnitude of the impacts of the coupling. Like in this thesis, also Rutgersson et al. (2010) found significant impacts of the waves on the atmosphere on a regional scale. They, however, used long term simulations in order to assess the significance of the impacts of the coupling. In addition to the assessment of the significance, in this thesis it is found that the coupling of the wave model to the atmospheric model reduces the internal variability of the latter.

3 Conclusions and Outlook

In this dissertation potentials to reduce the uncertainty in wave and atmospheric model results, with the aim of enhancing the quality of the model output especially during extreme events, are illustrated. For the stand-alone wave model it is shown that high quality and high temporal resolved wind input data improve the depiction of significant wave height during extreme events. In addition, it is demonstrated that the coupling of waves to the atmospheric model improves the depiction of extreme events and reduces the uncertainty in the model. A good estimation of extreme events as well as a reduction of uncertainty is particularly important for the safety of humans at sea, but also required for hindcast and climate studies.

Major sources of uncertainty for the wave model are the quality and resolution of the available wind input data. In this study it is shown that an hourly temporal resolution is necessary to depict the significant wave height during extreme events. This is important

for both the estimation of the magnitude as well as the location of the peak. The shift in location by approximately 290 km and the difference in magnitude of around 0.5 m, in the extreme event analysed, can make differences in the decision making of wave forecast users. This study extends previous studies which illustrate the importance of high spatial resolution to improve the wave model results and that the wave model is very sensitive to the quality of the wind data (Cavaleri and Bertotti, 2004, 2006; Bolaños-Sanchez et al., 2007; de León and Soares, 2008; Van Vledder and Akpınar, 2015). This dissertation emphasises the necessity of hourly wind data being made available for wave model simulations. Especially when forecasting waves with stand-alone wave models this is fundamental for the depiction of extreme events in the area analysed. Also in hindcast and wave climate studies an hourly resolution of wind input data is recommended for the better depiction of extreme events.

To reduce the uncertainty in wave models, observational data can be assimilated into the model. The technique of data assimilation is mainly used for global simulations, where the model can benefit from the observations (Lionello et al., 1992; ECMWF, 2019). In coastal areas, however, the quality of satellite data decreases (Fenoglio-Marc et al., 2015). In this thesis it is found that within the first 10 km from the coast the RMSE, SI and correlation are improved by 20 %, 17 % and 5-10 %, respectively for the Sentinel-3A data compared to older satellite products. These results make its data interesting for potential data assimilation. Nevertheless, the Sentinel-3A data are still not accurate enough to completely force the wave model towards the observations, but can rather be used to guide the model into the right direction. Meanwhile a similar conclusion is made by Schulz-Stellenfleth and Staneva (2019), showing that the smallest error is still found for in situ measurements, while the amount of uncertainty of Sentinel-3A compares to the uncertainty of the wave model. Additionally, attempts have been made to reduce the uncertainty in remote sensing measurements by modifying the retracking algorithms for the data of Sentinel-3A (Dinardo et al., 2020; Schlembach et al., 2020). This path needs further exploration, since with lower uncertainties, remote sensing observations in coastal areas could become useful to reduce uncertainties in regional wave model simulations.

As shown in the first part of this thesis the quality of wind data affects the accuracy of the wave model. A strong tool to reduce the uncertainty of the atmospheric model and, hence, the wave model, as pointed out in this dissertation is the coupling between them. Due to the coupling the realism of the system is enhanced, coming closer to observational data and reducing the internal variability of the atmospheric model. This reduction is

quantified with around 7 % in the mean internal variability and even 23 % in the maximum internal variability in wind speed for simulations only forced at the lateral boundaries. Therefore, the coupling is advantageous for operational forecasting systems, as well as for regional climate models. Significant wave height and wind speed are crucial parameters for operations at sea including shipping as well as building and conducting maintenance of offshore energy structures. These sectors can benefit from the the increased model reliability, through the reduction in uncertainty.

A substantial step towards fully coupled atmosphere-wave-ocean models is made by estimating the internal variability in the coupled atmosphere-wave system and reducing the uncertainty via the coupling. While regional climate models have transitioned from stand-alone models to coupled ocean-atmosphere systems, the waves are rarely incorporated (Cavaleri et al., 2012a; Schrum, 2017). The results of this thesis clearly demonstrate the reduction in internal variability of the atmospheric model due the coupling between waves and atmosphere, which indicates a reduction in model uncertainty due to the coupling. This reduction in uncertainty can be beneficial for regional climate studies. Schrum et al. (2003) and Ho-Hagemann et al. (2020) have shown a stabilising effect of the ocean component on the atmospheric model. Consequently, the next major step is to couple all three components and assess the effects regarding uncertainties and reliability of the model system.

Additionally, the way of exchanging parameters between the components is an ongoing research topic. This further addresses the reduction of model uncertainty in coupled systems and enhances the description of physical processes at the interface between ocean and atmosphere through the waves. For the calculation of the roughness length within the wave model, different approaches exist. While this study uses the approach by Janssen (1991) (ECMWF, 2019), other approaches, like the use of a wave boundary layer model (Moon et al., 2004; Du et al., 2017, 2019), could be tested within the system. Since waves are located right at the interface between the ocean and atmosphere, they determine the momentum, heat, energy and mass fluxes between the two components (Cavaleri et al., 2012a; Staneva et al., 2014). In this thesis, the effects of wave dependent surface roughness on the momentum are analysed, showing differences in surface parameters but also within the PBL, however, the effects on latent and sensible heat fluxes are not assessed. For that assessment, an active ocean model in the coupled system is desirable, with especially the sensible heat flux being highly dependent on the ocean surface temperature. Lately the attempt of a more integral approach towards energy conserving models and model

systems is made (TRR181, 2020). This further tackles the reduction of model uncertainty but also enhances the description of the physical processes. For energy conserving transfer between ocean and atmosphere, the waves at their interface play a crucial role. Hence, the waves need to be paid attention and better understood of exactly how the energy is transferred between the ocean and the atmosphere through the waves (Buckley and Veron, 2019; TRR181:M6, 2020). Furthermore, the mass transfer between the ocean and the atmosphere is determined by the waves in the form of sea spray and air intrusion into the ocean, which needs to be incorporated into coupled models as well (Cavaleri et al., 2012a; Wu et al., 2015). This again shows the need for fully coupled systems of ocean, waves and atmosphere, as also the ocean and the waves impact each other (Breivik et al., 2015; Staneva et al., 2016a,b). In the context of hurricane studies fully coupled systems of ocean, waves and atmosphere have already been used and proven superior over models not incorporating all three components (Chen et al., 2007; Olabarrieta et al., 2012; Zambon et al., 2014; Pant and Prakash, 2020). The necessity of including waves into the coupled model systems for hurricanes along with the studies of Wu et al. (2019) and Wu et al. (2020) on a fully coupled system in the extratropical region makes it inevitable to asses the waves impact within a fully coupled system in regional climate models, as well as operational forecasting systems.

Overall, this dissertation illustrates potentials to reduce uncertainties in atmospheric and wave model results. It is shown that high-quality and high temporal resolved wind data are needed to improve the ability to depict the sea state during extreme events. An additional result of this dissertation is that the data quality of the Sentinel-3A satellite is improved compared to older satellite products and can be used to guide the wave model towards a better solution. Nevertheless, Sentinel-3A data quality needs further improvement to be able to enhance the accuracy of the wave model when completely forcing it towards the satellite data. For the coupled wave-atmosphere model it is shown that the coupling not only affects the surface parameters, but also that the differences between coupled and reference simulations can spread vertically within the atmosphere. Another important result presented in this dissertation is that the coupling of waves and atmosphere reduces the uncertainty in the atmospheric model, and hence in the wave model, by reducing the internal variability and getting closer to observational data. Also the impacts of the coupling are found to be significant during the majority of the time with large impacts during extreme events. Consequently, this dissertation makes one step forward to understand processes and reduce uncertainties in earth system models.

Appendices

A Synergy of wind wave model simulations and satellite observations during extreme events

Wiese, A., Staneva, J., Schulz-Stellenfleth, J., Behrens, A., Fenoglio-Marc, L., & Bidlot, J.-R. (2018). Synergy of wind wave model simulations and satellite observations during extreme events. Ocean Science, 14(6), 1503-1521, https://doi.org/10.5194/os-14-1503-2018.

The publication has been formatted according to the format of this dissertation. The references have been merged with the other references of the thesis to one reference list for the whole dissertation.

The contribution of Anne Wiese and the other authors to this paper is as follows:
Anne Wiese prepared the wind data for WAM format and performed all model simulations, except with ERA-Interim wind, did the analyses and wrote the paper. Anne Wiese and Dr. Joanna Staneva conceived the work. Dr. Arno Behrens prepared the wind data and performed the model simulation with ERA-Interim wind, provided assistance with the set-up and application of the wave model WAM, provided scripts for the preparation of wind data to WAM format and provided Jason-2 and DWD wind data. PD Dr. Luciana Fenoglio-Marc provided Sentinel-3A and CryoSat-2 data. Dr. Jean-Raymond Bidlot provided the ECMWF operational analysis/forecast and ERA5 wind and in situ observational data. Anne Wiese was guided by Dr. Johannes Schulz-Stellenfleth on the EOF analysis. All authors reviewed the manuscript. The manuscript was checked for English language.

Synergy of wind wave model simulations and satellite observations during extreme events

Anne Wiese[1], Joanna Staneva[1], Johannes Schulz-Stellenfleth[1], Arno Behrens[1], Luciana Fenoglio-Marc[2] and Jean-Raymond Bidlot[3]

[1]Institute of Coastal Research, Helmholtz-Zentrum Geesthacht, Geesthacht, Germany

[2]Institute of Geodesy and Geoinformation, University of Bonn, Bonn, Germany

[3]European Centre for Medium-Range Weather Forecasts, Reading, UK

(Received: 18 July 2018; Discussion started: 30 July 2018; Revised: 24 October 2018; Accepted: 29 October 2018; Published: 7 December 2018)

In this study, the quality of wave data provided by the new Sentinel-3A satellite is evaluated and the sensitivity of the wave model to wind forcing is tested. We focus on coastal areas, where altimeter data are of lower quality and wave modelling is more complex than for the open ocean. In the first part of the study, the sensitivity of the wave model to wind forcing is evaluated using data with different temporal and spatial resolution, such as ERA-Interim and ERA5 reanalyses, the European Centre for Medium-Range Weather Forecasts (ECMWF) operational analysis and short-range forecasts, German Weather Service (DWD) forecasts and regional atmospheric model simulations (coastDat). Numerical simulations show that the wave model forced using the ERA5 reanalyses and that forced using the ECMWF operational analysis/forecast demonstrate the best capability over the whole study period, as well as during extreme events. To further estimate the variance of the significant wave height of ensemble members for different wind forcings, especially during extreme events, an empirical orthogonal function (EOF) analysis is performed. In the second part of the study, the satellite data of Sentinel-3A, Jason-2 and CryoSat-2 are assessed in comparison with in situ measurements and spectral wave model (WAM) simulations. Intercomparisons between remote sensing and in situ observations demonstrate that the overall quality of the former is good over the North Sea and Baltic Sea throughout the study period, although the significant wave heights estimated based on satellite data tend to be greater than the in situ measurements by 7 cm to 26 cm. The quality of all satellite data near the coastal area decreases; however, within 10 km off

the coast, Sentinel-3A performs better than the other two satellites. Analyses in which data from satellite tracks are separated in terms of onshore and offshore flights have been carried out. No substantial differences are found when comparing the statistics for onshore and offshore flights. Moreover, no substantial differences are found between satellite tracks under various metocean conditions. Furthermore, the satellite data quality does not depend on the wind direction relative to the flight direction. Thus, the quality of the data obtained by the new Sentinel-3A satellite over coastal areas is improved compared to that of older satellites.

A.1 Introduction

Information on the state of the sea in coastal areas is of great interest, as waves are a crucial factor for important activities conducted at sea. Therefore, an accurate wave forecast and hindcast are very important for marine traffic, recreational activities on the water, urban development near the coast, ecosystem restoration, renewable energies and offshore management (Gautier and Caires, 2015; Thomas and Dwarakish, 2015). Global ocean wave forecasts with coarser spatial resolution have already reached a remarkable level of accuracy (Janssen and Bidlot, 2018). However, for inner basins and coastal areas, higher resolution is required, and numerical wave models still have some deficits (Cavaleri and Bertotti, 2003b; Van Vledder and Akpınar, 2015).

In many studies, the meteorological input has already been found to be a crucial factor for conducting good wave forecasts (Teixeira et al., 1995; Cavaleri and Bertotti, 2003b, 2004; Cavaleri et al., 2007; Thomas and Dwarakish, 2015; Van Vledder and Akpınar, 2015). The wind data used to force a wave model need to be very accurate since, in coastal areas, the fetch is limited and small islands can block wave propagation. Small changes in wind direction can lead to drastically different wave results. The wind speed is a crucial factor in determining the significant wave height. However, peaks and extreme events are frequently not well simulated by the wave model because the meteorological input underestimates the wind speed (Cavaleri et al., 2007; Cavaleri, 2009). More than 20 years ago, Cavaleri and Bertotti (1997) suggested that the general performance of the wave model as well as its performance during extreme events can be improved by using a wind input field with a higher spatial resolution. Since the most advanced wave models at that time were more accurate than the meteorological ones, the quality of the wave model output was a very good indicator of the quality of the meteorological input data. Cavaleri and Bertotti

(2003b, 2004) analysed the accuracy of the modelled wind and wave fields of enclosed seas, such as the Mediterranean Sea, with respect to the spatial resolution of the wind fields. They found that the modelled surface wind speeds are almost always underestimated, which they attributed to a lack of spatial resolution (Cavaleri and Bertotti, 2003b). When the meteorological input data have a higher spatial resolution, the average results of the wave model are indeed closer to the ground truth (Cavaleri and Bertotti, 2004). However, even today, wind data inaccuracy leads to discrepancies between wave model simulations (Thomas and Dwarakish, 2015; Van Vledder and Akpınar, 2015). Van Vledder and Akpınar (2015) assessed the sensitivity of the wave model SWAN (Simulating Waves Nearshore) to the spatial and temporal resolution of wind input data in the area of the Black Sea. They concluded that the wave model results are critically sensitive to the spatial resolution and less sensitive to the temporal resolution of the meteorological input data. Similar analyses have been conducted both globally (Feng et al., 2006) and for coastal areas such as that around the Mediterranean Sea (Cavaleri and Bertotti, 2003a,b, 2004; Signell et al., 2005; Bolaños-Sanchez et al., 2007; de León and Soares, 2008; de León et al., 2012), the Caribbean Sea and Gulf of Mexico (Appendini et al., 2013), the Black Sea (Van Vledder and Akpınar, 2015) and the Beaufort Sea (Nose et al., 2018) but not for the area of interest in the present study, i.e. that around the North and Baltic seas, and with the wind data available at present. Hence, the accuracy of the spectral wave model WAM is assessed for both normal and extreme conditions using different meteorological input data presently available. The sensitivity of the wave model to the meteorological input data as well as their temporal and spatial resolution are estimated. Also the wind data with which the wave model performs best with respect to the observations will be determined for the later comparisons of wave model with the newly available satellite data of Sentinel-3A.

Another way to increase the accuracy of the modelled significant wave height is by assimilating the significant wave height measured by satellites into a first-guess wave field (Thomas and Dwarakish, 2015). While altimeter data related to the open ocean are of good quality and used routinely, for coastal areas, their quality tends to deteriorate, which results in systematic discarding of up to a few tens of kilometres from the coast (Cipollini et al., 2010; Vignudelli et al., 2011; Fenoglio-Marc et al., 2015). One issue in coastal altimetry is land contamination in the footprint of the altimeter due to different ocean and land surface reflectivities, leading to incorrect interpreted waveforms and therefore incorrect significant wave heights (Cipollini et al., 2010; Vignudelli et al., 2011). Hence, the advantage of improving the sea state by assimilating altimeter data into the wave

model cannot be employed close to a coast, where people are interested in accurate wave forecasting to protect and design coastal structures, e.g. dykes (Thomas and Dwarakish, 2015). The difficulties in taking satellite measurements close to a coast, e.g. retracking at a land-sea interface, have already been reduced by CryoSat-2 and, even more so, by Sentinel-3A (Beneviste and Vignudelli, 2009). In this paper, the quality of the newly available Sentinel-3A data is analysed in comparison with the data from CryoSat-2 and Jason-2, especially those related to coastal areas. Also, the data quality of the Sentinel-3A wave measurements for onshore versus offshore flights, different metocean conditions and relative wind and flight direction is examined. Then, the data are merged with the wave model results to produce a best-guess wave field.

In the next section, the measured satellite and in situ data as well as the wind forcing data and the numerical wave model used are described (Section A.2). This is followed by an assessment of the sensitivity of the wave model to different wind input data (Section A.3). In Section A.4, the quality of the newly available satellite data from Sentinel-3A with respect to that of older satellites is analysed. Then, the satellite and model data are combined to generate a best-guess wave field (Section A.5). The summary and conclusions are given in the last section (Section A.6).

A.2 Data and model

Here, the ocean wave model WAM is forced using different meteorological input data to evaluate the sensitivity of the model to different wind input spatial and temporal resolutions. Therefore, the numerical model and wind input data used are introduced in this section. Information regarding the in situ measurements used here is also given. Furthermore, the satellite data, especially that of the new Sentinel-3A satellite, are presented.

A.2.1 Satellite altimeter data

In this study, wave height data derived from the Jason-2, CryoSat-2 and Sentinel-3A altimeter missions are used. Jason-2 is a classical pulse-limited altimeter operating in low-resolution mode (LRM) that was in operation, with a revisiting time of 10 days, from June 2008 to October 2016 (ftp://avisoftp.cnes.fr, last access: 16 November 2018).

The CryoSat-2 satellite, launched in April 2010, is the first space-borne instrument with synthetic aperture radar (SAR) capabilities. It can operate in one of three modes, i.e., SAR mode, interferometric SAR (SARIn) mode and low-rate mode (LRM), following a geographical mask, which is regularly updated. Compared to conventional pulse-limited (or conventional) altimetry (CA), SAR altimetry provides a better along-trajectory resolution and a higher signal-to-noise ratio (SNR). Over the northeastern Atlantic, CryoSat-2 operates in SAR mode. Data collected in SAR mode and processed similarly to LRM data are called reduced SAR (RDSAR) data. We use CryoSat-2 RDSAR data (C2-RDSARRADS-1Hz) from the Radar Altimeter Database System (RADS) (http://rads.tudelft.nl/rads/rads.shtml, last access: 16 November 2018) and SAR products from the grid processing on demand (GPOD) service at the ESA Centre for Earth Observation (ESRIN) (C2-SARGPOD-1Hz) (https://gpod.eo.esa.int, last access: 16 November 2018).

Sentinel-3A, launched in February 2016, is the first satellite operating entirely in SAR mode. RDSAR products are also available. Essentially, the altimeter data are 1-D profiles along the ground track of the satellite, with a footprint size of 1.5 km to 10 km depending on the sea state across the track. The resolution along the track of the satellite is approximately 7 km for 1 Hz measurements. Each track is repeated every 27 days, with a deviation of $\pm$ 1 km in longitudinal direction. "Ascending" passes are from south-southeast to north-northwest, whereas "descending" passes are from north-northeast to south-southwest. In the present study the official Sentinel-3 SAR (S3A-SARNTC-1Hz) and RDSAR products (S3A-RDSARNTC-1Hz) are used, which are made available directly by Copernicus (https://sentinels.copernicus.eu/, last access: 16 November 2018). The same data are available from RADS.

Table A.1: Type and availability of the satellite data.

Satellite	**S**	**Mode**	**Period**	**Product name**
Jason-2	J2	LRM	16.04.2016 - 20.08.2017	J2-LRMAVISO-1Hz
CryoSat-2	C2	SAR	01.01.2016 - 31.12.2016	C2-SARGOPD-1Hz
CryoSat-2	C2	RDSAR	31.12.2014 - 20.08.2017	C2-RDSARRADS-1Hz
Sentinel-3A	S3A	RDSAR	15.06.2016 - 15.11.2016	S3A-RDSARNTC-1Hz
Sentinel-3A	S3A	SAR	06.04.2016 - 20.08.2017	S3A-SARRADS-1Hz

A.2.2 In situ measurements

In situ observations have great accuracy, but their geographical distribution is highly inhomogeneous, being mainly along coastal regions of industrialized countries. Gaps in measurements and other types of inhomogeneities also occur frequently in in situ observational records (Bidlot et al., 2002). While remote sensing measurements can be seen as a viable alternative to buoy observations, the shortness of the existing time series and the poor temporal resolution pose limitations to their use in wave climate studies (Stopa, 2018).

The results of the wave model and the satellite measurements are evaluated via a comparison with in situ observations at 165 locations. Most of the data are from the Global Telecommunication System (GTS), which were obtained by and are archived at the European Centre for Medium-Range Weather Forecasts (ECMWF) (Bidlot and Holt, 2006); other data were gathered by the ECMWF as part of the Joint Technical Commission for Oceanography and Marine Meteorology (JCOMM) wave forecast verification project (Bidlot et al., 2002). This data set was augmented with in situ wave buoy data provided by the Federal Maritime and Hydrographic Agency (Bundesamt für Seeschifffahrt und Hydrographie, BSH). Figure A.1 shows the locations of these in situ data. Moored wave data buoys are anchored at fixed locations and regularly collect observations from different atmospheric and oceanographic sensors. Moored buoys are usually deployed to serve national forecasting needs, to serve maritime safety needs or to observe regional climate patterns (http://www.jcommops.org/dbcp/platforms/types.html, last access: 16 November 2018). Data are usually collected by either Argos, Iridium, ORBCOMM, GOES or METEOSAT, transmitted in real time and shared on the GTS of the World Meteorological Organisation (WMO). They are generally upgraded or serviced yearly. Over the North Sea and Norwegian Sea, the bulk of the data come from the oil and gas industry, kindly supplied to the meteorological community via the GTS. Generally, the data are from instruments mounted on a platform or a rig. Note, however, that due to a lack of metadata in the GTS record, it is impossible to determine exactly which sensor was used. Wave height, wind speed and wind direction measurements are available every hour. Following a basic visual inspection of the data, the wave height measurements are collocated with the wave model simulations, using the grid point closest to the location of the in situ measurements. The wind measurements, however, have to be adjusted to a height of 10 m above the surface to compare the measurements with the model data. For the wind

speed, the method used by Bidlot et al. (2002) is applied. With the steady-state neutrally stable logarithmic vertical wind profile relation (Equation A.1), the friction velocity ($u*$) is calculated from the wind speed at the measurement height ($U(z)$) with the assumption that the surface roughness (z_0) can be specified by the Charnock relation (Equation A.2) with a constant parameter (α) of 0.018 and g denoting the acceleration due to gravity. κ in Equation A.1 is the von Kármán constant and has a value of 0.41. After obtaining $u*$ via Equation A.1, the wind speed at z=10 m can be calculated using the same equation.

$$U(z) = \frac{u*}{\kappa} ln \left(\frac{z}{z_0} \right) \tag{A.1}$$

$$z_0 = \alpha \frac{u*^2}{g} \tag{A.2}$$

A.2.3 Wave model WAM and meteorological input data used

The spectral wave model WAM Cycle4.6.2 is used here (WAMDI Group, 1988; Komen et al., 1994; Staneva et al., 2017). The model runs as the shallow water version, taking into account depth refraction and wave breaking, and is therefore suitable for coastal applications. The 2-D wave spectra are calculated on a polar grid with 24 directional 15° sectors and 30 frequencies logarithmically spaced from 0.042 to 0.66 Hz. A spherical grid is used for the spatial dimensions, with ∼0.06° resolution in the x-direction (east-west) and ∼0.03° resolution in the y-direction (north-south). The bathymetry and the study area are shown in Figure A.1. The forcing values at the open boundaries of the model domain are calculated via a coarser model simulation for the whole North Atlantic driven by ERA-Interim winds. The coarser model has a spacial resolution of 0.25° in both directions and the same spectral resolution as the finer model described above. These forcing values are used for all model simulations conducted within this study.

To estimate the sensitivity of the wave model to the temporal and spatial resolutions of the meteorological input, different wind input data are used (Table A.2). The ERA-Interim, ERA5 and coastDat-3 reanalyses, as well as the ECMWF operational analysis/forecast and the German Weather Service (Deutscher Wetterdienst, DWD) forecast, are used as meteorological input data to force the wave model. ERA-Interim is a global reanalysis produced by the ECMWF (Dee et al., 2011). The temporal resolution of the output is

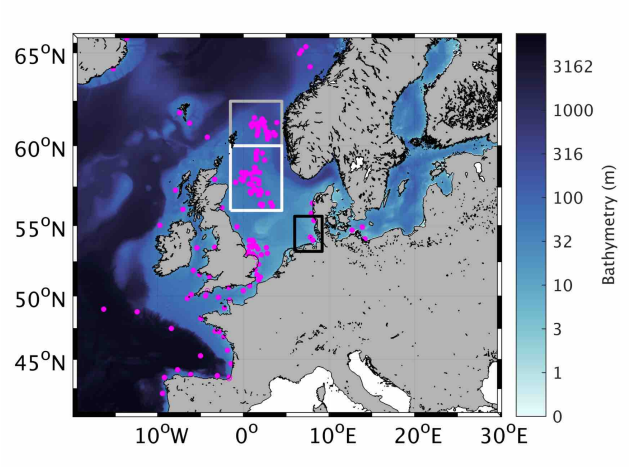

Figure A.1: Bathymetry of the model area and locations of the GTS measurements. The boxes indicate the area of the German Bight (black) and the GTS measurements in the northern part of the North Sea used for the comparisons in Sections A.3.2.1 and A.3.2.3 (grey and white).

6 h, and the grid resolution is approximately 79 km (Berrisford et al., 2009). The data are made available with a spatial resolution of 0.125°. The successor of ERA-Interim is ERA5 (Hersbach and Dee, 2016). The grid size of the model is reduced to 31 km (0.28125°). The output is made available on a 0.25° grid. Furthermore, very important for the wave model simulations is that the temporal resolution of the output ERA5 is increased to an hourly one (ECMWF, 2017b). For both reanalysis, near-surface in situ wind data were part of the data provided to the 4D-Var data assimilation. In addition, the ECMWF 6 h operational analysis is used to force the wave model. When hourly temporal resolution of the output is needed, the first 12 h of the forecast wind fields from 00:00 and 12:00 UTC are taken, with the operational analysis at 00:00 and 12:00 UTC being used to initialize the forecast. The horizontal resolution of the grid is ∼9 km (ECMWF, 2017a) and is available on a 0.125° grid. Also, the short range forecasts by the ECMWF have been influenced by the data assimilation from the 4D-Var system because the assimilation is performed over a 6 or 12 h window with data that can be more recent (by a few hours) than the start time of each forecast. Aside from the wind input provided by the ECMWF, the hindcast coastDat-3 produced by the Helmholtz-Zentrum Geesthacht (HZG) using the Consortium for Small-Scale Modelling Community Land Model (COSMO-CLM) (Rockel et al., 2008; Geyer, 2014) is used to force the wave model. The coastDat-3 output has a temporal resolution of 1 h and uses a rotated grid with a spatial resolution of 0.11° (HZG, 2017), which is about 7 km in the centre of the model domain. Vertically, 40 levels up to an altitude of 22.7 km are used. As boundary conditions for the model domain, ERA-Interim

is used. Here, no data are assimilated into the model. Another data set used to force the wave model is the DWD forecast, which is produced using the ICON_EU numerical model with a grid resolution of 6.5 km and an output that is available every hour (Reinert et al., 2018). For the DWD forecast, the in situ wind data are assimilated into the analysis used to initialize the forecast but for the forecast itself, no data are assimilated. The impact of the temporal resolution of the wind forcing on wave simulations is evaluated in the next section. Therefore, model experiments with 6 h wind forcing from ERA5 and the DWD forecast are conducted, with the wind data being updated every 6 h based on the hourly output.

Table A.2: Horizontal and temporal resolutions of the meteorological input data.

Meteo data set	**Resolution**	
	Horizontal	**Temporal**
ERA-Interim	79 km x 79 km	6 h
ERA5	31 km x 31 km	1 h/6 h
ECMWF operational analysis/forecast	9 km x 9 km	6 h/1 h
coastDat-3	7 km x 7 km	1 h
DWD forecast	6.5 km x 6.5 km	1 h/6 h

A.3 Sensitivity of wave model to wind conditions

In this section, the sensitivity of the wave model to different wind input data and their different spatial and temporal resolutions is analysed by assessing the general performance of the wave model under different wind forcings over the entire study period (from June to November 2016) and the entire model area. The quality of the simulated significant wave height during an extreme event in September 2016 is analysed in detail.

A.3.1 General performance of modelled waves and winds

A.3.1.1 Significant wave height

To study the sensitivity of the wave model simulations to the wind conditions, WAM is forced using eight different wind data sets, as described in Section A.2.3. The general performance of WAM on all different wind data sets is similar and good compared to the in situ observations (Figure A.2). Especially during normal conditions, the signifi-

cant wave heights in the eight model experiments are similar. However, during extreme events, the differences in the simulated significant wave height become more apparent. Particularly, the WAM simulation with coastDat-3 wind forcing overestimates the large significant wave heights (Figure A.2b). Also, the simulation with hourly wind forcing of the DWD forecast tends to slightly overestimate the large significant wave heights (Figure A.2g). On the other hand, WAM forced using ERA-Interim, the ECMWF operational analysis/forecast and ERA5 wind data slightly underestimates the large significant wave heights with respect to the measurements taken at the GTS stations (Figure A.2a, A.2c, A.2d, A.2e and A.2f). Regarding the statistical values, the best wave model performance is seen in the simulation forced using the hourly ECMWF operational analysis/forecast atmospheric data. Using the DWD forecast as wind forcing data led to a smaller bias (Equation A.A6). However, the root mean square error (RMSE) (Equation A.A4) of 29.9 cm and the scatter index (SI) (Equation A.A5) of 0.191 are the lowest, and the correlation coefficient (CORR) (Equation A.A7) of 0.959 is the largest for the model simulations performed using hourly ECMWF operational analysis/forecast wind data. The differences in the statistical values for the results of WAM with the ECMWF operational anaylsis/forecast and ERA5 data are very small and approximately 1 order of magnitude less than the differences in the results produced with the ERA-Interim, coastDat-3 and DWD forecast wind forcings. Therefore, the model simulations with wind forcings of either the ECMWF operational analysis/forecast or ERA5 produce good results that are closer to the GTS measurements than the simulations with the other wind forcings. Notably, the model results corresponding to hourly wind input have better statistical values than the corresponding simulation with 6 h wind input (compare Figure A.2c to Figure A.2d). This once again justifies the crucial importance of using high-frequency wind forcing data (with a minimum of 1 h) for wave simulations, especially for operational purposes.

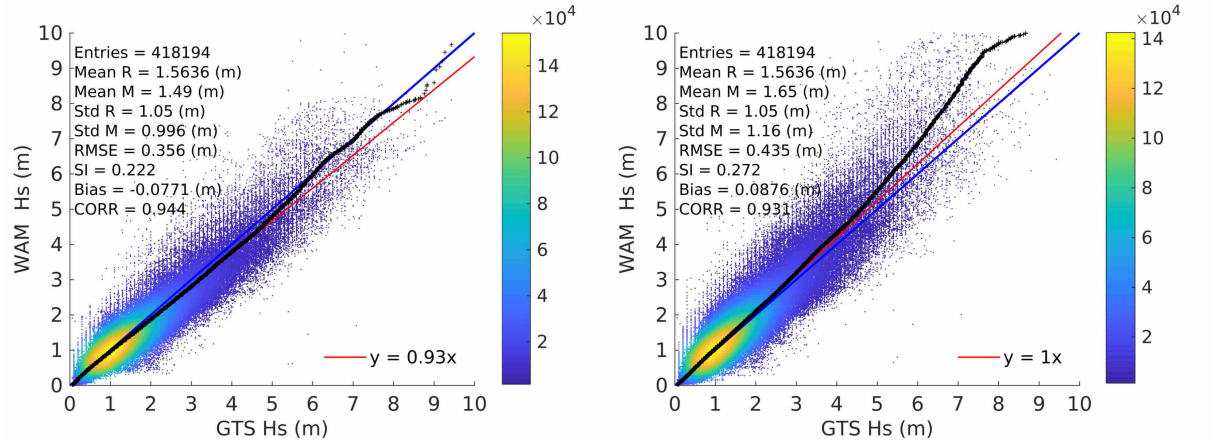

Figure A.2: Continued on the next page.

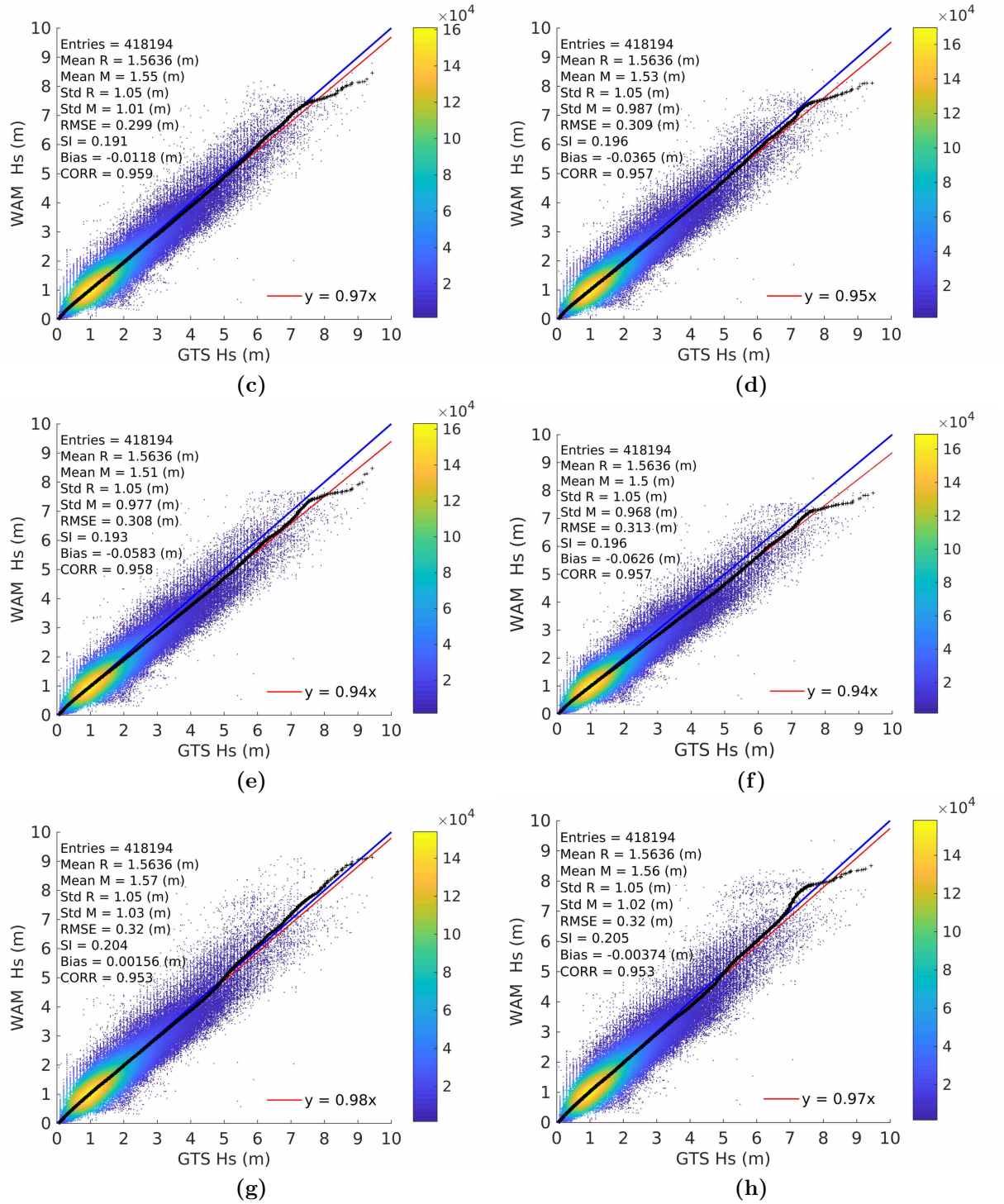

Figure A.2: Q-Q scatter plot for measured (GTS wave data) significant wave height as reference (R) and modelled (WAM) significant wave heights (M) with (a) ERA-Interim, (b) coastDat-3, (c) hourly and (d) 6 h ECMWF operational analysis/forecast; (e) hourly and (f) 6 h ERA5; and (g) hourly and (h) 6 h DWD forecast wind forcings from June to November 2016: Q-Q plot (black crosses), 45° reference line (blue line) and least-squares best-fit line (red line).

A.3.1.2 Wind input data

When comparing the wind speed with the in situ GTS measurements (Figure A.3), the best statistical values are achieved by ERA5 (Figure A.3d), although all performance is fairly similar. For this analysis, the original wind data are used; therefore, only the ERA-Interim data are taken every 6 h, whereas all other wind data are taken every hour. For high wind speeds, a slight underestimation of the modelled wind speed compared to the GTS measurements still occurs. However, this underestimation reflects a large improvement compared to the underestimation found by Cavaleri and Bertotti (2003b). The overprediction of coastDat-3, which can be seen for high significant wave heights, is not evident for the magnitude of the wind in the wind forcing (Figure A.3b). One possible reason for the higher significant wave heights during extreme events might be the wind direction, which has a bias of approximately 12° for the coastDat-3 data (not shown here). Hence, the wind direction is shifted to the right, affecting the fetch length in the North Sea, especially for northwesterly wind directions. For the other wind data, the bias of the wind direction is only approximately 1° to 2°. Since the fetch in coastal areas is limited because of the presence of land, this shift in wind direction can impact the simulated significant wave height.

The general performance of WAM under all different wind forcings is good and fairly similar, especially under normal conditions, where no major differences are found. During extreme events, however, the model simulations tend to be spread out, with the coastDat-3 wind forcing overestimating and the ERA-Interim, ECMWF operational analysis/forecast and ERA5 wind forcings underestimating the large significant wave heights. In the wind data, this cannot be found. The wind is only very slightly underestimated. Particularly, the overestimation of the significant wave height with the coastDat-3 wind forcing cannot be found in the wind data.

A.3.2 Evaluation of the ensemble during an extreme event

As described in the previous section, the modelled significant wave heights tend to spread out during extreme events for different model experiments. Here, a more detailed analysis of data variability during an extreme event is provided. During the study period from June to November 2016, an extreme event occurred on 29 September 2016. The centre of the low pressure system was located along the coast of Norway. Thus, the highest wind speeds

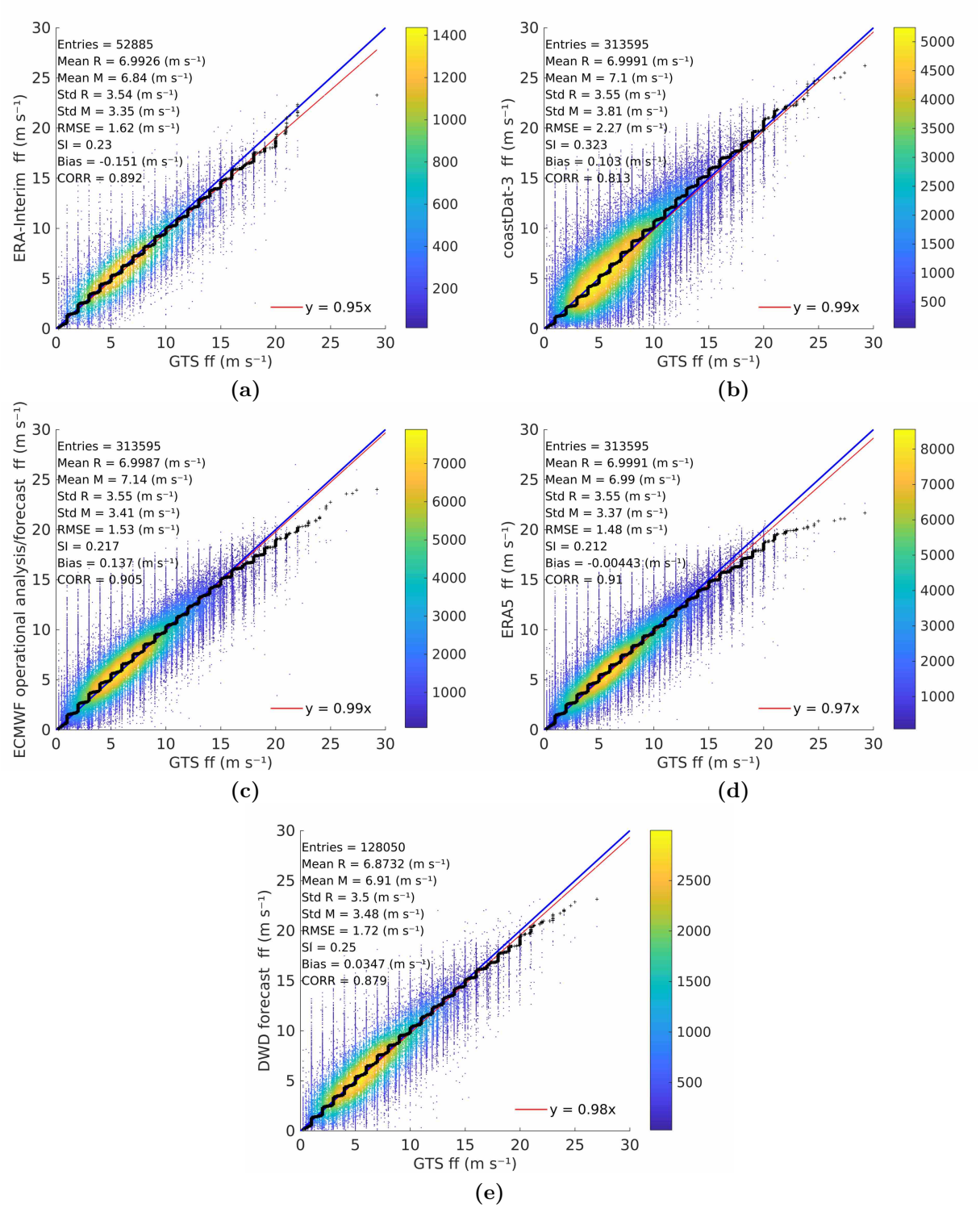

Figure A.3: Q-Q scatter plot for measured (GTS wave buoys) wind speeds as reference (R) and modelled wind speeds (M) from (a) ERA-Interim, (b) coastDat-3, (c) ECMWF operational analysis/forecast, (d) ERA5 and (e) DWD forecast from June to November 2016: Q-Q plot (black crosses), 45° reference line (blue line) and least-squares best-fit line (red line).

occurred in the northern part of the North Sea, and the corresponding highest significant wave heights could be found in the northern part of the North Sea. At 11:00 UTC, the area with maximum significant wave height coincided with the locations of the GTS measurements. Hence, this event is chosen for further analyses.

A.3.2.1 Significant wave height of each ensemble member

In Figure A.4, the wave height estimates of each ensemble member for 29 September 2016, 11:00 UTC, are shown together with the locations of the GTS measurements. The horizontal patterns of the eight model runs for this extreme event are quite different. The largest significant wave height is found in the model simulation with the coastDat-3 wind forcing of more than 9 m (Figure A.4b). The smallest maximum significant wave height is found for the model simulation with the 6 h ECMWF operational analysis wind forcing (Figure A.4d). Notably, the maximum of the model simulation with 6 h wind forcing (Figure A.4a, A.4d, A.4f and A.4h) is shifted further to the east than in the model simulations with hourly wind input (Figure A.4b, A.4c, A.4e and A.4g). Furthermore, in the model simulations with the 6 h wind input, the maximum of the significant wave height is smaller than that with the hourly wind input. This again emphasizes the importance of using higher-time-frequency wind data for wave simulations over the study area.

When comparing the modelled significant wave height with the GTS measurements in the northern part of the North Sea (55° N, 2° W to 62.5° N, 5° E, white and grey box in Figure A.1), none of the simulations are perfectly in line with the measurements, but the model simulation with the hourly ERA5 wind forcing has a bias of only -0.02 m and an SI of 0.144 (Figure A.4e). For the model simulation with the ERA5 wind forcing, the RMSE is 0.56 m, which is smallest compared to that of the other model experiments. The only simulation with a smaller SI is the run with the hourly ECMWF operational analysis/forecast wind forcing, achieving a value of 0.139 (Figure A.4c). The bias, though, is 0.1843 m, which is clearly larger than the bias for the model simulation with the hourly ERA5 wind forcing. The model experiment simulation with the 6 h ERA5 wind forcing has the largest SI (0.193) as well as the largest RMSE (Figure A.4f). Compared to the GTS measurements, the simulations with the ERA-Interim, 6 h ECMWF operational analysis and both ERA5 wind forcings underestimate the significant wave height, with the largest underestimation (0.57 m) being made by the model simulation with the 6 h ERA5 wind forcing (Figure A.4f). The model simulations with the coastDat-3, hourly ECMWF

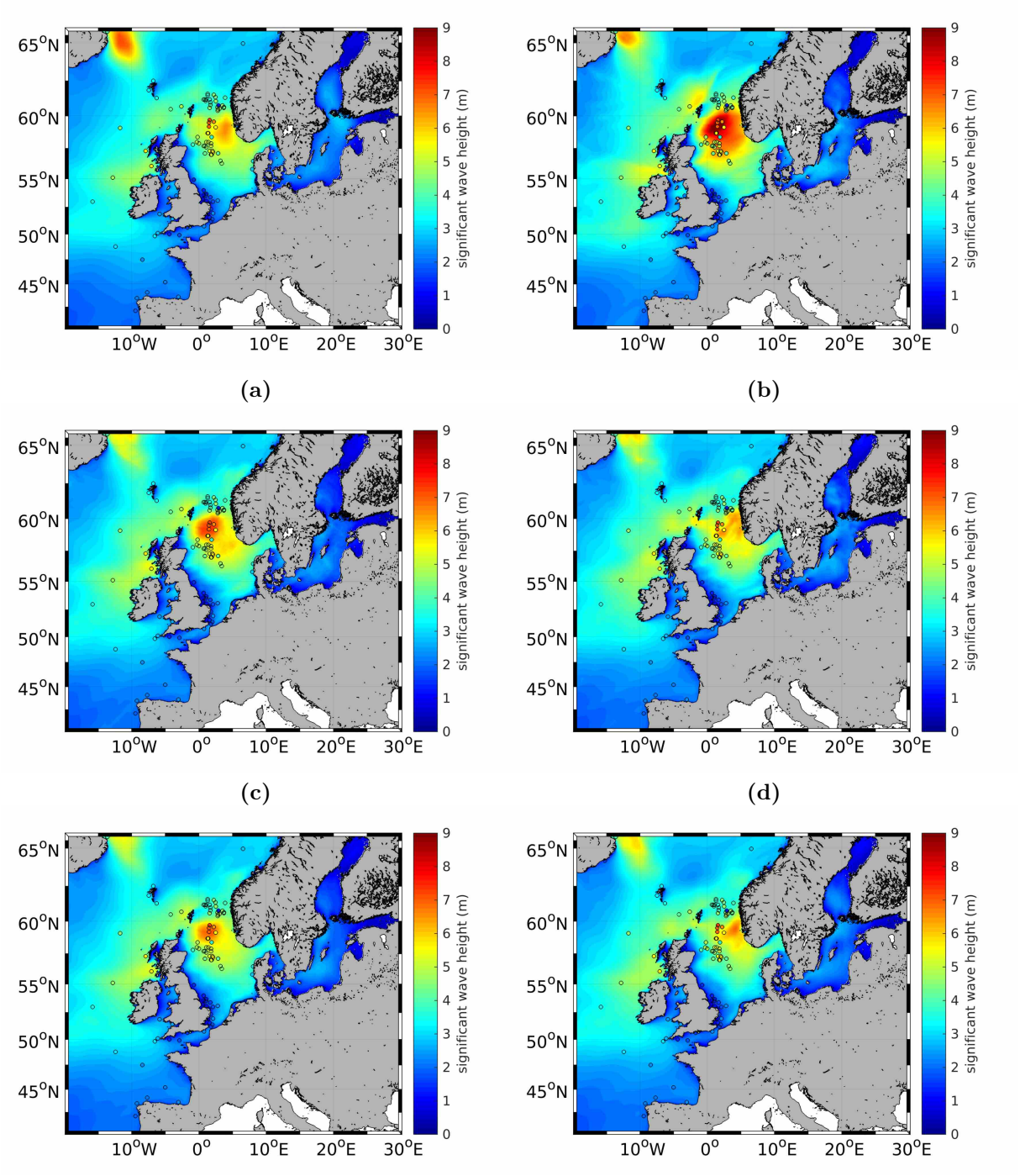

(a) **(b)**

(c) **(d)**

(e) **(f)**

Figure A.4: Continued on the next page.

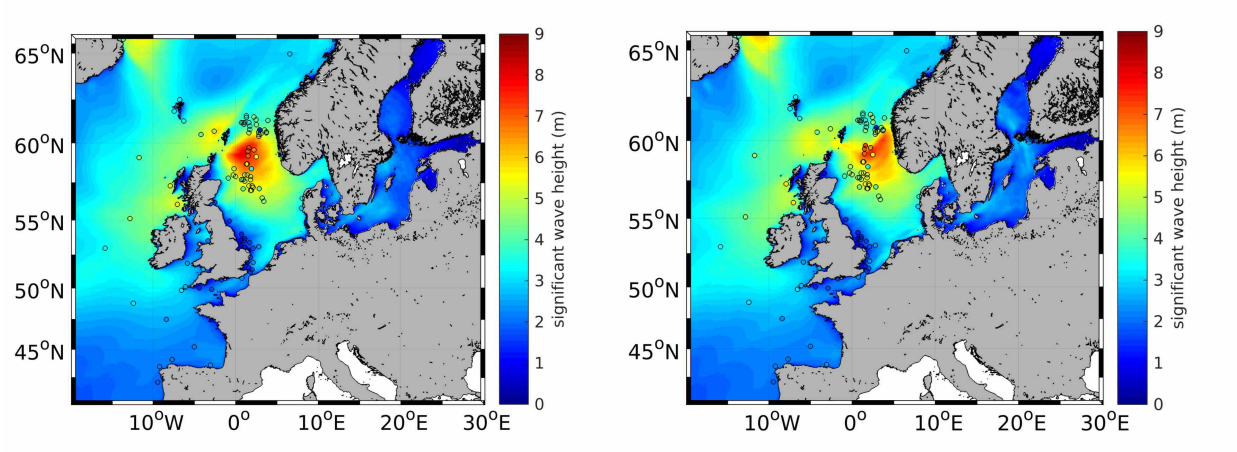

(g) **(h)**

Figure A.4: The significant wave height (m) of the ensemble for 29 September 2016, 11:00 UTC, as well as the GTS measurements for the model simulations with the (a) ERA-Interim, (b) coastDat-3, (c) hourly and (d) 6 h ECMWF operational analysis/forecast; (e) hourly and (f) 6 h ERA5; and (g) hourly and (h) 6 h DWD forecast wind forcings.

operational analysis/forecast and both DWD forecasts all overestimate the significant wave height in the northern part of the North Sea by up to 1.28 m for the case of coastDat-3 wind forcing (Figure A.4b).

A.3.2.2 Empirical orthogonal functions

To study the variance of the significant wave height of the eight ensemble members during the extreme event, an empirical orthogonal function (EOF) analysis of the extreme event on 29 September 2016, 11:00 UTC, is performed. The EOF analysis is carried out as described by Björnsson and Venegas (1997).

Figure A.5a shows the mean of the ensemble depicted in Figure A.4. The associated standard deviation with respect to the mean is given in Figure A.5b. Clearly, the largest difference between the ensemble members is located in the northern part of the North Sea. The ensemble members also differ substantially with respect to the local wave height maximum off the coast of Iceland.

The first EOF of the significant wave height represents 56.16 % of the total variance of the ensemble. The maximum variance is found in the area of the maximum significant wave height in the northern part of the North Sea (Figure A.5a and A.5c). This demonstrates

that the largest difference between the different model simulations is the magnitude of the significant wave height peak. In this case, the model simulation with the coastDat-3 wind forcing has the highest simulated significant wave height maximum (9.5 m), and the model simulation with the 6 h ECMWF operational analysis wind forcing has the lowest simulated significant wave height maximum (6.6 m).

The maximum of the second EOF of the significant wave height, which represents 19.31 % of the total variance, is located in the northern part of the model domain near the coast of Iceland (Figure A.5d), which overlaps the area of the second maximum significant wave height (Figure A.5a). This shows that the model simulations also differ in terms of the magnitude of the maximum significant wave height in the northern part of the model domain. In this area, the significant wave height in the model simulations with the ERA-Interim and coastDat-3 forcings is clearly larger than that in the model simulations with the other wind forcings. These two differences are also found regarding the standard deviation of the ensemble. Combining the first two EOFs explains 75.47 % of the total variance of the ensemble. However, with the EOF, more differences in the model simulations can be found.

The third EOF pattern shows a dipole in the northern part of the North Sea (Figure A.5e). This means that in the model simulations, the exact positions of the significant wave height maximum differ. The orientation of the dipole is in the east-west direction and therefore represents the variation of the peak location in the different model simulations in the zonal direction. In this context, larger differences are especially found between the model simulations with the hourly and 6 h wind forcings, with a peak shift of approximately 290 km. The third EOF represents 9.98 % of the total variance.

The fourth EOF explains 7.71 % of the total variance. This EOF reveals the larger-scale differences in the synoptic situation and, therefore, in the wind fields, which are also reflected in the wave field. In the wind forcing data, the exact location of the centre of the low-pressure system and, therefore, the area of light wind differs, which also leads to different wave heights off the coast of the northern part of Norway. In addition, due to the different strengths of the wind fields in the wind forcings, the significant wave height west of Ireland in the Atlantic as well as off the coast of Norway is larger relative to that east of Great Britain due to the fetch conditions (Figure A.5f).

In order to estimate the difference between the model simulations with hourly and 6-hourly wind forcing during the whole time period, a temporal EOF over the difference

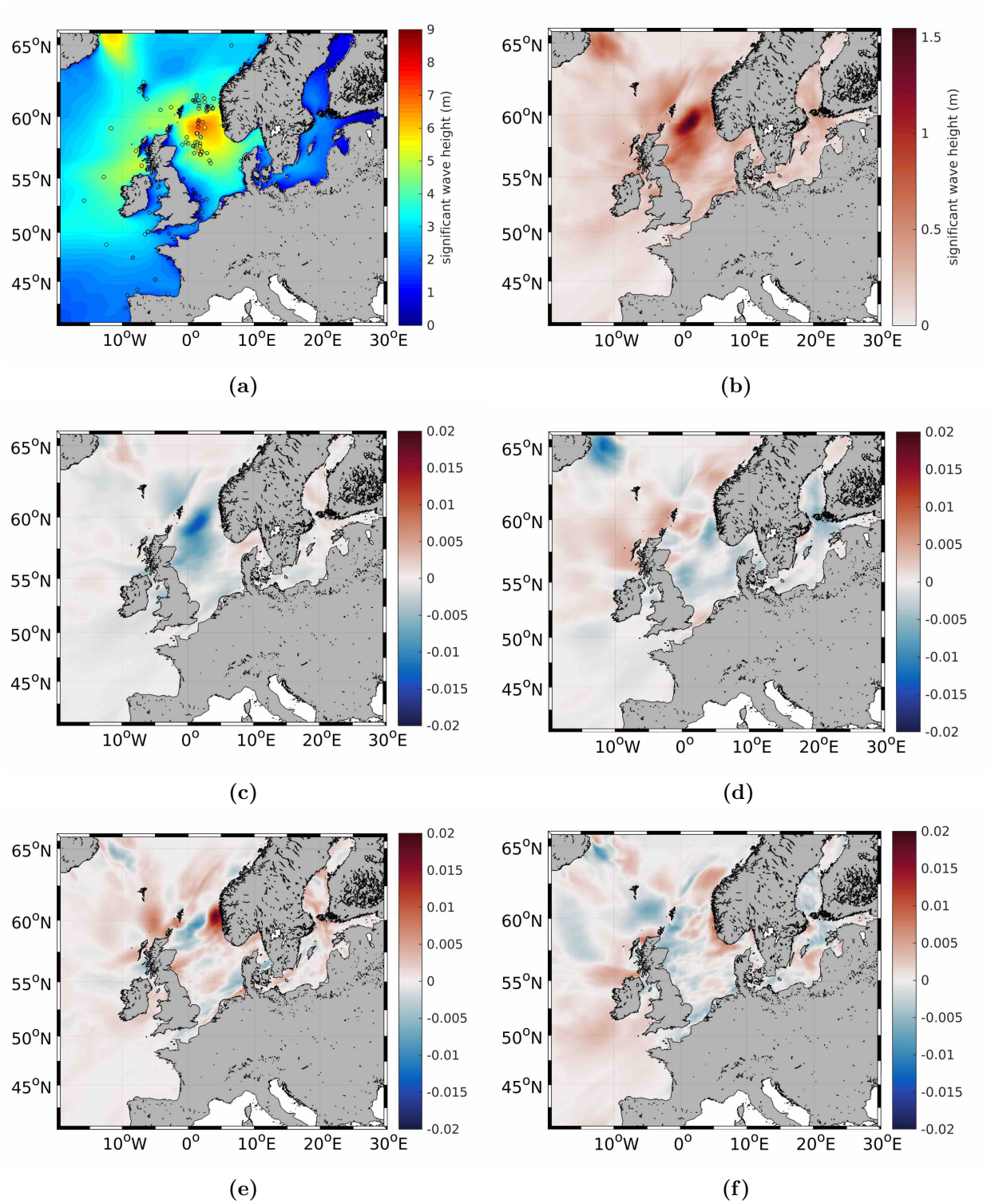

Figure A.5: (a) The mean significant wave height (m) of the ensemble for 29 September 2016, 11:00 UTC, as well as (b) the standard deviation and the EOFs representing (c) 56.16 %, (d) 19.31 %, (e) 9.98 % and (f) 7.71 % of the total variance.

between the model simulations with hourly and 6-hourly ERA5 wind forcings is conducted. Here, no dominant EOF can be found, since the first EOF has an explained variance of 3.13 %. This shows that the model simulations do not substantially differ during normal conditions, which are present most of the time during the whole time period analysed. However, as shown above the model simulations substantially differ during extreme events.

A.3.2.3 Time series of significant wave height, wind speed and wind direction

Further investigation of the magnitude in significant wave height of the respective peak is required, since this is the largest difference between the ensemble members. Time series extracted from the ensemble members are compared to the time series of the GTS measurements (Figure A.6). For this analysis, the mean of the GTS measurements in the northern part of the North Sea (55° N, 2° W to 60° N, 5° E, white box in Figure A.1) at each time step is taken, and the standard deviation is calculated to estimate the variation of the measurements within the considered area. The same is done for the significant wave height of each ensemble member at the locations of the GTS measurements. Here, only the southern part of the in situ measurements in the northern part of the North Sea is taken (only white box in Figure A.1 and not grey and white as in Section A.3.2.1), as the time series of the northern and southern parts differ due to the centre of the low-pressure system passing only over the northern part of the in situ measurements. Therefore, the mean is taken for in situ measurements with similar temporal behaviours.

Figure A.6a depicts the spread of the simulated significant wave heights between the experiments with different wind forcings. During the extreme event, the maximum significant wave height varies between 4.7 m for the simulation with the 6 h ERA5 wind forcing and 6.9 m for the simulation with the coastDat-3 wind forcing. The observed significant wave height from the GTS measurements lies in between the two extremes at 5.3 m. Therefore, coastDat-3 overestimates the significant wave height by approximately 1.6 m. During this extreme event, the overestimation is mainly due to coastDat-3 overestimating the wind speed at that time (Figure A.6b). Also, in coastDat-3, the wind direction is shifted in the clockwise direction by approximately 12° for the majority of time during this extreme event (Figure A.6c). This impact is likely to be small compared to the overestimation of the wind speed, as the fetch is rather limited with respect to the wind directions between south and west-northwest. The wind direction in other areas may affect the significant wave height in this area, though, due to swells travelling into the analysed area. For

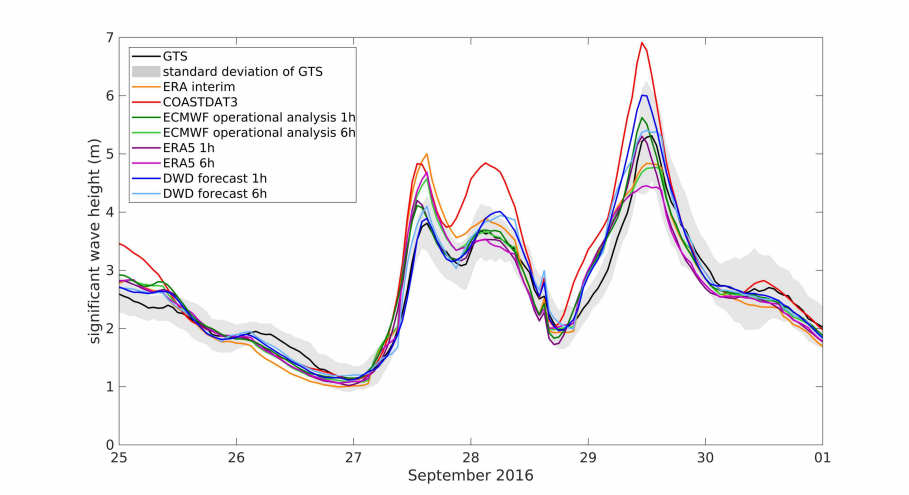

(a)

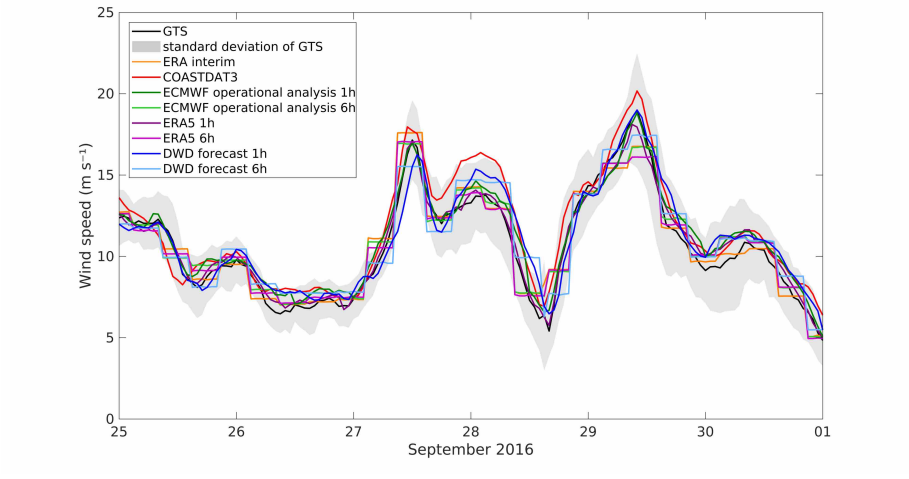

(b)

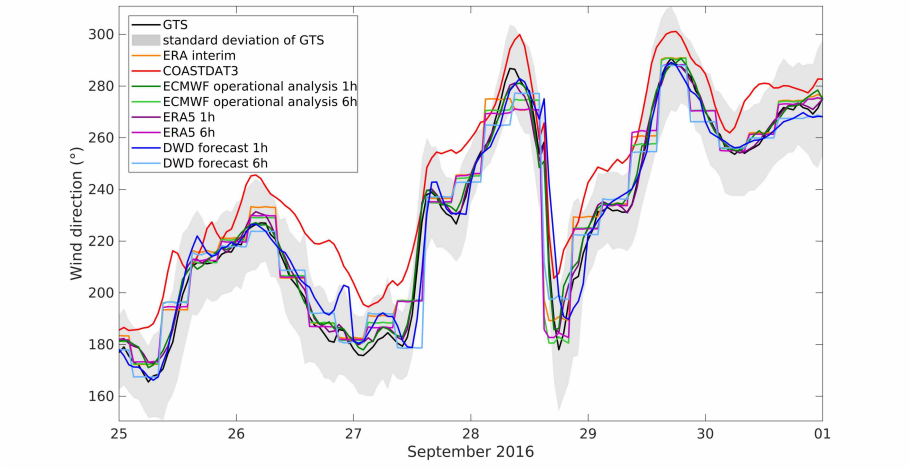

(c)

Figure A.6: Time series of significant wave height (m) as modelled by WAM with different wind forcings and GTS measurements within the northern part of the North Sea (55° N, 2° W to 60° N, 5° E, white box in Figure A.1).

coastDat-3, the area affected by high wind speeds and, therefore, also by high significant wave heights is larger than that for the other wind forcings (Figure A.4b). This might also contribute to the high significant wave height shown in Figure A.6a, as the values averaged in this analysis cover the northern part of the North Sea.

The model experiment with the 6 h ERA5 wind forcing yields the lowest significant wave heights for 29 September 2016 (Figure A.6a). In this simulation, the peak is underestimated by approximately 0.6 m. This underestimation of the significant wave height is also due to the underestimation of the wind speed (Figure A.6b). Since WAM receives the wind data only every 6 h, the wind speed peak is missed in the wind forcing; therefore, the peak in terms of the significant wave height is omitted. This problem can also be seen for the model simulations with the ERA-Interim and 6 h ECMWF operational analysis wind forcing. Although the wind speed of the hourly DWD forecast and ECMWF operational analysis/forecast matches the observed wind speed very well (Figure A.6b), WAM overestimates the peak in the significant wave height (Figure A.6a). This might indicate that WAM needs to be further tuned regarding the significant wave height during extreme events. Another possible reason for this overestimation could be the swells travelling into the area. To clearly conclude either reason, more extreme events need to be analysed. For this extreme event, WAM simulates the maximum significant wave height 2 h earlier, even though the timing of the wind speed peak fits well for the two wind forcings.

The peak in the observed significant wave height is best illustrated by the model simulation with the hourly ERA5 wind forcing (Figure A.6a). The maximum significant wave height differs by only approximately 0.01 m. However, in this run, similar to the simulations with the coastDat-3 data, hourly DWD forecast and hourly ECMWF operational analysis, the simulated peak in the significant wave height occurs 2 h earlier than the observed peak. The model simulation with the 6 h DWD forecast wind forcing slightly overestimates the observed peak (Figure A.6a), although the maximum wind speed is below the maximum observed wind speed (Figure A.6b). The duration of the peak for all model simulations with the 6 h wind forcing in terms of the significant wave height is longer than that for the model simulations with hourly wind forcing. Here, duration of the peak is estimated based on the time at which the significant wave height exceeds 99 % of the peak value. For this significant wave height peak, the duration of the peak for the model simulations with hourly wind forcing is 1 h, whereas for the model simulations with 6 h wind forcing, the duration of the peak is 3-4 h.

A few days earlier, two smaller wave height peaks occur. The first one on 27 September 2016 is overestimated by all of the model experiments, although the corresponding peak in the wind speed is captured well by the model simulations with the hourly ERA5 and ECMWF operational analysis/forecast wind forcings. The 6 h wind forcings capture this peak very well, but due to the wind speed being high 3 h prior to and after the peak, the simulated significant wave height is too high. The model simulation with the hourly DWD forecast wind forcing is the most successful at reproducing the significant wave height peak, although the estimated wind speed is lower than the observed wind speed. The second peak, which occurred on 28 September 2016, is best matched by both model simulations with the ECMWF operational analysis/forecast wind forcing. Both simulations with ERA5 wind forcings slightly underestimate the significant wave height peak. All other simulations overestimate the significant wave height.

During normal conditions both before and after the peaks, the results of all model simulations are very similar.

From the analyses above, it can be concluded that during extreme events, the wave model results are quite sensitive to the wind forcing. Hence, high-quality wind data are needed to improve the ability to predict the sea state.

For our area of interest, a higher temporal resolution of the wind forcing is more important than a higher spatial resolution. Although the spatial resolution of the DWD forecast and coastDat-3 is higher than that for ERA5 and the ECMWF operational analysis, the wave model simulations using the latter two increase the model capabilities. However, clearly better results can be found via model simulations with hourly wind forcing than via those with 6 h wind forcing. This conclusion differs from that of the study on the Black Sea by Van Vledder and Akpınar (2015). Notably, the different spatial resolutions tested are produced by different atmospheric models or model setups, which can also lead to differences. Therefore, the differences cannot only be traced back to the different spatial resolutions. In our study, wave model simulations with the hourly ECMWF operational analysis/forecast as well as the hourly ERA5 wind forcing produce results more similar to the observations made during the extreme event at the end of September 2016 than model simulations with the other wind forcings. Also, the statistical values for the entire study period and over the study area are better for the model simulations forced with hourly ERA5 and ECMWF operational analysis/forecast than for the model simulations with the six other wind data sets. Under normal conditions, the model simulations with all eight wind forcings produce fairly similar results.

A.4 Comparison of satellite data

In this section, the quality of the newly available Sentinel-3A satellite data is assessed and compared to that of older satellite data. The focus in this study is on coastal areas, where the quality of both the satellite and the model data tends to deteriorate. Also, the quality of the Sentinel-3A data is analysed based on the relative orientation of the coastline and satellite heading, varying metocean conditions, and the wind direction relative to the satellite flight direction. In this section, when comparing satellite data with the simulated significant wave height, the model simulation with the ERA5 wind forcing is used, as this simulation, along with that with the ECMWF operational analysis/forecast wind forcing, produced the best results during both extreme events and normal conditions (Section A.3).

A.4.1 General quality of measured significant wave height

To estimate the overall performance of the different satellite products during the entire study period and over the study area, scatter plots of the in situ measurements versus remote sensing measurements are analysed (Figure A.7). For these comparisons, the satellite data are allowed to have a maximum spatial distance of 20 km and a maximum time gap of 30 min with respect to the in situ measurements (Fenoglio-Marc et al., 2015). The general performance of all five satellite products is good and very similar. The correlation between all products varies by only 3 % with values ranging from 94 % to 97 %. The SI is the largest for the CryoSat-2 RDSAR product, being approximately 0.22. For the SAR products of Sentinel-3A and CryoSat-2 as well as for Jason-2, the SI is approximately 0.17. However, the satellites tend to overestimate the significant wave height of in situ measurements, especially Sentinel-3A SAR and both CryoSat-2 products, with biases of up to 26 cm. The smallest bias (only 6 cm) is found for the Jason-2 measurements.

A.4.2 Scatter index along the satellite track

To analyse the spatial distribution of the quality of the satellite data, the SI between the modelled and measured significant wave heights along the satellite tracks within each grid box is calculated for Jason-2 and Sentinel-3A SAR (Figure A.8). Since very few data

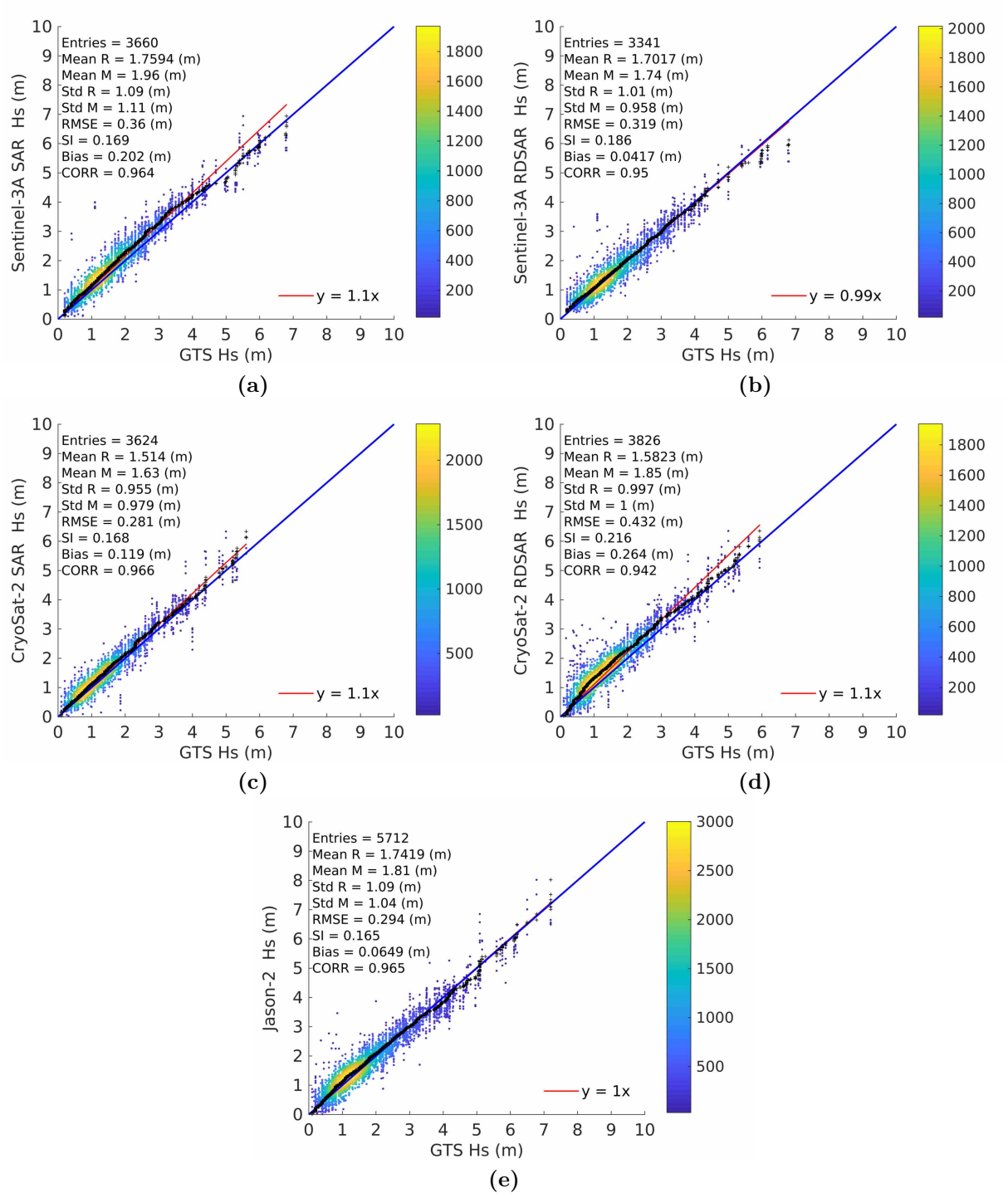

Figure A.7: Q-Q scatter plots of measured significant wave height – in situ GTS (R) vs. remote sensing data (M) of (a) Sentinel-3A SAR, (b) Sentinel-3A RDSAR, (c) CryoSat-2 SAR, (d) CryoSat-2 RDSAR and (e) Jason-2 from June to November 2016: Q-Q plot (black crosses), 45° reference line (blue line) and least-squares best-fit line (red line).

exist within each grid box during the study period, for this analysis, the study period is extended to the end of August 2017 to achieve a more robust SI result. For both satellites, the SI is small over the open ocean and becomes larger closer to the coast. Notably, in coastal areas, the SI for Sentinel-3A SAR is smaller than that for Jason-2. Especially in the northern part of the Baltic Sea, the Danish Straits and along the coastal areas of the southern North Sea, the SI is reduced for Sentinel-3A SAR compared to that for Jason-2. This clearly indicates that Sentinel-3A SAR performs better over coastal areas than Jason-2.

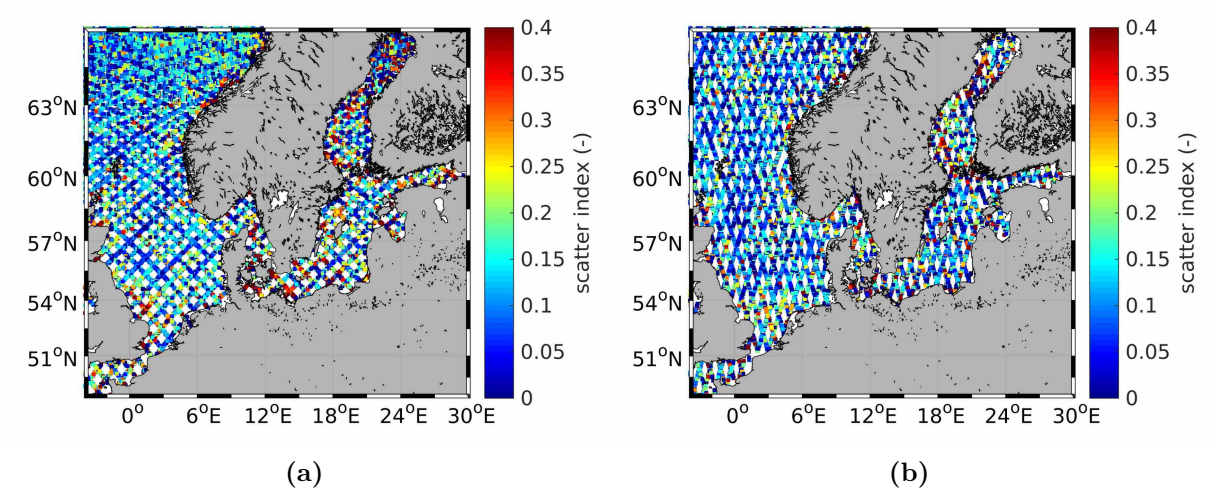

Figure A.8: Scatter index between satellite and modelled significant wave heights along the satellite tracks for (a) Jason-2 and (b) Sentinel-3A SAR.

To quantify this, the statistical values within the first 10 km off the coast are calculated for all three different satellites (Table A.3). In some earlier studies, this area was neglected due to the deteriorating quality of the satellite data (Fenoglio-Marc et al., 2015). For Sentinel-3A, the RMSE is reduced by approximately 0.1 m and the SI is reduced by 0.17 compared to the values for the other two satellites. The bias is reduced by 0.08 m compared to that for Jason-2 and 0.16 m compared to that for CryoSat-2. The correlation for Sentinel-3A is increased by 10 % compared to that for Jason-2 and 5 % compared to that for CryoSat-2. Furthermore, the statistics of Sentinel-3A within the first 10 km are closer to those over the whole study area, which is not the case for the other two satellites (Table A.3; see Figure A.7). This indicates that the quality of the data of Sentinel-3A over coastal areas is closer to that over the open ocean compared to the data quality of CryoSat-2 and Jason-2.

Table A.3: Comparison of the data quality within the first 10 km off the coast for all three satellites.

	Entries	**RMSE (m)**	**SI**	**Bias (m)**	**Correlation**
Jason-2	1076	0.5219	0.4977	0.2461	0.8075
CryoSat-2 RDSAR	1360	0.4860	0.4957	0.3334	0.8548
Sentinel-3A SAR	4192	0.3985	0.3324	0.1682	0.9138

A.4.3 Comparison of data quality for onshore and offshore flights

Due to the way satellite altimeter data are processed, the data quality can deteriorate in the vicinity of coastlines, particularly for passes from land to ocean. To test how much the satellite measurements over the study area are affected by this problem, the flights are separated into onshore and offshore flights, with onshore flights passing from the ocean to the shore and offshore flights passing from the shore to the ocean. For the analysis here, again, only measurements within the first 10 km off the coast are taken. When comparing the statistical values for Sentinel-3A SAR for both onshore and offshore flights, no substantial differences are found, and the statistical values are very similar (Table A.4). Therefore, the transition from land to water does not influence the quality of the satellite observations over our study area.

Table A.4: Comparison of the data quality, organized by onshore and offshore flights, for Sentinel-3A SAR. Only measurements taken within the first 10 km off the coast are used.

	Entries	**RMSE (m)**	**SI**	**Bias (m)**	**Correlation**
onshore	1694	0.3877	0.3244	0.1666	0.9151
offshore	2151	0.3981	0.3219	0.1695	0.9195

A.4.4 Comparison of data quality for long- and short-fetch conditions

Another assessment of the quality of the data measured by the satellites can be carried out by analysing their quality in terms of the fetch conditions. To test this, Sentinel-3A SAR data within the German Bight (53.23° N, 6° E to 55.62° N, 9.2° E, black box in Figure A.1) are split into two groups: that for long-fetch situations and that for short-fetch situations. Long-fetch situations within the German Bight are characterized by northwesterly winds,

while short-fetch conditions occur for southeasterly winds. The analyses demonstrate that the data quality for both situations is very similar (Table A.5). The SI and the correlation have better values for long-fetch situations. The correlation between modelled and measured significant wave heights for long-fetch situations is 98 %, being 4 % larger than that for short-fetch situations. The SI for long-fetch situations is 0.09. The SI for short-fetch situations is approximately twice as large, i.e. 0.19. The RMSE and the bias, though, are better under short-fetch conditions. The RMSE, which is 21.6 cm for short-fetch situations, is approximately 16 cm smaller under short-fetch conditions than under long-fetch conditions. The bias under short-fetch conditions is only 0.7 cm. This is due to the over- and underestimation of the measured data essentially cancelling each other. Under long-fetch conditions, this is not the case, as the bias amounts to 33 cm. When analysing all directions, the statistical values lie between those under long- and short-fetch conditions. Hence, it can be concluded that the satellite measurements do not yield clearly better results for any of the conditions.

Table A.5: Comparison of the data quality, organized by long- and short-fetch situations within the German Bight, for Sentinel-3A SAR.

	Entries	**RMSE (m)**	**SI**	**Bias (m)**	**Correlation**
Long fetch (NW)	143	0.3796	0.0943	0.3299	0.9809
Short fetch (SW)	86	0.2164	0.1854	0.0065	0.9411
All directions	993	0.2763	0.1658	0.1660	0.9524

A.4.5 Comparison of data quality for different relative wind and flight directions

In previous studies, e.g. Chelton and Freilich (2005), a dependency of the data quality on the wind and wave direction relative to the movement of a satellite was found, as satellites move while measuring the wind and wave conditions. Therefore, in this analysis, the measured significant wave height data are separated in terms of the wind direction relative to the satellite track. A slightly smaller RMSE, SI and bias can be found in situations where the wind comes from the direction opposite that of satellite motion (Table A.6). The best correlation, though, is achieved under cross-wind conditions, having a value of 96.7 %. Since the differences between all situations are quite small, i.e. 1.3 % for the correlation, 6 cm for the bias, 0.009 for the SI and 6.6 cm for the RMSE, the difference in the statistical values for all three situations cannot be regarded as substantial. Therefore,

it can be concluded that the quality of the Sentinel-3A measurements does not depend on the wind direction relative to the satellite flight direction.

Table A.6: Comparison of the data quality, organized by the wind direction relative to the satellite flight direction, for Sentinel-3A SAR.

	Entries	**RMSE (m)**	**SI**	**Bias (m)**	**Correlation**
Along wind	7366	0.4396	0.1643	0.2794	0.9645
Opposing wind	6257	0.3757	0.1553	0.2254	0.9544
Cross wind	14940	0.4416	0.1625	0.2886	0.9673

The newly available Sentinel-3A data yield better results for coastal areas compared to the data quality of older satellites such as Jason-2 and CryoSat-2. Especially within the first 10 km from the coast, the statistical values of Sentinel-3A are substantially better then the ones for Jason-2 and CryoSat-2. Also, for Sentinel-3A, no substantial differences are found regardless whether the satellites pass from land to water or vice versa. Furthermore, the quality of the Sentinel-3A data does not differ substantially under either long- or short-fetch conditions within the German Bight. When comparing the data quality based on the wind direction relative to the satellite flight direction, again, no substantial differences can be found. Therefore, the data quality is not affected by relative flight direction and the coastline or the wind direction, as well as different metocean conditions.

A.5 Synergy of satellite data and model ensemble

To enhance the quality of the significant wave height data of the ensemble mean, the satellite measurements and the ensemble of the modelled significant wave height are combined to produce a best-guess wave field using the EOFs. A more detailed explanation of this method, which is based on a maximum a posteriori approach, can be found in Schulz-Stellenfleth and Stanev (2010). The technique is illustrated for the extreme event on 29 September 2016, 11:00 UTC (Figure A.9). When comparing the ensemble mean of the significant wave height (Figure A.5a) to the GTS measurements in the northern part of the North Sea (55° N, 2° W to 62.5° N, 5° E, white and grey box in Figure A.1), where the maximum in significant wave height occurs, both are found to be in very good agreement, with an SI of 0.139, a bias of 0.11 m and an RMSE of 0.56 m. When using the satellite data with the satellite measurement standard deviation as an observation error, and when no bias correction is performed, the statistical values of the best-guess wave field

in terms of the GTS measurements become worse compared to the ensemble mean. To force the analysis to stay close to the already good ensemble mean, a rather high value of 3 m is assumed for the observation errors. The significant wave height reconstructed using the EOFs and the satellite measurements then has an SI of 0.138, a bias of 0.36 m and an RMSE of 0.65 m with respect to the GTS data (not used for the reconstructed significant wave height). As this is still not superior to the ensemble mean, a bias correction of the satellite measurements is carried out. The reconstructed significant wave height (Figure A.9) then has the same SI as that before the bias correction, but the standard deviation of the error is reduced from 0.70 m to 0.65 m, and the bias and RMSE are improved to 0.06 m and 0.54 m, respectively. For this extreme event, the results demonstrate that a bias correction is absolutely necessary before assimilating the satellite data into a wave model. The analyses show that the model can be guided towards the right direction by the satellite data but that the satellite data are still not accurate enough compared to the in situ observations to be used to strictly force the model towards the satellite observations.

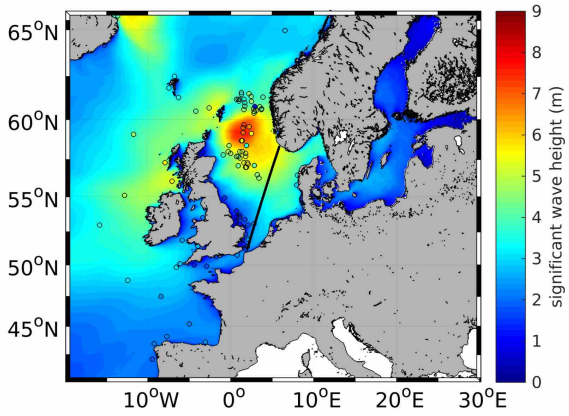

Figure A.9: Best guess of the significant wave height of the ensemble (coloured), together with the Sentinel-3A track (line) and the GTS measurements (dots), on 29 September 2016 at 11:00 UTC.

A.6 Summary and conclusions

In this study, the sensitivity of the wave model to wind forcing data with different spatial and temporal resolutions is tested. The analysis shows that the general performance of WAM for all different wind forcings is good and fairly similar. Especially during normal conditions, no major differences can be found. During extreme events, however, the model

simulations tend to be spread out, with the model simulation with the coastDat-3 and DWD wind forcings tending to overestimate the significant wave height and the model simulations with the ECMWF operational analysis/forecast, ERA-Interim and ERA5 wind forcings tending to underestimate the high significant wave heights. The EOF analysis shows that the largest difference between the model simulations is the magnitude of the peak significant wave height, with a difference of 2.92 m between the smallest and largest significant wave height peaks. Also, the location of the maximum differs, especially between the simulations with hourly and 6 h wind forcings, with approximately 290 km between the peaks. Furthermore, the larger-scale wind conditions change the wave conditions. The analysis of the time series clearly shows that hourly wind forcing data are needed to simulate the significant wave height peak correctly, as a 6 h wind forcing often misses the wind speed peak and, therefore, also the significant wave height peak. The best results of the wind wave model WAM are obtained by the simulations with the ECMWF operational analysis/forecast and ERA5 wind forcings.

Furthermore, the quality of the newly available Sentinel-3A data is assessed in comparison with data from older satellites, i.e. Jason-2 and CryoSat-2. The general performance is good and fairly similar between all satellite products, although all products tend to overestimate the in situ significant wave height measured within the GTS. The analysis of the spatial distributions of the satellite data quality reveals better results for Sentinel-3A over coastal areas than for Jason-2. Especially within the first 10 km off the coast, these differences become apparent. In further analyses, no substantial differences between onshore and offshore satellite flights as well as for different metocean conditions can be found. Also, the satellite data quality does not depend on the wind direction relative to the flight direction. Therefore, Sentinel-3A has a clear advantage over the other satellites when utilized over coasts, exhibiting better skills than those of the other satellites compared to the wave model.

In the last section, where the ensemble and satellite data are merged, the carrying out of bias correction before assimilating satellite data into a wave model is shown to be necessary. Also, for an extreme event, satellite data can be used to guide an ensemble towards a better best-guess wave field, though it cannot be used to strictly force the ensemble towards the satellite data, as they are not accurate enough compared to the in situ measurements.

Data availability

The WAM model code can be found at http://mywave.github.io/WAM/ (WAM, 2018). The satellite data of Jason-2 and CryoSat-2 are available as follows: Jason-2: ftp://avisoftp.cnes.fr (Jason-2, 2018); CryoSat-2 SAR: https://gpod.eo.esa.int (CryoSat-2 SAR, 2018); CryoSat-2 RDSAR: http://rads.tudelft.nl/rads/rads.shtml (CryoSat-2 RDSAR, 2018). The wind forcing data used for this study are available as follows: ERA-Interim: ECMWFdataserver; ERA5: https://cds.climate.copernicus.eu/cdsapp#!/search?type=dataset (ERA5, 2018); coastDat-3: https://cera-www.dkrz.de/WDCC/ui/cerasearch/entry?acronym=coastDat-3_COSMO-CLM_ERAi (HZG, 2017).

Appendix AA: Calculation of statistical values

Mean value:

$$\overline{R} = \frac{1}{N} \sum_{i=1}^{N} R_i. \tag{A.A1}$$

Errors:

$$E = M - R. \tag{A.A2}$$

Standard deviation of the errors:

$$s_E = \sqrt{\frac{1}{N-1} \sum_{i=1}^{N} \left(E_i - \overline{E}\right)^2}. \tag{A.A3}$$

Root mean square error:

$$RMSE = \sqrt{\frac{1}{N} \sum_{i=1}^{N} \left(M_i - R_i\right)^2}. \tag{A.A4}$$

Scatter index:

$$SI = \frac{s_E}{\overline{R}}. \tag{A.A5}$$

Bias:

$$bias = \overline{E}. \tag{A.A6}$$

Correlation:

$$CORR = \frac{1}{N-1} \sum_{i=1}^{N} \left(\frac{M_i - \overline{M}}{s_M} \right) \left(\frac{R_i - \overline{R}}{s_R} \right). \tag{A.A7}$$

Competing interests

The authors declare that they have no conflict of interest.

Special issue statement

This article is part of the special issue "Coastal modelling and uncertainties based on CMEMS products". It is not associated with a conference.

Acknowledgements

This publication has received funding from the European Union's H2020 Programme for Research, Technological Development and Demonstration under grant agreement no. H2020-EO-2016-730030-CEASELESS. Luciana Fenoglio acknowledge the support of the European Space Agency (ESA) within the project SAR Altimetry Coastal & Open Ocean Performance (SCOOP). The authors would like to thank Beate Geyer for providing coastDat-3 wind data.

B The Impact of the Two-Way Coupling between Wind Wave and Atmospheric Models on the Lower Atmosphere over the North Sea

Wiese, A., Stanev, E., Koch, W., Behrens, A., Geyer, B., & Staneva, J. (2019). The Impact of the Two-Way Coupling between Wind Wave and Atmospheric Models on the Lower Atmosphere over the North Sea. Atmosphere, 10(7), 386, https://doi.org/10.3390/atmos10070386.

The publication has been formatted according to the format of this dissertation. The references have been merged with the other references of the thesis to one reference list for the whole dissertation. Changes in the text and the figure caption both on page 79 compared to the original publication are marked in italic.

The contribution of Anne Wiese and the other authors to this paper is as follows:
Anne Wiese performed the analyses and wrote the paper. Anne Wiese, Prof. Dr. Emil Stanev and Dr. Joanna Staneva conceived the work. Wolfgang Koch conducted the model simulations. Dr. Arno Behrens provided assistance with the wave model WAM. Dr. Beate Geyer provided assistance with the atmospheric model COSMO-CLM. All authors reviewed the manuscript. The manuscript was checked for English language.

The Impact of the Two-Way Coupling between Wind Wave and Atmospheric Models on the Lower Atmosphere over the North Sea

Anne Wiese, Emil Stanev, Wolfgang Koch, Arno Behrens, Beate Geyer and Joanna Staneva

Institute of Coastal Research, Helmholtz-Zentrum Geesthacht, 21502 Geesthacht, Germany

(Received: 24 May 2019; Accepted: 9 July 2019; Published: 11 July 2019)

The effects of coupling between the atmospheric model of the Consortium for Small-Scale Modelling-Climate Limited-area Modelling (CCLM) and the wind wave model (WAM) on the lower atmosphere within the North Sea area are studied. Due to the two-way coupling between the models, the influences of wind waves and the atmosphere on each other can be determined. This two-way coupling between these models is enabled through the introduction of wave-induced drag into CCLM and updated winds into WAM. As a result of wave-induced drag, different atmospheric parameters are either directly or indirectly influenced by the wave conditions. The largest differences between the coupled and reference model simulation are found during storm events as well as in areas of steep gradients in the mean sea level pressure, wind speed or temperature. In the two-way coupled simulation, the position and strength of these gradients vary, compared to the reference simulation, leading to differences that spread throughout the entire planetary boundary layer and outside the coupled model area, thereby influencing the atmosphere over land and ocean, although not coupled to the wave model. Ultimately, the results of both model simulations are assessed against in situ and satellite measurements, with a better general performance of the two-way coupled simulation with respect to the observations.

B.1 Introduction

Wind induced waves at the surface of the ocean are well known to affect the overlying atmosphere. In 1989, Janssen (1989) investigated the wave-induced stress and airflow drag over sea waves. Three years later, Janssen reported experimental evidence of the effects of surface waves on the airflow (Janssen, 1992). Since then, coupled atmosphere-wave models have been utilised in many studies to analyse the effects of wind waves on the atmosphere and vice versa. These studies addressed mainly the effects of coupling on idealised cyclones (Doyle, 1995; Lionello et al., 1998), hurricanes (Bao et al., 2000), wind waves (Wahle et al., 2017), atmospheric (Janssen et al., 2002) and wave forecasts (Wahle et al., 2017) and climate (Janssen et al., 2002).

The flow of air within the free atmosphere is determined by the balance between the pressure gradient and the Coriolis force. Closer to the surface, friction also plays a major role in the momentum balance. This friction leads to a cross-isobar flow. As a result, low-pressure systems fill more quickly (Janssen, 2004). Over the ocean, this friction is dependent on the sea state. In particular, young sea states are associated with rough airflow and high friction (Donelan et al., 1993; Janssen, 2004). Hence, the largest changes in the surface roughness and friction velocity occur in areas of young sea states (Katsafados et al., 2016). Consequently, this increased friction leads to more direct airflow into the centre of the low-pressure system, and thus the system fills up more quickly. On the other hand, enhanced friction leads to enhanced heat fluxes, which tend to deepen low-pressure systems (Janssen, 2004). Therefore, the effects wind waves have on the evolution of a low-pressure system are determined by the dominant processes through which the system develops. Momentum fluxes play a major role in the development of extratropical lows. Where an atmospheric model is coupled to a wave model, the momentum flux affected by wind waves causes less deepening of the lows during the model simulation (Doyle, 1995; Lionello et al., 1998; Janssen et al., 2002; Janssen, 2004). For hurricanes, however, the temperature difference between the ocean and the atmosphere can become quite large. In this case, the heat flux can also play a major role in the development of the low. Bao et al. (2000) demonstrated that a hurricane can become deeper due to the coupling between the atmospheric model and the wave model. Furthermore, feedbacks between wind waves and the atmosphere create nonlinear interactions within the dynamic structure of a storm or cyclone (Katsafados et al., 2016). Katsafados et al. (2016) also found that the planetary boundary layer (PBL) is

thicker and more turbulent due to atmosphere-wave coupling. The impact of coupling on a single depression is also dependent on the model resolution. If the resolution is too coarse to resolve the processes involved, the effect caused by coupling the wave model to the atmospheric model vanishes (Janssen et al., 2002; Janssen, 2004; Wu et al., 2017). Wu et al. (2017) also analysed the effects of different roughness length parametrisations on the predictability of a storm, but none of the tested parametrisations could reproduce the results of the coupled model simulation.

The two-way coupling of wave and atmospheric models was introduced into the operational forecasts of the European Centre for Medium-Range Weather Forecasts (ECMWF) in 1998. This led to substantial improvements in various surface parameters, such as the 10 m wind speed and the significant wave height, and had modest impacts on the 1000 hPa and 500 hPa geopotential heights (Janssen et al., 2002; Janssen, 2004).

This two-way coupling also affects the climate across the troposphere. Janssen and Viterbo (1996) and Janssen et al. (2002) found significant impacts in the storm track area in both hemispheres, although the effect is more pronounced in the Southern Hemisphere. This discrepancy was attributed to the larger water surfaces surrounding the Antarctic continent and the less precise forecasts for the Southern Ocean due to the lack of observational data there (Janssen and Viterbo, 1996). These findings show that the effects of local wind waves produce teleconnections in the large-scale atmospheric system. Furthermore, the wind wave climate itself is affected by the coupling of wave and atmospheric models (Babanin et al., 2012). Weisse et al. (2000) and Weisse and Schneggenburger (2002) investigated the sensitivity of a regional atmospheric model to sea-state dependent roughness regarding the mean sea level pressure in the region of the North Atlantic Ocean. They, on the other hand, found no significant impact on the mean sea level pressure, when introducing wave-depended roughness to the atmospheric model.

The above mentioned studies focused on the impacts of the coupling between atmospheric and wave models close to the surface, whereas they paid little attention to differences that occur above the surface layer. Therefore, the present study further investigates under which conditions the coupling lead to differences in the atmospheric parameters within and at the height of the atmospheric boundary layer. The models and measurement data used for the analysis are described in the next section (Section B.2). This is followed by an analysis of the general differences between the reference simulation and the coupled model simulation regarding the roughness length, 10 m wind speed and significant wave

height (Section B.3). In Section B.4, an event with large changes close to the boundary layer height is identified and analysed in more detail. This is followed by a discussion of the results (Section B.5). Finally, a summary and the conclusions of this analyses are given in Section B.6.

B.2 Numerical Models, Model Set-Up and Measurement Data

B.2.1 Numerical Models

B.2.1.1 Atmospheric Model CCLM

This study employs the atmospheric model known as Consortium for Small-Scale Modelling (COSMO)-Climate Limited-area Modelling (CLM) Community (CCLM) version 4.8 (Rockel et al., 2008), a non-hydrostatic regional climate model developed and applied by the CLM Community (CLM-Community, 2019) on the basis of the numerical weather prediction model COSMO (COSMO, 2019). CCLM is based on the primitive equations that describe compressible flow in a moist atmosphere and uses the primitive momentum equations. The continuity equation is replaced by a prognostic equation for pressure perturbations from a reference state, which represents a time-independent dry atmosphere at rest. This atmosphere is prescribed as being horizontally homogeneous, vertically stratified and in hydrostatic balance.

The model domain of CCLM covers Northern Europe with a spatial resolution of 0.1°. In the vertical direction, 40 grid levels are used. The initial and boundary conditions are taken from 6-hourly ECMWF Re-analysis (ERA)-Interim analysis data (Berrisford et al., 2009; Dee et al., 2011).

B.2.1.2 Wave Model WAM

Here, the wind wave model (WAM) Cycle 4.5.4 is used (WAMDI Group, 1988; Komen et al., 1994; Wahle et al., 2017). In this version, depth refraction and wave breaking are taken into account. Consequently, this model set-up is suitable for shallow water applications. The directional resolution of the model is 15°. The model uses 30 frequencies

logarithmically spaced from 0.04 to 0.66 Hz. The model domain covers the North Sea and has a spatial resolution of approximately 5 km (Figure B.1). The values at the open boundaries of the model domain are taken from the European WAM (EWAM), the regional model of the Deutscher Wetterdienst (DWD).

B.2.1.3 Coupling between CCLM and WAM

The OASIS3-MCT version 2.0 coupler is used to couple the CCLM and WAM (Wahle et al., 2017). The fields that are exchanged in this study are the wind components as well as the roughness length. In the one-way coupled model simulation (hereafter called the reference model simulation), WAM receives the wind components from CCLM, and CCLM uses the Charnock parametrisation to calculate the roughness length over water surfaces (COSMO, 2019). In the two-way coupled model simulation (hereafter known as the coupled model simulation), WAM still receives the wind components from CCLM and additionally sends the roughness length calculated directly from the wind wave field back to CCLM. In order to determine the effects of the coupling of the wind wave model and the atmospheric model, the results of the two model simulations are compared. This is illustrated through the differences between the model simulations (reference and coupled) close to the surface but also in higher parts of the atmosphere.

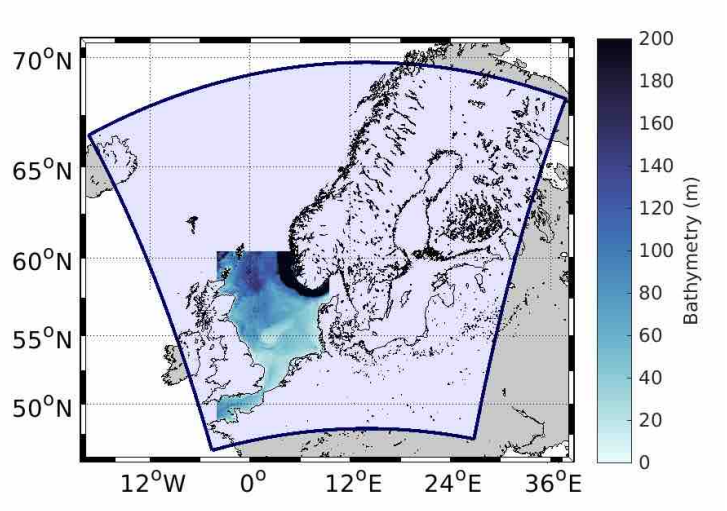

Figure B.1: Bathymetry of the wave model WAM (shaded) and area of the atmospheric model CCLM (box).

B.2.2 Measurement Data

To determine whether the two-way coupling improves the model results, the simulations are compared with observational data. For this purpose, in situ measurements within the North Sea from the Global Telecommunication System (GTS) and satellite measurements from Sentinel-3A are chosen. The two data sets are described in the following sections.

B.2.2.1 In Situ Measurements

Most of the in situ measurement data of the significant wave height and wind speed used in this study are from the GTS. The data are obtained from and archived at the ECMWF (Bidlot and Holt, 2006). Alternatively, the data are gathered by the ECMWF as part of the Joint Technical Commission for Oceanography and Marine Meteorology (JCOMM) wave forecast verification project (Bidlot et al., 2002). The data are recorded either by moored wave data buoys, anchored at fixed locations to serve national forecasting needs, or by instruments mounted on platforms or rigs of the oil and gas industry. These data have been kindly provided to the meteorological community. As in Wiese et al. (2018), the wave height measurements are collocated with the model data using the closest grid point to the location of the in situ measurement and the wind speed measurements are interpolated to a height of 10 m above the surface and then collocated with the model using the closest grid point to the location of the observation. The locations of the in situ measurements are depicted in Figure B.2.

B.2.2.2 Satellite Data

The significant wave height and wind speed observations from the Sentinel-3A satellite are used to compare the model results with satellite measurements. Sentinel-3A, which was launched in February 2016, is the first satellite that operates entirely in synthetic aperture radar (SAR) mode (ESA, 2015). The revisit time of Sentinel-3A is 27 days. The data acquired by Sentinel-3A are retrieved from 1D profiles along the ground track of the satellite. The footprint size is between 1.5 and 10 km depending on the sea state across the track. The along-track resolution of Sentinel-3A is approximately 7 km for 1 Hz measurements. Figure B.2 shows the locations of the satellite measurements. Because

the quality of the data from Sentinel-3A is better than that of data from other satellites, especially close to the coast, the data from this satellite are chosen for comparisons with the model results (Wiese et al., 2018). The satellite data are collocated according to the nearest model grid point and the closest time with a maximum time lag of 30 min.

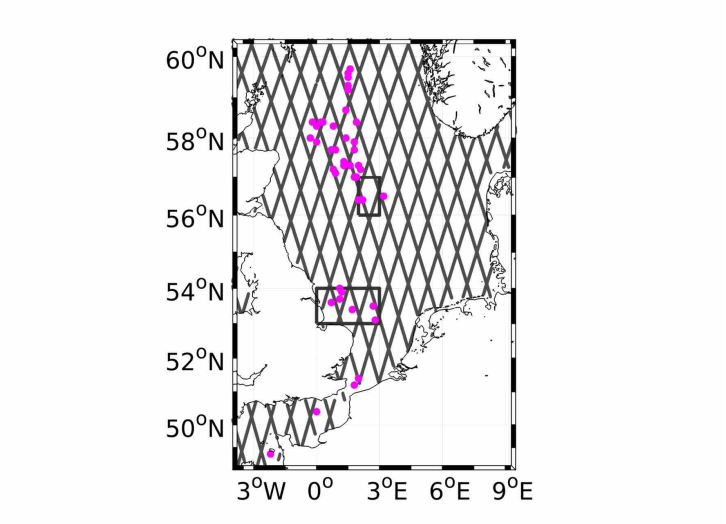

Figure B.2: Locations of the in situ measurements (magenta dots) and the satellite measurements (grey tracks). The southerly box indicates the area of the in situ measurements used for the comparisons in Section B.3. The northerly box indicated the area of the Hovmöller diagrams in Section B.4.1.

B.3 General Impacts of the Wave-Atmosphere Coupling

In the coupled model simulation, the roughness length calculated by WAM is passed to CCLM to ensure a roughness length over the ocean that is more precise than the parametrised roughness length used within the reference model simulation. Figure B.3 shows the dependency of the roughness length on the wind speed (Figure B.3a) and the friction velocity (Figure B.3b). Clearly, the roughness length in the reference model simulation is underestimated compared with that in the coupled model simulation. In particular, at wind speeds exceeding 10 m s^{-1}, the roughness length of the wave model becomes substantially larger than the parametrised roughness length. Additionally, the least-squares best-fit lines through the roughness lengths of the coupled model simulation show that the parametrised roughness length in CCLM is too small, especially at high wind speeds. The colour of the roughness lengths of WAM in Figure B.3 indicates the corresponding wave age. These results illustrate that a young sea state creates a

large surface roughness, as was also found by Janssen et al. (2002); Janssen (2004) and Katsafados et al. (2016). For wind speeds below approximately 15 m s^{-1}, the largest roughness lengths are due to swell with large wave ages. However, this effect cannot be captured by parametrisations in the stand-alone atmospheric model (Cavaleri et al., 2012a). The roughness length for areas covered by sea ice is set to 0.001 by CCLM, as shown by the black lines in Figure B.3.

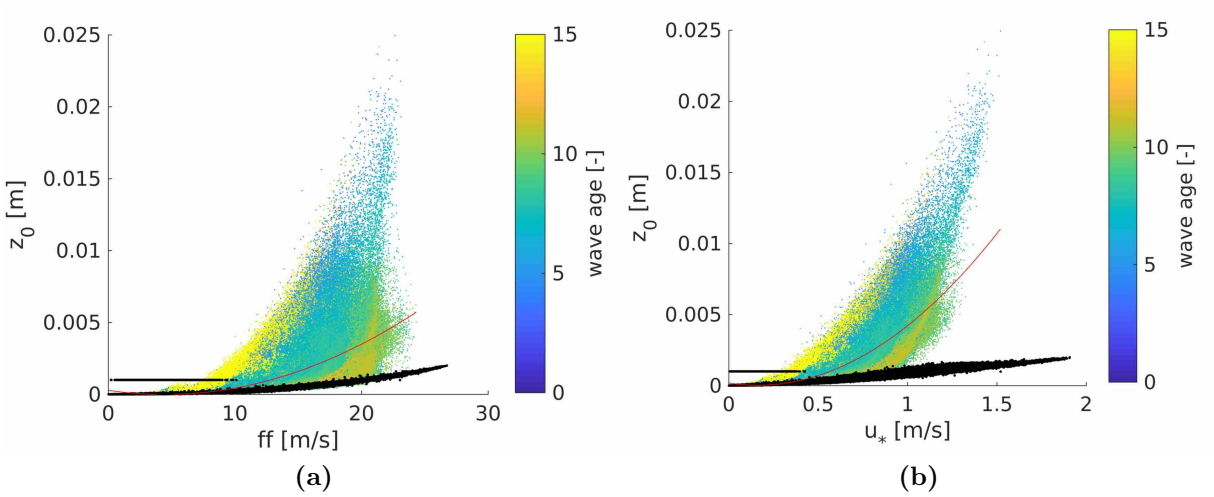

Figure B.3: Scatter plots of the (a) wind speed (ff) and (b) friction velocity (u_*) against the roughness length (z_0) for the reference model simulation (black dots) and the coupled model simulation (coloured dots). The red lines indicate the least-squares best-fit lines of the roughness lengths calculated by WAM. Values of 0.001 represent the roughness length of sea ice.

The wind speed and significant wave height are the most obvious parameters influenced by the coupling between the atmospheric model and wind wave model, since the wind is exchanged between the models and directly influences the significant wave height and, the other way round, the wave height directly influences the roughness length given back to the atmospheric model. Hence, the general influences of the two-way coupling on the wind speed and significant wave height are investigated. In Figure B.4, the wind speeds modelled with both the reference model simulation (Figure B.4a) and the coupled model simulation (Figure B.4b) are compared with the wind speeds measured by the Sentinel-3A satellite. The reference model overestimates the wind speeds exceeding approximately 7 m s^{-1} (Figure B.4a). Below 7 m s^{-1}, CCLM underestimates the Sentinel-3A wind speeds. In the coupled model simulation, the overestimation of wind speed above approximately 7 m s^{-1} is reduced compared to the reference simulation. Furthermore, for

high wind speeds (exceeding 15 m s^{-1}), the overestimation is eliminated entirely (Figure B.4b). However, at wind speeds below 7 m s^{-1}, the coupled model simulation tends to produce a slightly larger underestimation than the reference model simulation. According to the statistical values calculated between the measured and modelled wind speeds, the results of the coupled model simulations are closer to the measurements than the results of the reference model simulation (Table B.1).

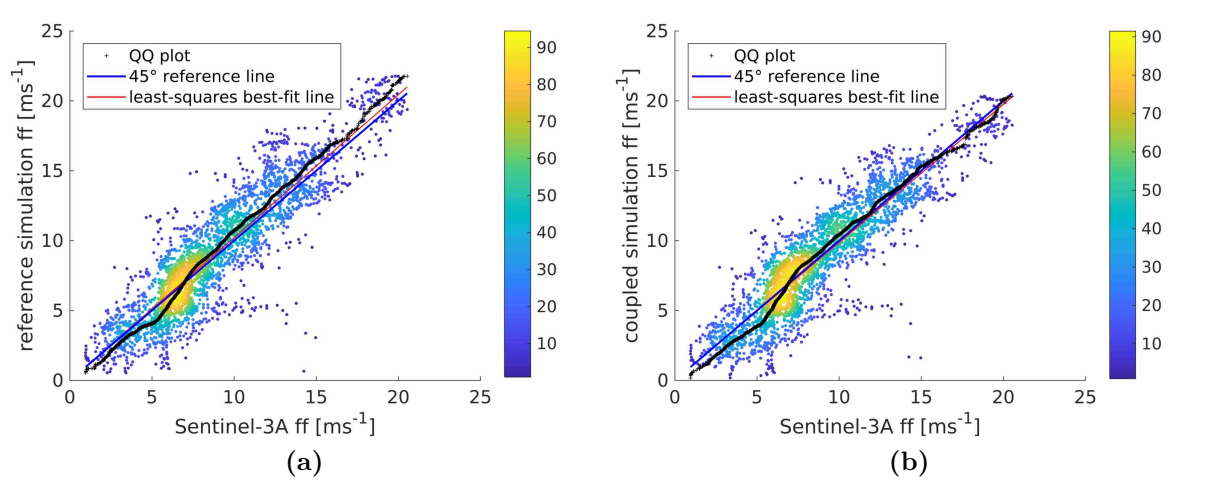

Figure B.4: Q-Q scatter plots for the measured (Sentinel-3A) wind speeds and modelled wind speeds with the (a) reference and (b) coupled model simulations for January 2017. The Q-Q plot is shown as black crosses, the 45° reference line is denoted by the blue line, and the least-squares best-fit line is the red line.

In the coupled model simulation, the significant wave height is influenced by changes in the wind speed, resulting in nonlinear feedback in both the atmospheric model and the wave model. The modelled significant wave heights below 4 m in both model simulations are in good agreement with the satellite measurements (Figure B.5). In contrast, significant wave heights between 4 m and 7 m are overestimated by the reference model simulation, whereas larger significant wave heights are represented quite well by the reference model (Figure B.5a). In the coupled model simulation, the significant wave height is depicted very well until the significant wave height reaches 6 m, while larger significant wave heights tend to be underestimated by the coupled model simulation relative to the satellite measurements during January 2017 (Figure B.5b). Regarding the root mean square error, the scatter index and the correlation, the statistical parameters are improved for the coupled model simulation compared with those for the reference model simulation (Table B.1).

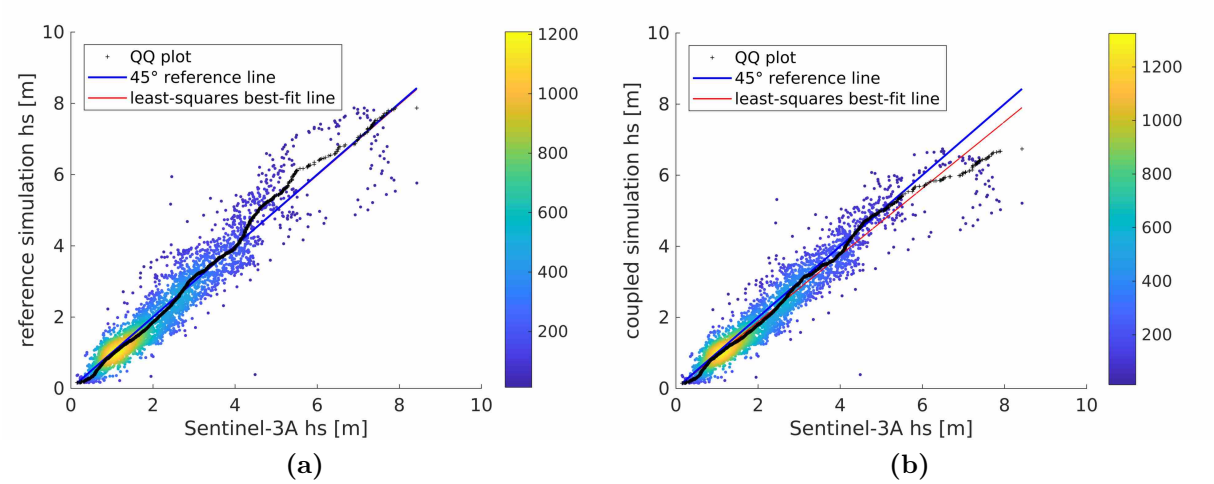

Figure B.5: Q-Q scatter plots for the measured (Sentinel-3A) significant wave heights and modelled significant wave heights with the (a) reference and (b) coupled model simulations for January 2017. The Q-Q plot is shown as black crosses, the 45° reference line is denoted by the blue line, and the least-squares best-fit line is the red line.

Table B.1: Statistical values of the comparison between the wind speeds (ff) and significant wave heights (hs) measured by Sentinel-3A and the modelled wind speeds and significant wave heights.

	ff		**hs**	
	Reference	**Coupled**	**Reference**	**Coupled**
Entries	3286		3284	
Mean (Sentinel-3A)	8.85 m s^{-1}		2.28 m	
Mean (Model)	9.05 m s^{-1}	8.77 m s^{-1}	2.25 m	2.14 m
Standard Deviation (Sentinel-3A)	3.82 m s^{-1}		1.38 m	
Standard Deviation (Model)	4.35 m s^{-1}	4.13 m s^{-1}	1.49 m	1.35 m
Root Mean Square Error	1.94 m s^{-1}	1.81 m s^{-1}	0.49 m	0.45 m
Scatter Index	0.218	0.204	0.213	0.188
Bias	0.199 m s^{-1}	−0.082 m s^{-1}	−0.029 m	−0.136 m
Correlation	0.896	0.899	0.945	0.951

The largest differences both in the wind speed and in the significant wave height occur during extreme events with large wind speeds and significant wave heights (Figures B.4 and B.5). Therefore, the model results are compared with GTS measurements recorded

during one extreme event in January 2017 by buoys located off the coast of England (53° N, 0° E to 54° N, 3° E). For this comparison, the measurements acquired at the same time from the seven buoys within that small area (see the black box in Figure B.2) are averaged. The results of the models collocated with the buoys are then averaged as well. As shown in Figure B.6, the results of the coupled model simulation are closer to the observations than are the results of the reference model simulation. In particular, under the high wind speeds and large significant wave heights observed on the 11th/12th and 13th/14th of January 2017, the coupled model performs substantially better than the reference model. During these periods, the results of the reference model simulation are outside the standard deviation range of the GTS measurements, while the results of the coupled model simulation are well within the range of standard deviations. During the calm conditions after the storm, both model simulations produce rather similar results that are close to the measurements (Figure B.6).

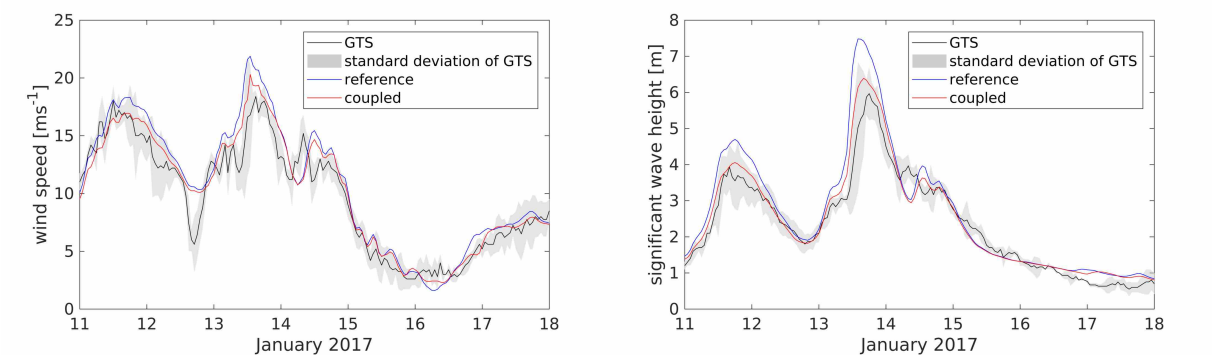

Figure B.6: Time series of GTS measurements versus the simulated results of the (a) wind speed (m s^{-1}) and (b) significant wave height (m) off the coast of England (53° N, 0° E to 54° N, 3° E).

These findings illustrate that the overall agreement between the coupled model simulation and the observational data are better than the agreement between the reference model simulation and the observational data. This result is especially valid during extreme events. During calm conditions, the results of both model simulations are quite similar. The discrepancies in these model performances result from the underestimation of the roughness lengths by the CCLM parametrisation compared to the roughness lengths calculated by WAM. This underestimation is larger at higher wind speeds, which causes larger differences for extreme events.

B.4 Impact of the Two-Way Coupling of the Models on Processes within the PBL and Higher Layers of the Atmosphere

B.4.1 Temporal Variability within the PBL

Hovmöller diagrams are generated to determine the events corresponding to large effects within the PBL due to the coupling between CCLM and WAM. Figure B.7 presents the Hovmöller diagrams for an area of 1° by 1° in the middle of the North Sea (symmetric around the point 56.5°N, 2.5°E, Figure B.2) for January 2017. On 16 January 2017, an event can be observed that is associated with large differences in the pressure, temperature and wind speed close to the PBL height. A second event can be observed on 24 January 2017 with a recognizable temperature change. Both events are associated with quickly rising temperatures along warm fronts (Figure B.7e). Additionally, during these events, the wind speed is relatively low (Figure B.7c), and the surface pressure exceeds 1010 hPa (Figure B.7a). To analyse these changes close to the PBL height, the time period between 11 January and the event on 16 January 2017 is investigated in more detail because the largest changes in all three parameters occur during this period. Additionally, on 13 January 2017, an event emerges that is characterised by pressure changes throughout the atmosphere.

B.4.2 Synoptic Situation

First, the synoptic situation during the time period from 11 to 16 January 2017 is discussed using the mean sea level pressure (MSLP) results from the reference model simulation. On 11 January 2017, the centre of the low-pressure system is located between Iceland and Norway, and a secondary low-pressure system is located over the southern coast of Norway close to Oslo (Figure B.8a). The associated pressure gradient across the North Sea is quite steep, causing high northwesterly winds in the North Sea area. The secondary low moves northeastwards with increasing pressure in the centre and eventually vanishes over Norway. The main low-pressure system moves towards the coast of Norway, after which it moves south along the coast and crosses the North Sea with a convergence zone evolving from the centre to the British coast (Figure B.8b). During this storm period, the wind speeds and significant wave heights are quite large. On 13 January 2017 at 9:00 p.m. UTC, the centre of the low-pressure system hits the East Frisian Islands along

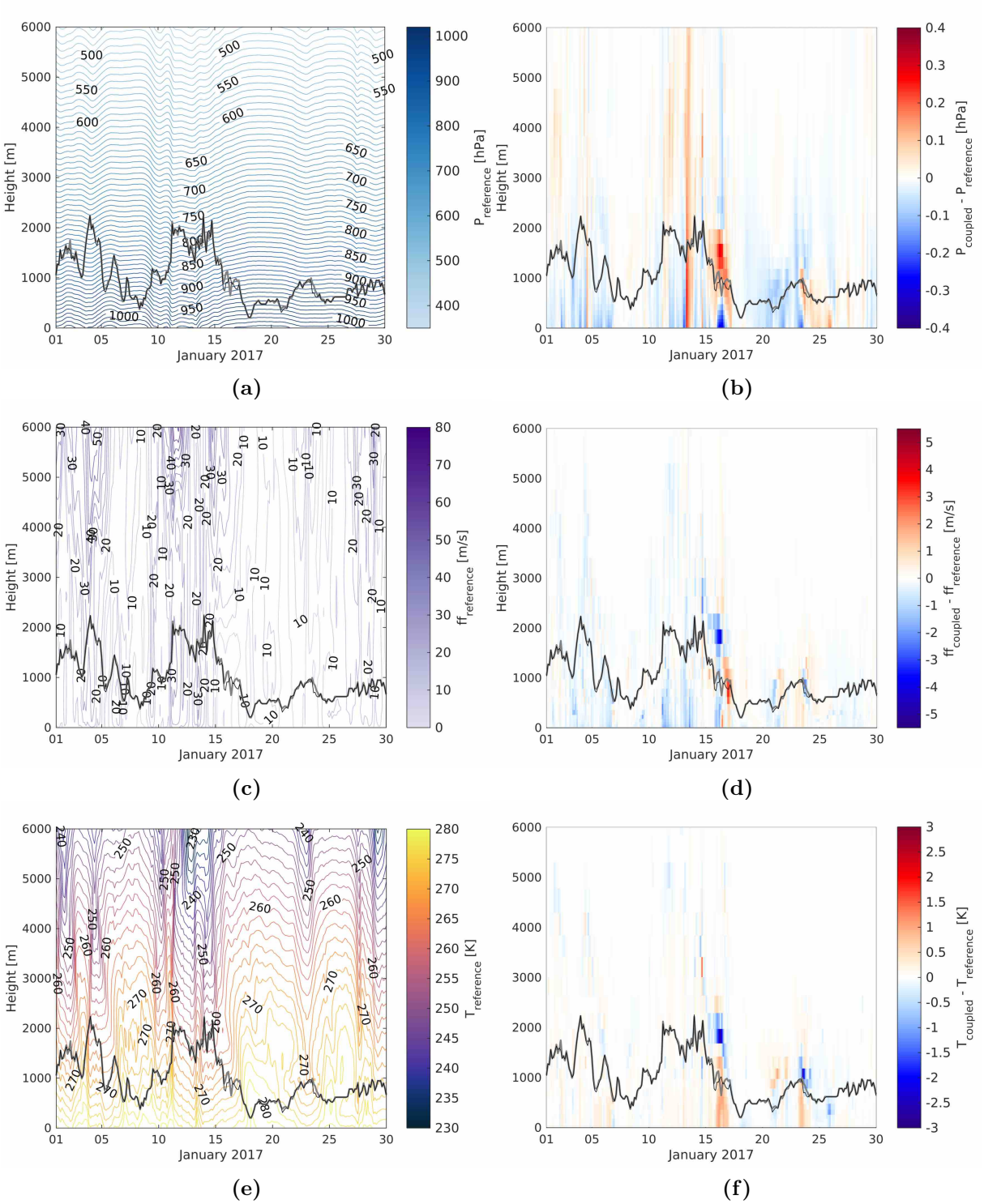

Figure B.7: Hovmöller diagrams (a,c,e) of the results from the reference model simulation and (b,d,f) of the differences between the reference and coupled model simulations in the North Sea for January 2017 for the (a,b) air pressure, (c,d) wind speed and (e,f) temperature. The black lines indicate the planetary boundary layer (PBL) height in the reference model simulation, and the grey lines indicate the PBL height in the coupled model simulation.

the German coast, after which it moves further southeastwards and fills up. After this low-pressure system moves out of the area, a high-pressure system develops over the North Sea (Figure B.8c) in association with low wind speeds and low significant wave heights throughout that area.

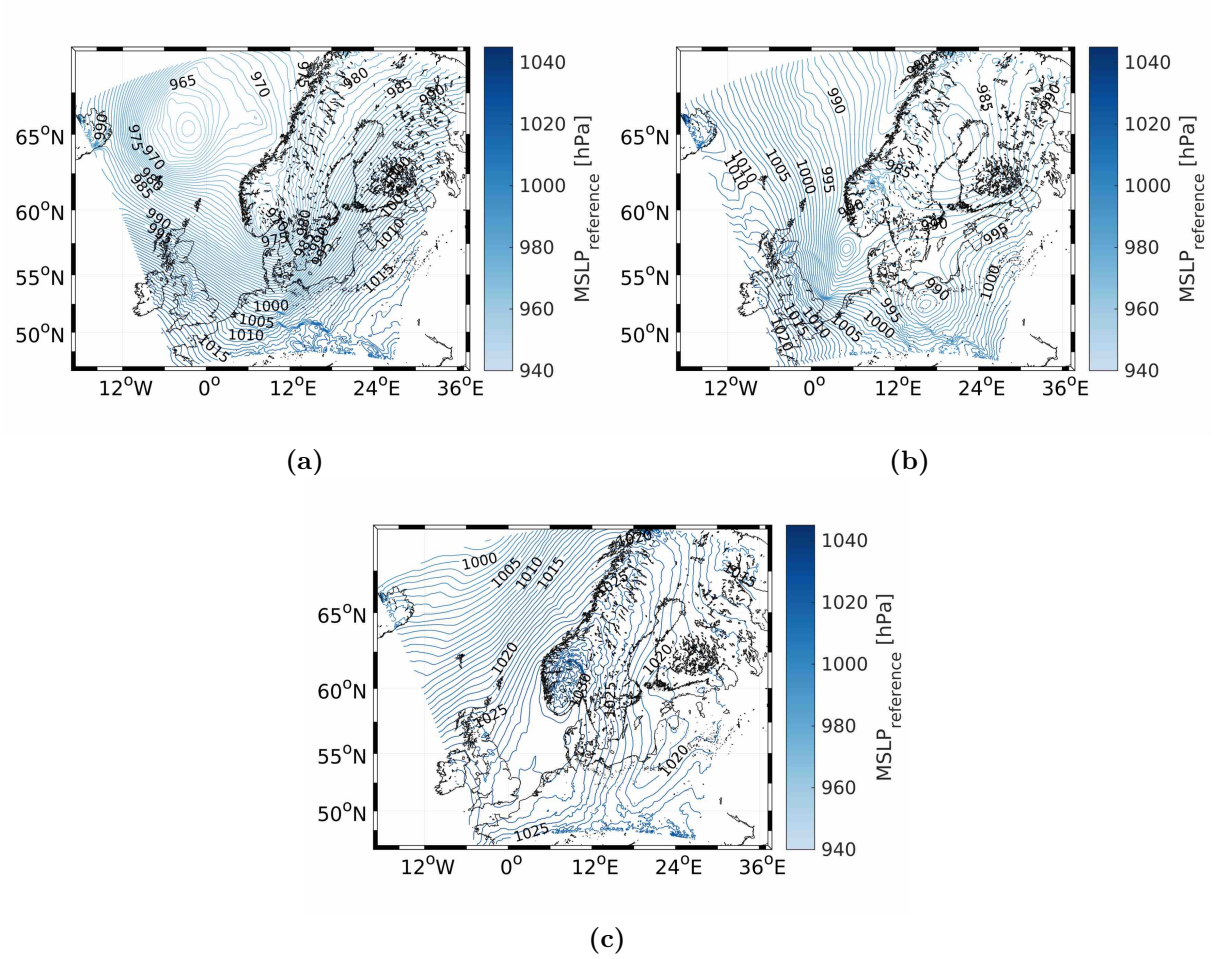

Figure B.8: Mean sea level pressure (MSLP) on (a) 11 January 2017 at 12:00 p.m. UTC; (b) 13 January 2017 at 12:00 p.m. UTC; and (c) 16 January 2017 at 6:00 a.m. UTC.

B.4.3 Tracks of the Low-Pressure System

Next, the tracks of the low-pressure system in the reference and coupled model simulations are compared (Figure B.9). The track of the low-pressure system is defined as the path of the minimum MSLP with time. The tracks in both model simulations are quite similar. The largest difference occurs when the system approaches the Norwegian coast. The

core of the system is quite large, which makes the definition of the centre inaccurate. Nevertheless, the structure of the low-pressure system is very similar in both cases. The tracks in the reference and coupled model simulations of the low-pressure system across the North Sea before hitting the German coast are also very similar. Therefore, the two-way coupling between the wind wave model and the atmospheric model does not influence the track of this low-pressure system. One possible reason for this might be that the coupled area in this set-up is too small, with the low pressure system moving across that area quite fast. Therefore, the time the low pressure system has to adjust to the changed roughness length might be too short to develop a different track, as this was found by other studies (Janssen et al., 2002).

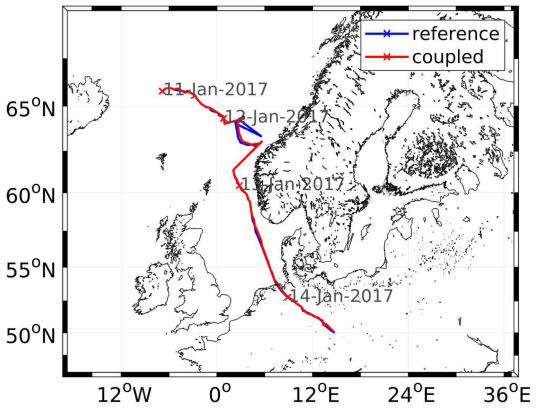

Figure B.9: Track of the low-pressure system from 11 January 2017 to 15 January 2017 for the reference model simulation (blue) and the coupled model simulation (red).

B.4.4 Impact on the Roughness Length

The parameter within the atmospheric model that is directly changed by the coupling with the wind wave model is the roughness length. In the coupled model simulation, the roughness length is calculated in the wind wave model and then passed to the atmospheric model, whereas in the reference model simulation, the roughness length is calculated using the Charnock parametrisation (COSMO, 2019).

On 11 January 2017 at 12:00 p.m. UTC, the roughness length in the coupled model simulation is enhanced compared to that in the reference model simulation (Figure B.10a). When the low-pressure system moves across the North Sea, the roughness lengths are also enhanced west of the convergence zone (Figure B.10b). These enhancements are

associated with high wind speeds and large significant wave heights. On 16 January 2017 at 6:00 a.m. UTC, when the high-pressure system is located over the North Sea, these differences in the roughness length vanish (Figure B.10c).

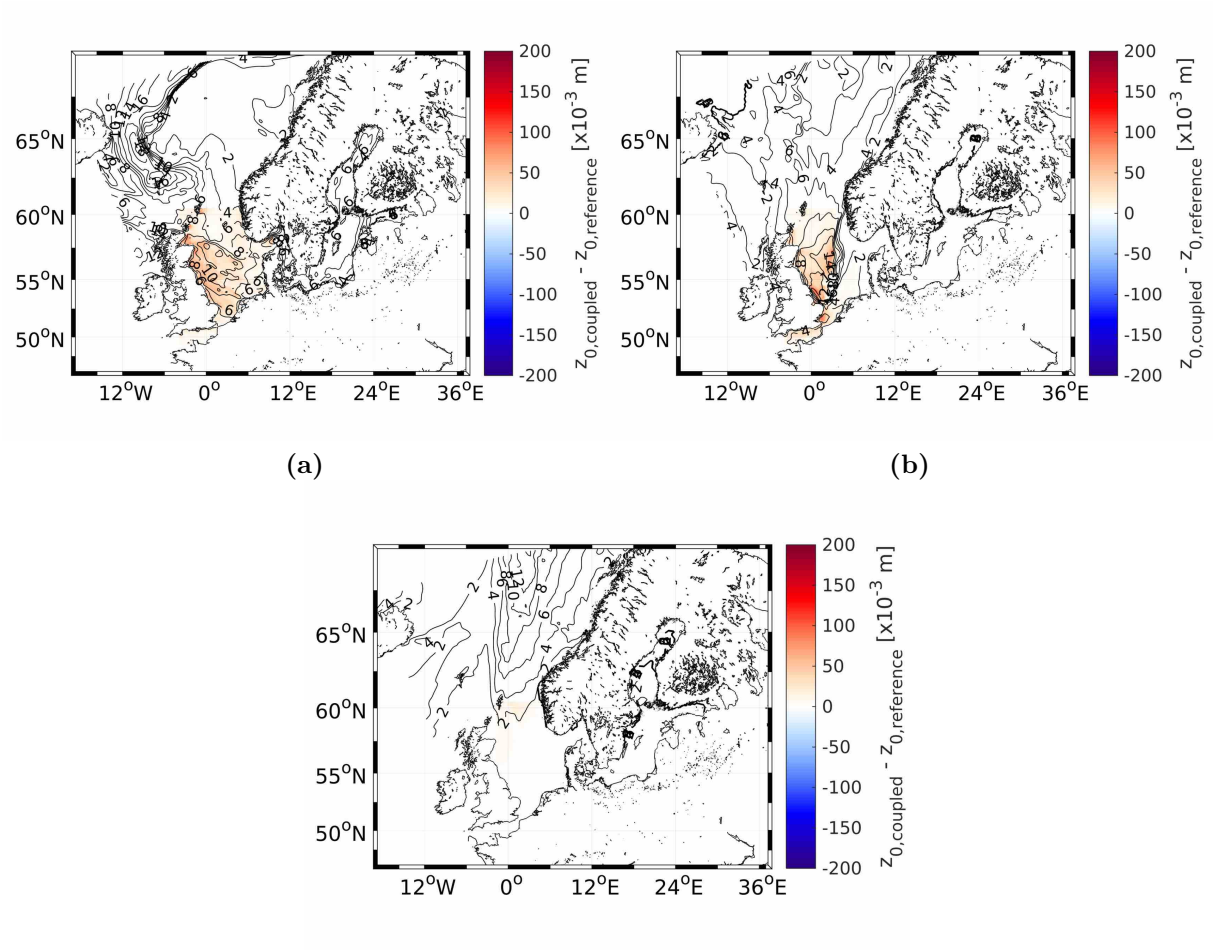

(a) **(b)**

(c)

Figure B.10: Absolute values of the roughness length in the reference model simulation (contours) and the differences in the roughness length between the coupled and reference model simulations (coloured) on (a) 11 January 2017 at 12:00 p.m. UTC; (b) 13 January 2017 at 12:00 p.m. UTC; and (c) 16 January 2017 at 6:00 a.m. UTC.

B.4.5 Impact on the Mean Sea Level Pressure

The differences in the roughness length discussed in the previous section (Section B.4.4) lead to differences in the MSLP because the roughness length determines the direction of airflow into the low-pressure system (Janssen, 2004). Due to the enhanced surface

roughness on 11 January 2017 at 12:00 p.m. UTC (Figure B.10a), the airflow moves more directly into the low-pressure system, allowing the low-pressure system to fill up faster. Therefore, the pressure increases in the centre of the low-pressure system and decreases around the outside, letting the gradient across the North Sea decrease (Figure B.11a).

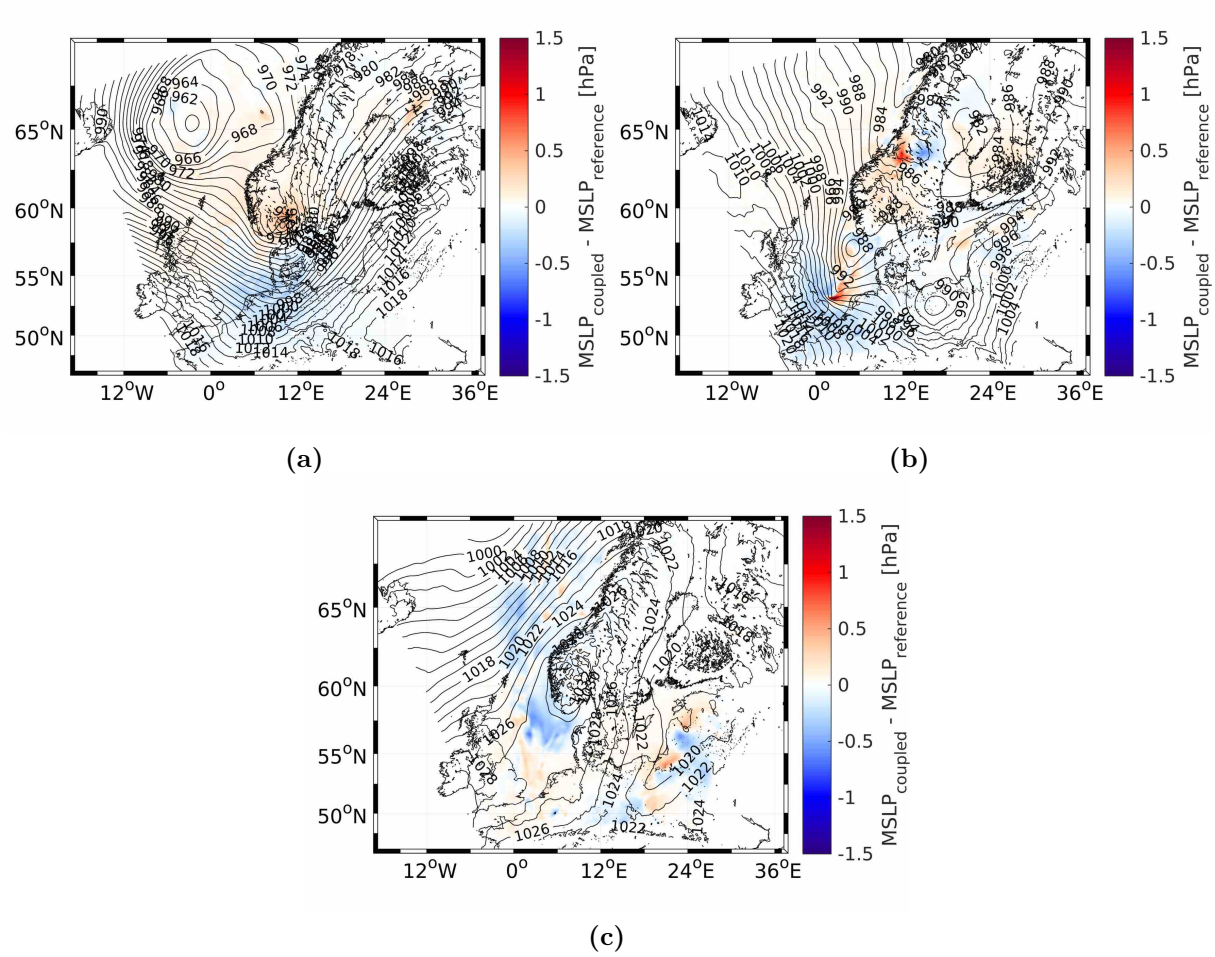

Figure B.11: Absolute values of the MSLP in the reference model simulation (contours) and the differences in the MSLP between the coupled and reference model simulations (coloured) on (a) 11 January 2017 at 12:00 p.m. UTC; (b) 13 January 2017 at 12:00 p.m. UTC; and (c) 16 January 2017 at 6:00 a.m. UTC.

Two days later, the largest changes in the MSLP can be found in the area of the convergence zone (Figure B.11b) because the exact position of the convergence zone varies between the reference and coupled model simulations. This convergence zone moves farther to the east in the coupled model simulation. This effect can also be seen in the Hovmöller diagrams (Figure B.7). At this time, a steep increase in the pressure can be detected throughout the entire atmosphere (Figure B.7a). Because the convergence zone

enters the investigated area earlier in the coupled model simulation, due to the shift towards the east, the pressure is increased throughout the entire atmosphere in the coupled model simulation (Figure B.7b). On 16 January 2017 at 6:00 a.m. UTC, the high-pressure system is located over the North Sea.

B.4.6 Impact on the 10 m Wind Speed

On 11 January 2017 at 12:00 p.m. UTC, the wind speed is also reduced due to the two-way coupling between the atmosphere and the wind waves (Figure B.12a). This is

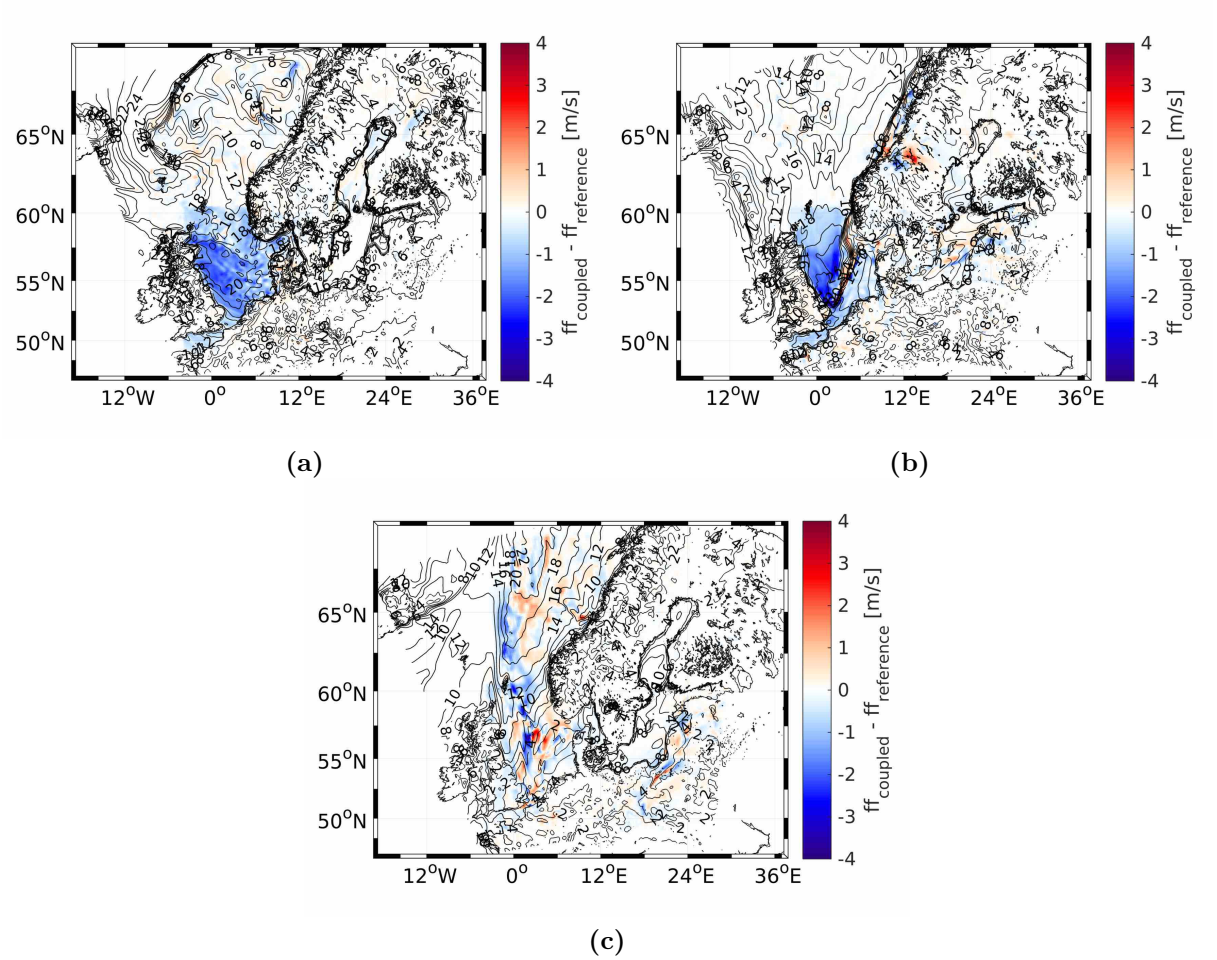

(a) **(b)**

(c)

Figure B.12: Absolute values of the 10 m wind speed in the reference model simulation (contours) and the differences in the 10 m wind speed between the coupled and reference model simulations (coloured) on (a) 11 January 2017 at 12:00 p.m. UTC; (b) 13 January 2017 at 12:00 p.m. UTC; and (c) 16 January 2017 at 6:00 a.m. UTC.

mainly due to the enhanced surface roughness (Figure B.10a) of the ocean surface because enhanced friction reduces the wind speed close to the surface. In addition, the reduced pressure gradient (Figure B.11a) contributes to a reduced wind speed within the North Sea area. Two days later, the largest impacts on the wind speed are observed along the convergence zone (Figure B.12b). Slightly east of the convergence zone, the wind speed is enhanced. This corresponds to the shift of the convergence zone towards the east, as seen in the MSLP (Figure B.11b). West of the convergence zone, where high wind speeds occur, the wind speed is again reduced due to the enhanced surface roughness. Due to the small pressure gradient across the North Sea on 16 January 2017 at 6:00 a.m. UTC (Figure B.8c), the wind speed is considerably low (Figure B.12c).

B.4.7 Impact on the Significant Wave Height

The significant wave height is reduced on 11 January 2017 at 12:00 p.m. UTC (Figure B.13a). This reduction is due to the wind speed being reduced (Figure B.12a), as the wind speed is passed from the atmospheric model to the wind wave model and therefore directly influences the significant wave height. This reduction reaches up to 1.4 m. The same can be seen two days later, when the significant wave height is reduced by up to 2.3 m west of the convergence zone, where significant wave heights reaching 10.5 m occur. On 16 January 2017 at 6:00 a.m. UTC, these changes in the significant wave height vanish, as the significant wave height is quite small during that time (Figure B.13c) due to low wind speeds.

B.4.8 Impact on the Temperature at the 850 hPa Geopotential Height

On 16 January 2017 at 6:00 a.m. UTC, a warm front is located across the North Sea, which can be clearly seen in the map of the temperature at the 850 hPa geopotential height (Figure B.14). The position and strength of this front differs between the coupled and reference model simulations. This explains the changes close to the PBL height seen in the Hovmöller diagrams (Figure B.7). These changes also extend outside the coupled model area.

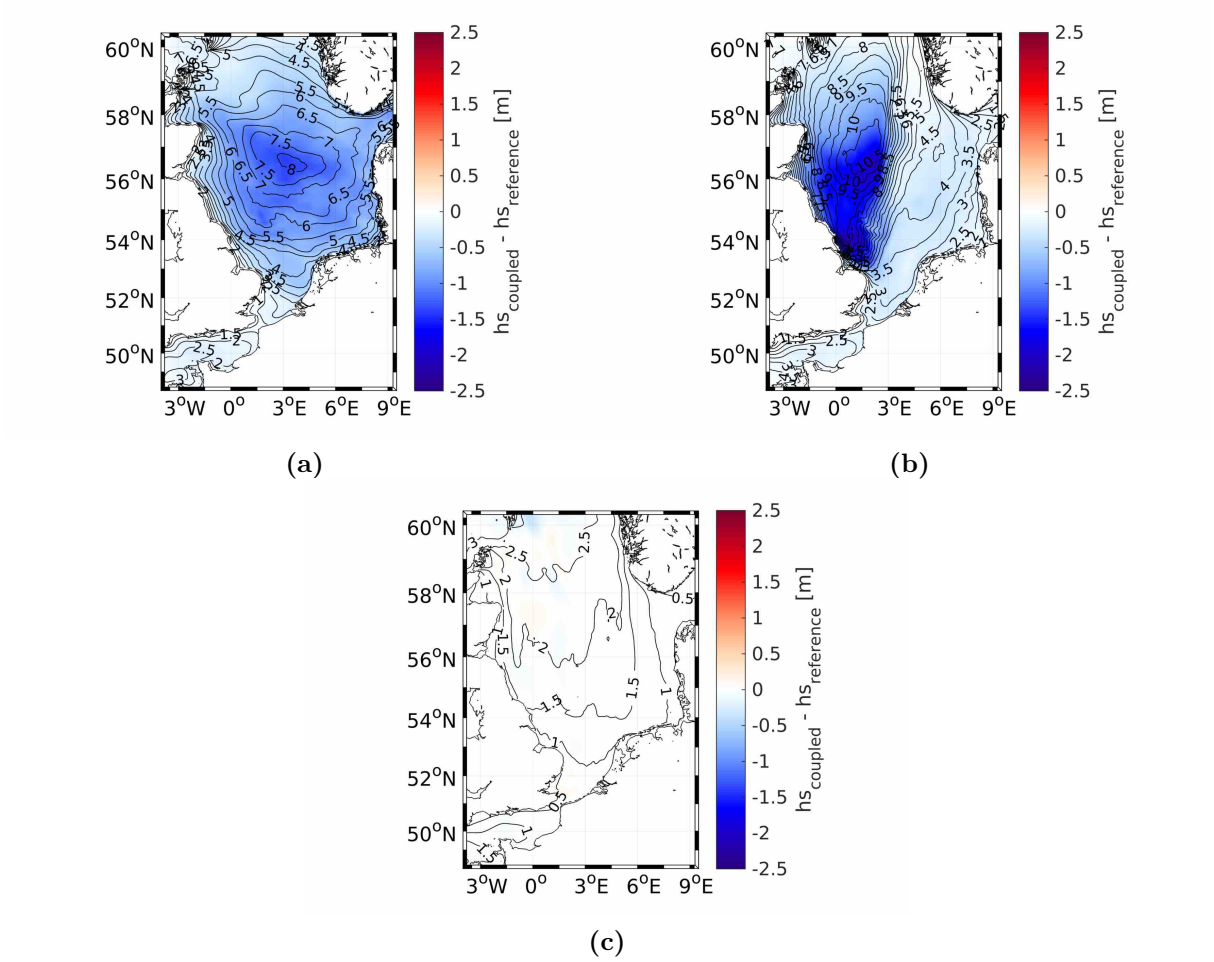

Figure B.13: Absolute values of the significant wave height in the reference model simulation (contours) and the differences in the significant wave height between the coupled and reference model simulations (coloured) on (a) 11 January 2017 at 12:00 p.m. UTC; (b) 13 January 2017 at 12:00 p.m. UTC; and (c) 16 January 2017 at 6:00 a.m. UTC.

B.5 Discussion

In this study, we depicted the differences between single run experiments of one-way and two-way coupled model simulations, showing that the differences between coupled and reference simulation can still be detected at the height of the PBL for the event studied. One approach to test the significance of the findings is using ensemble simulations. The significance of the role of sea state dependent roughness for the performance of coupled wave-atmospheric models has been differently estimated in several previous publications (Janssen and Viterbo, 1996; Weisse et al., 2000). The opinions range widely. Janssen and Viterbo (1996) reported a significant impact of the sea-state dependent momentum

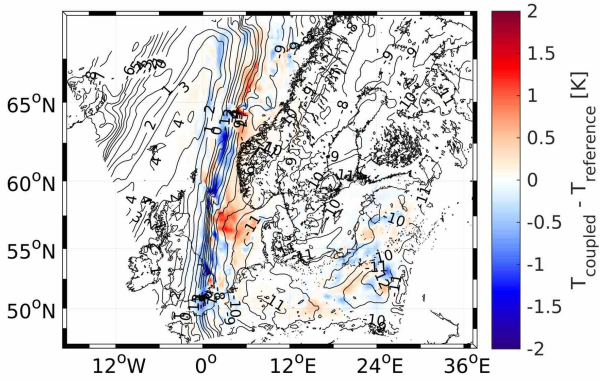

Figure B.14: Absolute values of the temperature *(°C)* at the 850 hPa geopotential height in the reference model simulation (contours) and the differences in the temperature *(K)* between the coupled and reference model simulations (shaded) on 16 January 2017 at 6:00 a.m. UTC.

exchange in their ensemble mean of a global model using 15 ensemble members and a horizontal resolution of *around 200 km*. Furthermore, they showed that the effects of waves are propagating up to the higher levels in the atmosphere. On the contrary, Weisse et al. (2000) and Weisse and Schneggenburger (2002), who analysed the sea level pressure over the North Atlantic, claimed that the effects of wind waves in the coupled model are weaker than the natural variability and can not easily be discerned. In their analysis they used an ensemble of six members with a horizontal resolution of 0.5°, but did not analyse the propagation of signals in the atmospheric boundary layer and above.

Although the ensemble approach proved useful to compare the significance of effects resulting from using new parametrisation against the natural variability, there are a number of studies which do not use this approach (Katsafados et al., 2016; Wu et al., 2017). Our study is one such example. We use a much finer resolution with the aim to illustrate situations under which the sea-state dependent momentum transfer would lead to substantial effects in both models. Our conclusions of the importance of sea state depended momentum exchange, in order to come closer to observational data, are more in line with these of Janssen and Viterbo (1996). *As Janssen and Viterbo (1996) found, the spatial resolution on a global scale is crucial for the significance of the effects of coupling, this might be similar on the regional scale, as our resolution is much finer, than the one of Weisse et al. (2000) and Weisse and Schneggenburger (2002). This needs further investigation in future studies.* Knowing that the natural variability is strongly dependent on some other processes, which we did not address here, we will mention below some important issues

first to address. One of these is to improve the model formulation of the atmospheric boundary layer. Another problem, when addressing the sea state dependent momentum exchange, would be to consider the coupled system of currents, waves and atmosphere. When addressing these issues in further studies, a deeper analysis with using model ensembles will be presented. Since the coupled model area in this study is rather small, the dependency of the changes found in this study on the size of the model domain, as well as different boundary conditions or different parametrisations of the roughness length, would be of interest.

B.6 Summary and Conclusions

In this study, the effects of coupling between an atmospheric model and a wind wave model, especially those on the PBL, are analysed. This coupling is enabled through the introduction of wave-induced drag in the atmospheric model and updated winds in the wind wave model.

The general performance of the coupled model system is better compared to the reference simulations with respect to observational data. The improvements in the coupled model system occur especially during extreme events because the influence of the enhanced surface roughness due to the coupling being largest at high wind speeds. During conditions of low wind speeds, both simulations are quite similar because the surface roughnesses calculated by WAM do not differ substantially from the surface roughnesses calculated by the parametrisation provided in CCLM.

Through the analysis of one event that affects the entire PBL, it becomes clear that the reference and coupled model simulation differ, especially along steep gradients, such as convergence zones and fronts. These differences are still present, when the significant wave height is already very small, and, therefore, the roughness length and variations in the roughness length are very small either. The differences between the reference and coupled simulation further extend outside the coupled model area over land and over uncoupled water surfaces.

This study demonstrates that the coupling between an atmospheric model and a wind wave model is necessary to obtain model results of wind speed and significant wave height closer to observational data with a better estimation of the roughness lengths over the

oceans, also accounting for different wave conditions at similar wind speeds, following the conclusions from Janssen and Viterbo (1996), Janssen et al. (2002) and Wu et al. (2017).

Author Contributions

Data curation, W.K., A.B. and B.G.; Formal analysis, A.W.; Funding acquisition, J.S.; Methodology, A.W., E.S. and J.S.; Software, A.W., W.K., A.B. and B.G.; Visualization, A.W.; Writing - original draft, A.W.; Writing - review and editing, A.W., E.S., W.K., A.B., B.G. and J.S.

Funding

This publication has received funding from the European Union's H2020 Programme for Research, Technological Development and Demonstration under Grant No. H2020-EO-2016-730030-CEASELESS.

Conflicts of Interest

The authors declare no conflict of interest. The funders had no role in the design of the study; in the collection, analyses, or interpretation of data; in the writing of the manuscript, or in the decision to publish the results.

C Internal Model Variability of Ensemble Simulations With a Regional Coupled Wave-Atmosphere Model GCOAST

This appendix contains a paper, which was accepted for publication when submitting the thesis and has now been published in the journal of "Frontiers in Marine Science" under the terms and conditions of the Creative Commons Attribution License (CC BY) (https://creativecommons.org/licenses/by/4.0/) as:

Wiese, A., Staneva, J., Ho-Hagemann, H.T.M., Grayek, S., Koch, W., & Schrum, C. (2020). Internal Model Variability of Ensemble Simulations With a Regional Coupled Wave-Atmosphere Model GCOAST. Front. Mar. Sci. 7:596843, https://doi.org/10.3389/fmars.2020.596843.

The publication has been formatted according to the format of this dissertation. The references have been merged with the other references of the thesis to one reference list for the whole dissertation. Changes on page 92 compared to the original publication are marked in italic.

The contribution of Anne Wiese and the other authors to this paper is as follows:
Anne Wiese set up the COSMO-CLM, performed all coupled and reference model simulations, conducted the analyses, and wrote the paper. Anne Wiese and Dr. Joanna Staneva conceived the work. Dr. Ha Thi Minh Ho-Hagemann provided assistance with the set-up of the COSMO-CLM regional climate model and the initialisation of the ensembles. Dr. Sebastian Grayek and Wolfgang Koch implemented the coupling in CCLM and WAM and provided technical support with the model system. Prof. Dr. Corinna Schrum and Dr. Joanna Staneva provided guidance on the overall course of the manuscript. All authors reviewed the manuscript. The manuscript was checked for English language.

Internal Model Variability of Ensemble Simulations With a Regional Coupled Wave-Atmosphere Model GCOAST

Anne Wiese[1], Joanna Staneva[1], Ha Thi Minh Ho-Hagemann[1], Sebastian Grayek[1], Wolfgang Koch[1] and Corinna Schrum[1,2]

[1]Institute of Coastal Research, Helmholtz-Zentrum Geesthacht, Geesthacht, Germany

[2]Center for Earth System Research and Sustainability, Institute of Oceanography, University of Hamburg, Hamburg, Germany

(Received: 20 August 2020; Accepted: 30 September 2020; Published: 4 November 2020)

Ensemble simulations are performed to quantify the internal variability of both regional atmospheric models and wave-atmosphere coupled model systems. Studies have shown that the internal variability in atmospheric models (e.g., wind or pressure fields) is increased during extreme events, such as storms. Comparing the magnitude of the internal variability of the atmospheric model with the internal variability of the coupled model system reveals that the internal variability can be reduced by coupling a wave model to the atmospheric model. While this effect is most evident during extreme events, it is still present in a general assessment of the mean internal variability during the whole study period. Furthermore, the role of this wave-atmosphere coupling can be distinguished from that of the internal variability of the atmospheric model since the impact of the wave-atmosphere interaction is larger than the internal variability. This is shown to be robust to different boundary conditions. One method to reduce the internal variability of the atmospheric model is to apply spectral nudging, the role of which in both the stand-alone atmospheric model and the coupled wave-atmosphere system is evaluated. Our analyses show that spectral nudging in both coupled and stand-alone ensemble simulations keeps the internal variability low, while the impact of the wave-atmosphere interaction remains approximately the same as in simulations without spectral nudging, especially for the wind speed and significant wave height. This study shows that in operational and climate research systems, the internal variability of the atmospheric model is reduced when the ocean waves and atmosphere are coupled. Clear influences of the wave-atmosphere inter-

action on both of these earth system components can be detected and differentiated from the internal model variability. Furthermore, the wave-atmosphere coupling has a positive effect on the agreement of the model results with both satellite and in situ observations.

C.1 Introduction

Air-sea interaction processes and the feedbacks of their interdependence must be better understood to further improve both the operational and the climate research capabilities of model systems. On the one hand, improving operational forecasts is particularly important for all human activities at sea, such as maintaining and installing offshore wind farms, ship routing, and recreational activities (Gautier and Caires, 2015; Thomas and Dwarakish, 2015). On the other hand, precise and low-uncertainty climate projections are crucial for coastal protection and offshore activities, which are highly vulnerable to extreme weather events and waves (Quante and Colijn, 2016). One approach for reducing these model uncertainties is the coupling of different earth system elements. In this context, the exchange processes near the ocean surface are described more realistically by considering two-way fully coupled sea surface waves and atmospheric components. Using stand-alone models of the atmosphere, the roughness length of the water surface is usually parameterised as a function of wind speed (e.g., Lionello et al., 1998; Doms et al., 2013; Wu et al., 2017). When waves interact with the atmosphere, wave models estimate the sea surface roughness using wave parameters, which can account for influencing factors, such as swells and wave age (e.g., Janssen et al., 2002; Wu et al., 2017; ECMWF, 2019). The linkage between waves and atmospheric components can lead to increased roughness lengths over the ocean surface (e.g., Lionello et al., 1998; Cavaleri et al., 2012a; Katsafados et al., 2016; Wu et al., 2017). This increase in roughness then affects the overlying atmosphere, resulting in diminished wind speeds and significant wave heights. For extratropical lows, an increased roughness length weakens low-pressure systems, which Doyle (1995) and Lionello et al. (1998) have shown for idealised cases. Doyle (1995) employed an idealised cyclone to study the responses of the boundary-layer, mesoscale and synoptic-scale environment associated with marine cyclogenesis to the sea state. They found that the boundary-layer structure is influenced by ocean waves in the vicinity of a marine cyclone, reducing the wind speed by as much as 12 % in coupled simulations as a result of high surface roughness due to young waves along the warm front and behind the cyclone. Furthermore, in coupled simulations, they detected an increase in pressure at the centre

of the low. Lionello et al. (1998) found similar effects of the two-way coupling between waves and atmosphere and tested the sensitivity of the wave-atmosphere interaction to the cyclone intensity and horizontal model resolution. They stated that the impact of waves on cyclogenesis depends on the storm intensity and is proportionally larger for extreme storms since intense and continuously changing winds maintain young waves. Furthermore, the influence on the increase in the minimum pressure is enhanced with increasing model resolution, which the authors lead back to a more detailed description of the cyclone centre.

In addition to studies on idealised cyclones, researchers have previously studied realistic cases in the North Atlantic (Perrie and Zhang, 2001; Janssen et al., 2002; Wu et al., 2017), the North Sea (Wahle et al., 2017; Wu et al., 2017; Wiese et al., 2019; Wu et al., 2019) and the Mediterranean Sea (Cavaleri et al., 2012b; Varlas et al., 2018, 2020). In all these areas, the general consequence of wave-atmosphere coupling on cyclones is very similar to that depicted for the idealised cases described above. While Cavaleri et al. (2012b) and Varlas et al. (2018) concentrated on the effects of the interaction between waves and atmosphere during intense cyclone events, Varlas et al. (2020) assessed the impacts of this coupling over the Mediterranean and Black Seas during a whole year and discovered significantly improved forecast skills for the one-year time period due to this interaction. However, they detected the largest improvements due to the wave-atmosphere linkage under intense wind and sea state conditions. In the North Sea, a decline in storm intensity due to the wave-atmosphere interaction was found to be caused by the enhanced surface roughness due to young waves (Wu et al., 2017; Wiese et al., 2019). Since the roughness length is often underestimated by atmospheric models, Wu et al. (2017) sought to improve the Charnock parameterisation by increasing the Charnock parameter and adding variance to the roughness emulating the variance in the surface roughness presented by wave models. However, both attempts to tune the Charnock parameterisation in the atmospheric model failed to replace the wave-atmosphere linkage under storm conditions. Having shown the importance of waves for atmospheric responses, Wu et al. (2019) assessed the impacts of waves in a fully coupled system considering atmospheric, waves and oceanic components on the transfer of momentum and heat between the ocean and atmosphere and showed significant effects on coastal areas. As coupled systems consisting of waves and atmospheric components have superior forecast skills over stand-alone models, such a system have been used at the European Centre for Medium-Range Weather Forecasts (ECMWF) for operational wind and wave forecasting since 1998 (Janssen et al., 2002; Janssen, 2004).

Recently, the interactions among waves and oceanic and atmospheric components have been shown to have important impacts on predicting the power generated by offshore wind farms (Larsén et al., 2019; Wu et al., 2020). In addition to studies on synoptic time scales, the influences of coupling on the atmospheric and wave climates have also been investigated. Significant impacts on the atmosphere by the wave-atmosphere linkage have been shown on both the global scale (Janssen and Viterbo, 1996) and the regional scale (Perrie and Zhang, 2001; Rutgersson et al., 2010). Furthermore, coupled systems showed superior forecast skills over stand-alone models for the estimation of the wind climate for the choice of offshore wind turbines (Larsén et al., 2019).

The increased roughness length calculated by wave models compared to atmospheric models also leads to enhanced heat flux, which is important for hurricane studies, as enhanced heat fluxes lead to an intensification of hurricanes (Bao et al., 2000). When simulating hurricanes, a decrease in or saturation of the roughness length at very high wind speeds is particularly important, as this allows the hurricane to intensify further (Chen et al., 2013; Donelan, 2018). Accordingly, Chen et al. (2007) showed the importance of waves in a coupled atmosphere-wave-ocean model for the prediction of hurricane winds.

In the context of both operational and climate research capabilities, it is important to examine and quantify the variability and levels of uncertainties. One source of uncertainty in atmospheric model simulations stems from ambiguous initial conditions since the dynamic evolution varies among different model simulations when the models are initialised with slightly different initial conditions. This uncertainty is usually referred to as internal model variability, hereafter called internal variability. (Laprise et al., 2012; Sieck, 2013; Rummukainen, 2016; Sanchez-Gomez and Somot, 2018; Ho-Hagemann et al., 2020). This is not be confused with the internal climate variability, which is the natural variability of the climate system (Ho-Hagemann et al., 2020). Internal variability can be estimated from the spread of ensemble simulations using slightly varying initial conditions (e.g., Sieck, 2013; Ho-Hagemann et al., 2020) and is often larger on a regional scale than on the global scale (Rummukainen, 2016). Internal variability was shown to be reduced by the coupling between oceanic and atmospheric models, resulting in a stabilising influence on the atmospheric model (Schrum et al., 2003; Ho-Hagemann et al., 2020). Therefore, incorporating the effects of waves on the atmosphere might have a similar consequence of stabilising the atmospheric model, which has not yet been investigated to the best of our knowledge.

In addition, the internal variability of a regional atmospheric model can be reduced by applying spectral nudging to the model (von Storch et al., 2000; Weisse and Feser, 2003; Schaaf et al., 2017). This method is widely used to keep the large-scale atmospheric state close to the forcing data, while the regional scale can develop (Feser et al., 2001; Alexandru et al., 2009; Weisse et al., 2009; Geyer, 2014). This technique is beneficial for studies reconstructing past climates or specific events with the maximum possible precision since reanalysis data can be used for spectral nudging under these circumstances (von Storch et al., 2000; Weisse and Feser, 2003). However, the performance of regional climate models using spectral nudging strongly depends on the accuracy of the global data. Moreover, in research on the future climate, this technique might not be advantageous since the global data contain uncertainties (Ho-Hagemann et al., 2020). This source of uncertainty, called the forcing uncertainty, is introduced into a regional model through the boundary forcing driven by global simulations (Sieck, 2013; Ho-Hagemann et al., 2020). Consequently, the choice of global climate model simulations as the boundary forcing for a regional climate model has been shown to greatly influence the regional model solution (Déqué et al., 2007; Kjellström et al., 2011; Keuler et al., 2016). Moreover, previous studies have shown that the use of both different global climate models and differing reanalysis data as the boundary forcing can have large impacts on regional model simulations (Meißner, 2008).

Furthermore, models contain inherent uncertainty called structural model uncertainty, hereafter called model uncertainty, which can be explained by the parameterisations, dynamical core and spatial resolution of the model (Murphy et al., 2004). Since numerical models cannot resolve processes smaller than twice their resolution, these processes have to be parameterised as a function of resolved large-scale features. These parameterisations lead to uncertainties in numerical models (Rummukainen, 2016). Furthermore, processes occurring in the real atmosphere-wave system are neglected in the model system or only insufficiently understood and for that reason not incorporated. At the interface between atmosphere and ocean, energy and momentum are exchanged through the waves (Cavaleri et al., 2012b). These exchanges are one example of processes that are not fully incorporated in uncoupled models, since they have to be parameterised in the absence of models for the other components of the earths system. Hence, when coupling the two models the model uncertainty might be reducible. By replacing the wind dependent parameterisation in the atmospheric model with the wave-atmosphere coupling a step towards a better depiction of the real atmosphere-wave system is made.

Previous studies on assessing the impacts of atmosphere-wave interaction relative to the internal variability of atmospheric models, have discussed the significance of the coupling in comparison with the extents of uncertainties with differing conclusions. For instance, Weisse et al. (2000) and Weisse and Schneggenburger (2002) stated that the regional-scale effects of linking the wave model to the atmospheric model on the mean sea level pressure (MSLP) in the North Atlantic are not significant, indicating that the internal variability is similarly large during events with large influences due to this coupling, and thus, the impacts cannot be differentiated from the internal variability. In contrast, Janssen and Viterbo (1996) reported a significant impact of the sea state-dependent momentum exchange on their ensemble mean of a global model and suggested that the spatial resolution is crucial for studying the significant consequences of waves on the atmosphere. Similarly, Wu et al. (2017) showed that the impacts of coupling increase with increasing model resolution. Rutgersson et al. (2010) demonstrated significant effects of the wave-atmosphere interaction on the regional climate but did not use an ensemble approach. Rather, they employed longer time scales to assess the significance of this coupling. Since the studies of Weisse et al. (2000) and Weisse and Schneggenburger (2002), the formulation and resolution of regional models have been improved and refined, enabling us to re-evaluate the sensitivity of extremes to the influences of waves and atmosphere in regional models. Therefore, in this study, a state-of-the-art high-resolution regional wave-atmosphere coupled model system for the North and Baltic Sea in the framework of the Geesthacht COAstal model SysTem (GCOAST) is used to investigate the effects of the wave-atmosphere coupling relative to the internal variability of atmospheric models, especially during extreme events, by conducting ensemble simulations. Furthermore, the influence of the coupling on the model uncertainty is assessed, as is the sensitivity of the impacts of coupling to the application of spectral nudging in atmospheric models, and the choice of boundary conditions.

The structure of this paper is as follows. The numerical models, measurement data and design of the numerical experiments are described in Section C.2. Then, the ensemble simulations are analysed with regard to the differences between coupled and reference simulations, and the internal variability is compared between them, as is the impact of the coupling on the internal variability (Section C.3). This is followed by an analysis of the sensitivity of the effects of coupling to the use of spectral nudging and different boundary conditions (Section C.4). Furthermore, one extreme event in January 2017 is investigated in more detail (Section C.5). Finally, a summary and conclusions along with a discussion of the results are given (Section C.6).

C.2 Numerical Models, Experimental Design, and Measurement Data

C.2.1 Numerical Models

The atmospheric model used herein is the Consortium for Small-Scale Modeling (COSMO)-Climate Mode (CLM) (CCLM) regional climate model (Rockel et al., 2008; Doms and Baldauf, 2013). CCLM is the community model of the German regional climate research community and has already been utilised in several studies employing coupled systems with waves (e.g., Cavaleri et al., 2012b; Wahle et al., 2017; Li et al., 2020) or oceanic and other earth system components (e.g., Ho-Hagemann et al., 2013, 2015; Van Pham et al., 2014; Ho-Hagemann et al., 2017; Will et al., 2017; Kelemen et al., 2019; Ho-Hagemann et al., 2020). CCLM is based on the primitive thermo-hydrodynamical equations describing a compressible flow in a moist atmosphere. The equations are solved on a rotated geographical Arakawa-C grid and generalised terrain-following height coordinates. The domain of the atmospheric model extends north to Iceland and Norway and south to Spain and Italy. The domain is just large enough to cover the area of the wave model (Figure C.1a), and the horizontal grid spacing is 0.0625°. A high horizontal resolution is desirable since the impacts of the coupling increase at higher resolutions, where the structure of cyclones is better resolved (Janssen and Viterbo, 1996; Lionello et al., 1998; Wu et al., 2017).

The wave model utilised in this study is the third-generation WAve Model WAM (WAMDI Group, 1988; ECMWF, 2019). WAM has also been used successfully in several studies that assessed the wave-atmosphere coupling together with CCLM (e.g., Cavaleri et al., 2012b; Wahle et al., 2017; Li et al., 2020). However, WAM has also been employed with other atmospheric models, such as the ECMWF model (e.g., Janssen and Viterbo, 1996; Janssen et al., 2002) or the Weather Research and Forecasting (WRF) model (e.g., Wu et al., 2017). WAM is a spectral wave model (WAMDI Group, 1988; ECMWF, 2019) that includes parameterisations for shallow water, depth refraction and wave breaking, making it applicable for the area studied herein. The 2-D wave spectra are calculated on a polar grid with 24 directional 15° sectors and 30 frequencies logarithmically spaced from 0.042 to 0.66 Hz. For the spatial dimensions, a spherical grid is used with a 0.06° longitudinal resolution and a 0.03° latitudinal resolution. The domain of the wave model covers the Baltic and North Seas and the Northeast Atlantic Ocean. The model domain

and bathymetry are shown in Figure C.1a. At the open boundaries of the model domain, the forcing values come from simulations with a coarser model covering the whole North Atlantic driven by ECMWF Reanalysis Version 5 (ERA5) winds (Copernicus Climate Change Service (C3S), 2017). The coarser model has a spatial resolution of 0.25° in both directions and the same spectral resolution as the finer model described above.

These two models are coupled through the OASIS3-Model Coupling Toolkit (MCT) version 2.0 *(Valcke et al., 2015)* with a coupling time step of 300 s. In the reference simulation, CCLM sends the 10 m wind components to WAM and applies its own parameterisation to calculate the roughness length over the ocean using the Charnock formula (Doms et al., 2013), and therefore, the roughness length is dependent only on wind:

$$z_0 = \frac{\alpha_c}{g} max(u_*^2, w_*^2) \tag{C.1}$$

In Equation C.1, the Charnock constant α_c is set to 0.0123, g denotes the acceleration due to gravity, u_* is the friction velocity, and w_* is the scaling velocity for free convection. The roughness length over ice is set to a constant value of 0.001 m.

In the coupled simulation, WAM still receives the wind components but also sends the roughness length calculated through the wave parameters to the atmospheric model. Hence, over the ocean surface, waves are taken into account when estimating the roughness length by using the wave-induced stress (τ_w) for the calculation of z_0 *(ECMWF, 2019)*.

$$z_0 = \frac{\hat{\alpha}\tau}{g} \frac{1}{\sqrt{1 - \frac{\tau_w}{\tau}}} \tag{C.2}$$

The total stress ($\tau = u_*^2$), the acceleration due to gravity (g) and the modified Charnock constant ($\hat{\alpha} = 0.0062$) are also taken to calculate the roughness length over the ocean.

C.2.2 Experimental Design

To analyse the internal variability of the atmospheric model in comparison with the internal variability of the coupled model system and the effects of the wave-atmosphere coupling on the atmospheric model, six different ensemble simulations are carried out and described in Table C.1. The ensembles are designed such that there is always a corresponding reference and coupled simulation. The basic set of ensembles is conducted using ERA5 boundary conditions (Copernicus Climate Change Service (C3S), 2017), and no

spectral nudging is applied in CCLM to allow the atmospheric model to freely develop and to estimate the impacts of coupling on the freely evolving atmosphere. Furthermore, two sensitivity experiments are carried out: one set of ensembles is conducted with spectral nudging, and another set of ensembles is performed using different boundary conditions. Spectral nudging is used to ensure that the large-scale circulation and positions of low-pressure systems are approximately correct using coarser global data, such as reanalyses (von Storch et al., 2000; Weisse and Feser, 2003). For the simulations with spectral nudging, boundary values for the open lateral boundaries as well as for spectral nudging are taken from ERA5 (Copernicus Climate Change Service (C3S), 2017) similar to simulations without spectral nudging. To estimate the sensitivity of coupling to the choice of boundary conditions and to assess the impacts of the boundary conditions of the atmospheric model on the effects of the coupling, one set of ensembles is performed using ERA-Interim as boundary conditions (Berrisford et al., 2009; Dee et al., 2011).

Table C.1: Experimental design.

Name	**Coupling**	**Spectral nudging**	**Boundary conditions**	**Time period**
ref.nsn	No	No	ERA5	01.12.2016 - 01.04.2017
cpl.nsn	Yes	No	ERA5	01.12.2016 - 01.04.2017
ref.sn	No	Yes	ERA5	01.12.2016 - 01.04.2017
cpl.sn	Yes	Yes	ERA5	01.12.2016 - 01.04.2017
ref.bc	No	No	ERA-Interim	01.12.2016 - 01.04.2017
cpl.bc	Yes	No	ERA-Interim	01.12.2016 - 01.04.2017

In the atmospheric model, the soil moisture content needs time to adapt (Geyer, 2014). This adaptation occurs faster closer to the surface than for deeper soil layers and depends both on the accuracy of the initial conditions and on the regional conditions. Considering the model domain and that the evaluation of the results is performed mainly for ocean areas, one year of spin up is performed starting on 1 January 2016. This spin-up simulation is conducted with the reference set-up involving spectral nudging, which is initialised with ERA5 data. The ensemble initialisation is accomplished following Ho-Hagemann et al. (2020) using different dates. Other studies have adopted a similar approach to assess the internal variability of atmospheric models (Alexandru et al., 2007; Lucas-Picher et al., 2008; Sieck, 2013). Lucas-Picher et al. (2008) further assessed other ways to disturb the initial ensemble conditions and found that neither the source nor the magnitude of the perturbations of initial conditions has an impact on the internal variability 15 days

past the initialisation. Like in Sieck (2013), each experiment consists of 10 ensemble members using restart fields from 1 to 10 December 2016 from the spin-up simulation, as Alexandru et al. (2009) showed 10 members are required for a robust estimate of the internal variability. All restart fields are then used to initiate the ensemble on 1 December 2016, which spans one winter season until 1 April 2017. For the study period the month of December is then discarded as a spin up for the ensemble. This period is chosen to account for the effects of coupling, especially during extreme events that occur during this time of the year (Janssen et al., 2002; Wahle et al., 2017; Wu et al., 2017; Wiese et al., 2019).

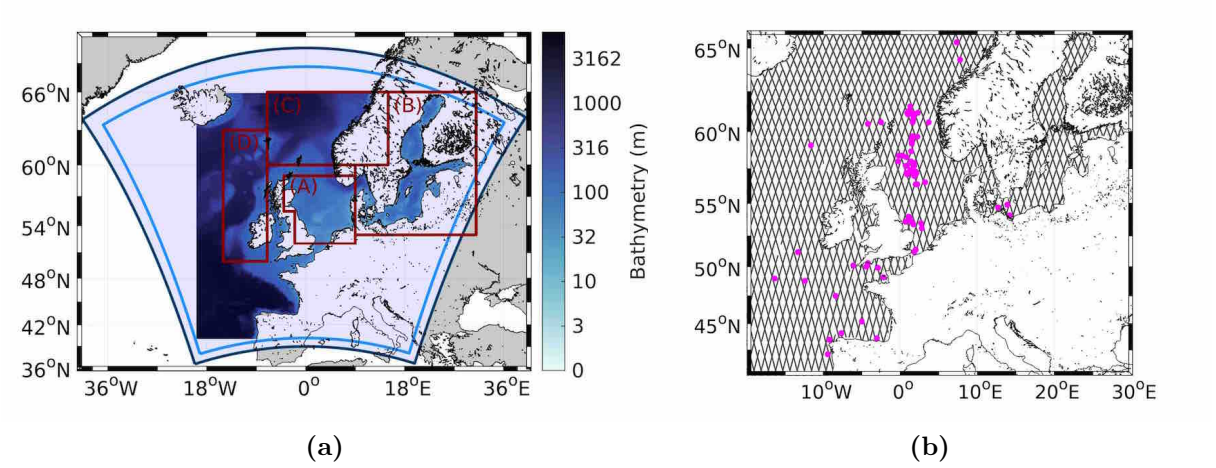

Figure C.1: Bathymetry of the wave model WAM (shaded) and domain of the CCLM regional climate model (dark blue box). The area between the dark and light blue boxes is regarded as the buffer zone and is neglected in the analysis. The four different study areas are indicated by the grey boxes in (a): the North Sea (A), the Baltic Sea (B), the southern Norwegian Sea (C) and the North Atlantic Ocean west of the British Isles (D). The locations of the GTS (magenta dots) and Sentinel-3A measurements (grey lines) are shown in (b).

C.2.3 Observations

C.2.3.1 In situ Measurements

Observations from the Global Telecommunication System (GTS) of the significant wave height and wind speed are used to estimate the agreement between the model simulations and observations. The data are obtained from and archived at ECMWF (Bidlot and Holt,

2006). Moreover, data are gathered by ECMWF as part of the Joint Technical Commission for Oceanography and Marine Meteorology (JCOMM) wave forecast verification project (Bidlot et al., 2002). The data are recorded either by moored wave buoys anchored at fixed locations to serve national forecasting needs or by instruments mounted on platforms or rigs managed by the oil and gas industry. As in Wiese et al. (2018), the wave height measurements are collocated with the model data using the closest grid point to the location of the in situ observations. The wind speed measurements are interpolated to a height of 10 m above the surface and then collocated with the model using the closest grid point to the location of the observation. The locations of in situ observations are presented in Figure C.1b.

C.2.3.2 Satellite Data

The significant wave height and wind speed observations from the Sentinel-3A satellite are used to assess the realism of the simulated wave characteristics. Sentinel-3A, which was launched in February 2016, is the first altimeter to operate entirely in synthetic aperture radar (SAR) mode (ESA, 2015). The revisit time of Sentinel-3A is 27 days. The data gathered by Sentinel-3A are retrieved from 1D profiles along the ground track of the satellite, and the footprint size is between 1.5 and 10 km depending on the sea state across the track. The along-track resolution of Sentinel-3A is around 7 km for 1 Hz measurements. Figure C.1b shows the locations of the satellite measurements. The satellite data are collocated with the model using the nearest model grid point and the closest time with a maximum time lag of 30 min. The in situ and Sentinel-3A observational data are also described in Wiese et al. (2019).

C.3 Impacts of the Wave-Atmosphere Coupling

Wind is directly influenced by the coupling through changes in the roughness length that alter the wind speed and direction. Furthermore, the roughness length impacts the MSLP since the roughness determines the angle of wind with respect to the isobars and therefore drives the mass transport from higher to lower pressures (Janssen, 2004). Hence, hourly outputs of wind speed and the MSLP are chosen for more detailed analyses in the following.

In addition, the effects of the internal variability in the atmospheric model and the impacts of coupling on the significant wave height are analysed. For these analyses, four regions are chosen with different wave conditions and storm activity characteristics: the North Sea (A), the Baltic Sea (B), the southern Norwegian Sea (C) and the North Atlantic Ocean west of the British Isles (D). The Baltic Sea exhibits only a very small opening to the North Sea through the Danish Straits and is therefore classified as a closed area for waves. As a result, the fetch conditions are limited within the Baltic Sea, especially in the longitudinal direction. The North Sea is open to the Atlantic Ocean through the English Channel, and swells stemming from the North Atlantic regularly enter the North Sea from the northern opening between Scotland and Norway. The Norwegian Sea and the North Atlantic west of Great Britain are exposed to large swells and long fetch conditions, which are conducive to the development of large waves.

C.3.1 Differences Between Coupled and Reference Ensembles

The average synoptic situation of ref.nsn during the whole study period and the differences between ref.nsn and cpl.nsn are analysed. For this, the mean values over the ensemble members and over the whole study period of ref.nsn along with the differences between the mean values over the ensemble members and the study period of cpl.nsn and ref.nsn are depicted (Figure C.2a, C.2c, C.2e and C.2g). In general, over the entire study period, an increase in the roughness length leads to decreases in the wind speed, significant wave height and pressure gradient. Moreover, while the effects of the coupling on the wind speed and roughness length are limited to the domain coupled to the wave model, changes in the MSLP and geopotential height extend over the whole atmospheric model domain, outside the coupled area and over the European continent.

The mean MSLP conditions are characterised by lower pressures west of Iceland and higher pressures over southern Europe. However, due to the wave-atmosphere coupling, this pressure gradient is slightly reduced (Figure C.2a). This reduction can be traced directly to the enhancement of the roughness length (Figure C.2e) since the surface roughness determines the ageostrophic wind component, responsible for cross-isobar mass transport. This corresponds to the results found by Lionello et al. (1998), Janssen et al. (2002) and Wu et al. (2017). Additionally, the wind speed at 10 m is reduced over the coupled ocean surface (Figure C.2c), which can also be attributed directly to the enhanced surface roughness (Figure C.2e). This similarly corresponds to several previous studies (e.g.,

Doyle, 1995; Lionello et al., 1998; Wahle et al., 2017). While the MSLP changes spread over the whole model area, the effect of the reduced wind speed is mostly limited to the coupled model area. The significant wave height is accordingly reduced with the wind speed (Figure C.2g). The largest reduction is observed between Norway, Great Britain and Iceland. In this area, the significant wave height, wind speed and roughness length in the reference simulation are the largest, and consequently, the roughness length is considerably enhanced, which results in the largest wind speed and the greatest significant wave height reduction. Smaller reductions in wind speed occur in the Bay of Biscay, the southeastern North Sea and the Baltic Sea, especially in the northern and southern Baltic Sea. The largest part of these small wind speed reductions can be traced to the weaker winds and smaller significant wave heights in those areas, leading to smaller roughness lengths and therefore smaller reductions in wind speed. This leads to a pattern featuring the whole southern North Sea having a relatively small reduction in wind speed, but along the British coast, the reduction in wind speed is larger than in the rest of the North Sea. Moreover, the impacts of the coupling extend further upwards. At 850 hPa, the change in geopotential displays a similar pattern as the change in MSLP with a reduction over the European continent and an increase between Iceland and Scotland (Figure C.S1a). This pattern leads to a reduced geopotential gradient since the geopotential is higher over the southeastern part of the model domain and lower over the northwestern part. At a height of 500 hPa, this pattern is still visible, but the increase in the geopotential between Iceland and Scotland is larger than the decrease over the continent (Figure C.S1c), which is contrary to the changes in the 850 hPa geopotential and MSLP. Nevertheless, this pattern can be interpreted as a reduction in the geopotential gradient at 500 hPa.

Ensemble simulations are conducted with the aim of making conclusions about the significance of differences between the coupled and reference simulations in comparison with the internal variability of the models. This is carried out in order to distinguish whether the coupling has a significant effect on the atmosphere or the impacts are within the range of internal variability of the atmospheric model. To ascertain the significance of these changes, for each grid cell and time step, it is determined whether cpl.nsn and ref.nsn differ significantly from each other using a t-test with a significance interval of 95 % (Janssen and Viterbo, 1996; Weisse et al., 2000). With the results of the t-test for each grid cell and time step, the percentage of time in each grid cell where cpl.nsn and ref.nsn differ significantly from one another is calculated, and the results are shown in Figure C.2b, C.2d, C.2f and C.2h. For the results presented in Table C.2, the mean values over the different areas are calculated. This analysis reveals that cpl.nsn and ref.nsn differ

significantly during the majority of the study period not only for parameters close to the surface but also for parameters in higher parts of the atmosphere.

The enhancement of the roughness length is significant 89 % of the time within the whole coupled area (Figure C.2f and Table C.2). This is also the case for the Baltic Sea, whereas in the North Sea, the Norwegian Sea and the North Atlantic Shelf, the changes are significant more than 90 % of the time. Regarding the wind speed, the differences between ref.nsn and cpl.nsn are significant 71 % of the time within the whole coupled area (Figure C.2d). Again, the Baltic Sea has the lowest value with just under 70 %, while the other three areas have significant changes in wind speed due to the coupling for approximately 72 % of the study period. For the roughness length and wind speed, the significance of changes decline outside the coupled area, while for the MSLP, significant changes are observed over the entire model area (Figure C.2b). In the case of the MSLP, the changes due to coupling are significant 75 % of the time within the whole coupled area. As before, the Baltic Sea has the smallest value with 74.86 % out of the four areas analysed, while the North Sea has the largest value with significant changes 80.17 % of the time due to the coupling. The percentages of time in the Norwegian Sea and the North Atlantic west of the British Isles range between the values in the Baltic and North Sea.

The changes in significant wave height are significant 93 % of the time within the whole model area (Figure C.2h). In the Baltic Sea, this percentage is reduced to 80.22 %, and in contrast to the other parameters, the North Sea has lower values than those elsewhere with significant changes almost 90 % of the time. For the Norwegian Sea and the North Atlantic

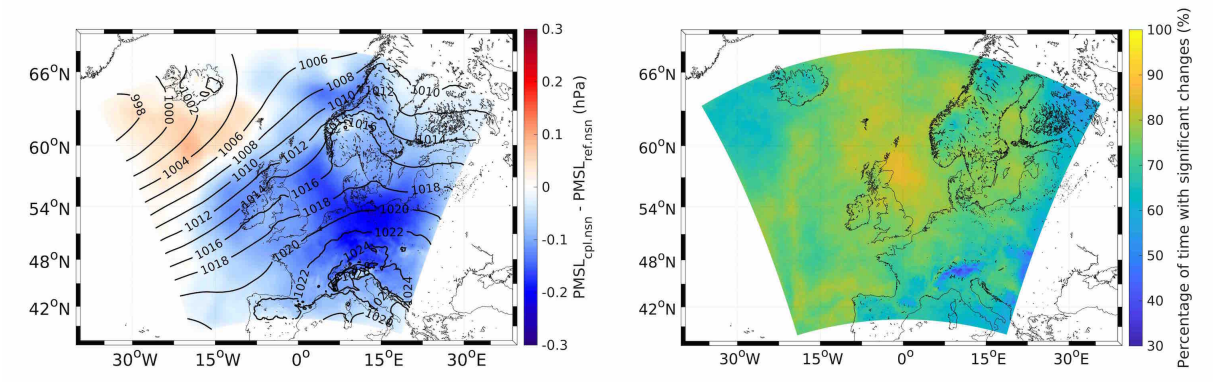

(a) **(b)**

Figure C.2: Continued on the next page.

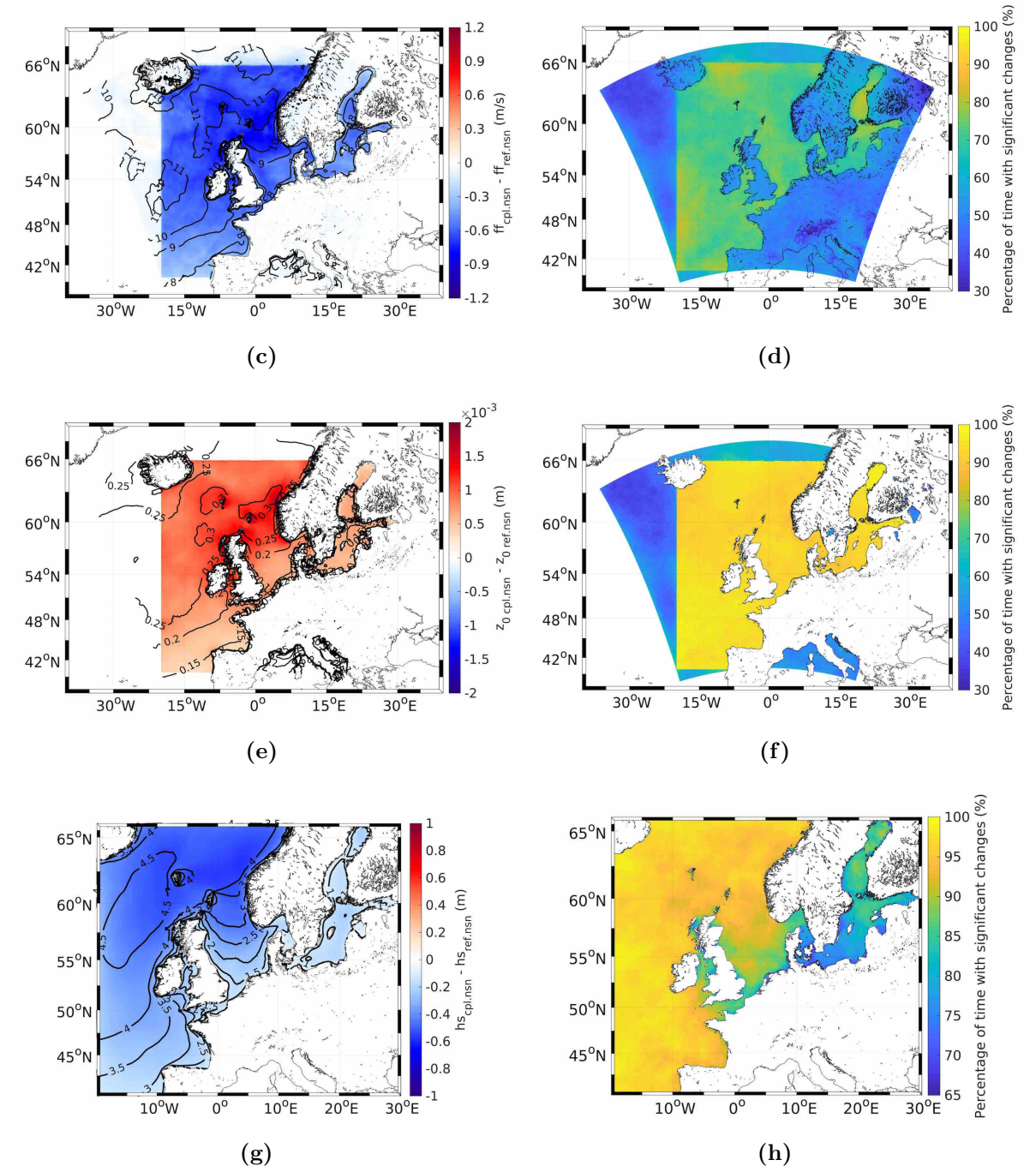

Figure C.2: Mean values over 3 months of the MSLP (a), wind speed (c), roughness length (e) and significant wave height (g). The contours reflect the values of the reference simulation, while the colours represent the difference between the coupled (cpl.nsn) and reference (ref.nsn) ensembles for the ensembles without spectral nudging. The percentage of time with significant differences between the coupled and reference ensembles in the MSLP (b), wind speed (d), roughness length (f) and significant wave height (h) are also shown (Note the different colour bar range for (h)).

Shelf, which are more exposed to higher significant wave heights and larger changes, the changes are significant for approximately 93 % of the study period.

The coupling also has significant impacts higher in the atmosphere. At 850 hPa, the changes are significant 73 % of the time (Figure C.S1b). The changes are significant for the most time within the North Sea region and for the least amount of time in the Baltic Sea, whereas the other two areas have values between those in the North and Baltic Seas. The time with significant differences between cpl.nsn and ref.nsn reduces with increasing height. At 500 hPa, the time characterised by significant differences averaged over the whole coupled area is 70.76 % (Figure C.S1d). The longest percentage of time with significant changes is detected in the Norwegian Sea at 76.1 %, while the percentages in the North Sea and the North Atlantic Shelf are 73.39 % and 73.49 %, respectively. The shortest amount of time with significant changes is again found in the Baltic Sea at 68.25 %. Hence, it can be concluded changes in roughness length still lead to significant changes higher in the atmosphere.

Table C.2: Time with significant differences between the coupled (cpl.nsn) and reference (ref.nsn) ensembles (%).

Variable	**Coupled area**	**North Sea**	**Baltic Sea**	**Norwegian area**	**Atlantic shelf**
MSLP	75.49	80.17	74.86	78.54	76.47
Wind speed	70.82	72.28	69.78	72.03	71.98
Roughness length	89.11	92.22	89.39	91.57	93.46
Significant wave height	93.22	89.99	80.22	92.81	93.42
Geopotential at 500 hPa	70.76	73.39	68.24	76.10	73.49
Geopotential at 850 hPa	72.95	78.27	72.70	76.66	74.10

C.3.1.1 Probability of Ensemble Differences

Figure C.3 shows histograms of the probability of differences between ref.nsn and the cpl.nsn for the four study areas over the whole study period. In general, the wind speed is reduced in cpl.nsn compared to ref.nsn since energy is needed for wave growth. These strengthened waves subsequently enhance the surface roughness, which leads to a reduction in wind speed. However, the magnitude of this reduction varies among the four areas.

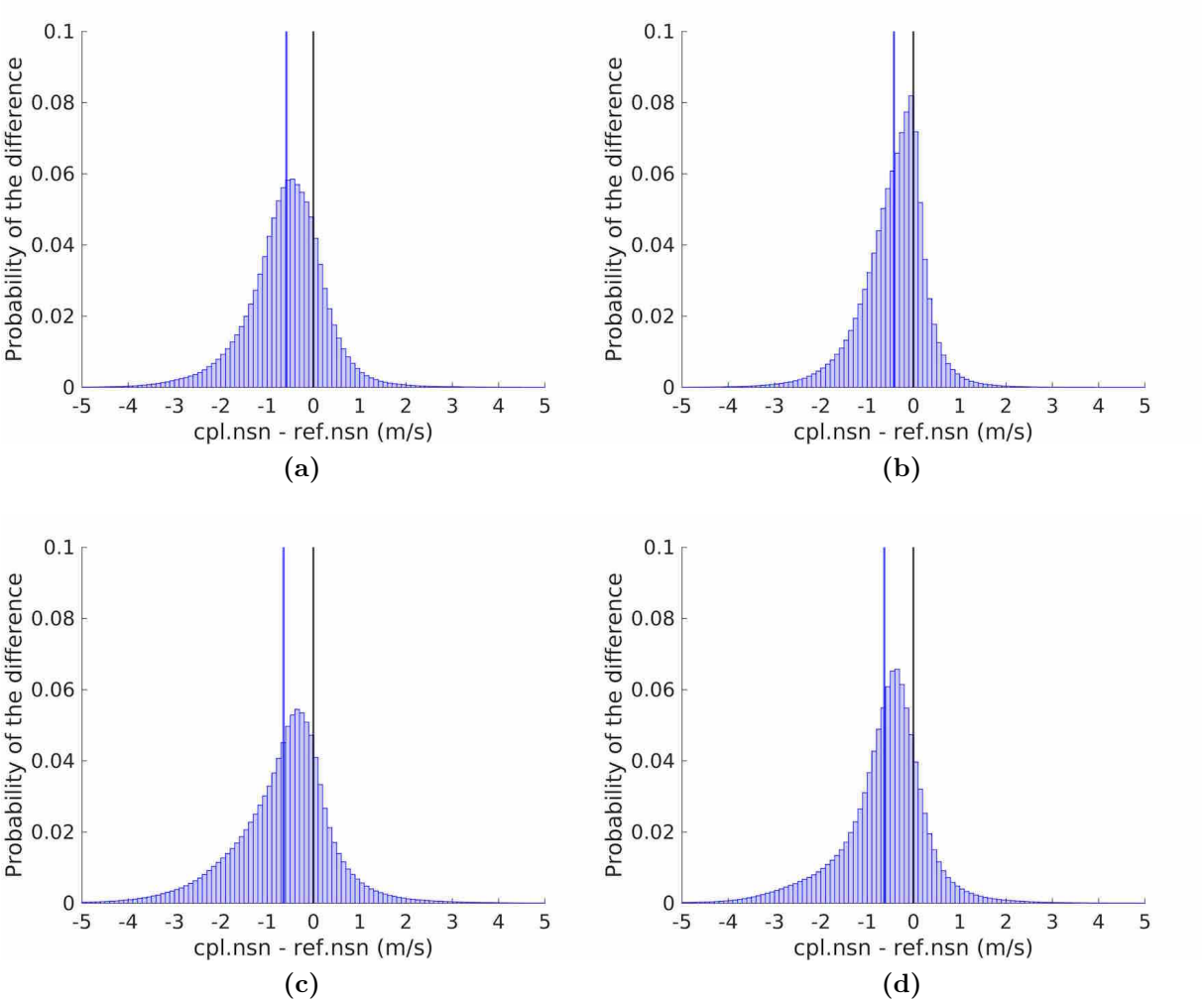

Figure C.3: Histogram of the difference in the wind speed between the coupled (cpl.nsn) and reference (ref.nsn) ensembles within the North Sea (a), the Baltic Sea (b), the southern Norwegian Sea (c) and the North Atlantic Ocean west of the British Isles (d). The blue line indicates the mean of the distribution, and the black indicates the zero line.

The mean reductions in the wind speed within the Norwegian Sea and the North Atlantic Ocean west of the British Isles are very similar with values of $-0.64\,\mathrm{m/s}$ (Figure C.3c) and $-0.63\,\mathrm{m/s}$ (Figure C.3d), respectively. In the North Sea, the mean reduction is $-0.58\,\mathrm{m/s}$ (Figure C.3a), while the Baltic Sea has the smallest mean reduction of $-0.42\,\mathrm{m/s}$ (Figure C.3b). These differences can be explained by the significant wave heights in these areas (Figure C.4). The Baltic Sea is a very sheltered area surrounded by coastline on all sides. Therefore, the fetch is very limited, and only swells travelling north-south can become larger. Due to mostly short fetches, the wave field cannot develop fully at higher wind speeds, as the distance to the coast is too short. For a fully developed sea state

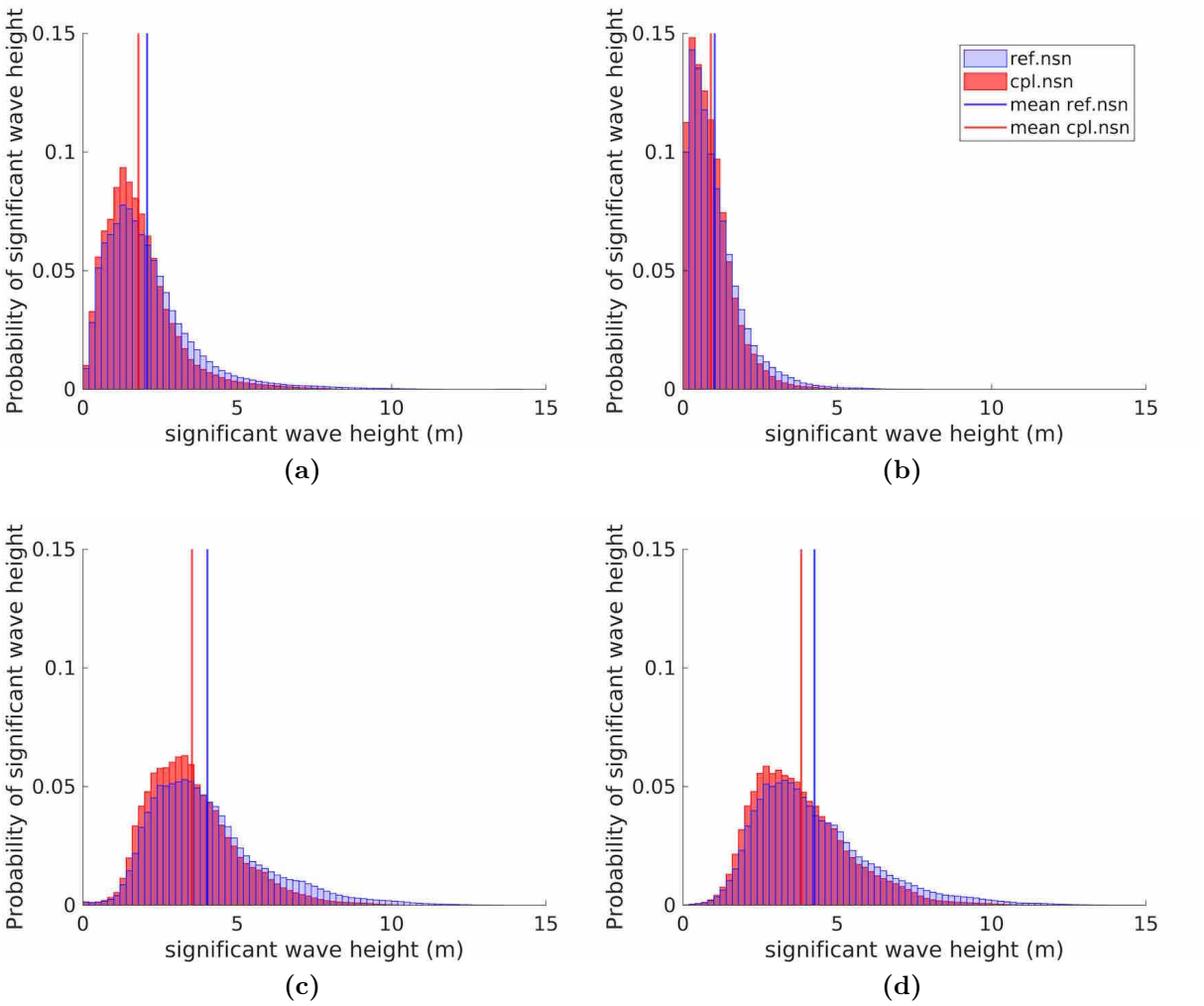

Figure C.4: Histogram of the significant wave heights of the reference (ref.nsn) and coupled (cpl.nsn) ensembles within the North Sea (a), the Baltic Sea (b), the southern Norwegian Sea (c) and the North Atlantic Ocean west of the British Isles (d).

at a wind speed of 20 m/s, a fetch well exceeding 1000 km is needed (Komen, 2002), which is far greater than the Baltic Sea can provide in most directions. Therefore, winds provide less energy and momentum to waves, and thus, the waves cannot reach their full height, which results in smaller wind speed reductions. Another aspect of wave growth important for fully developing the sea state is the wind speed and the duration of wind speeds. Full development takes more time for high wind speeds, than low wind speeds. The mean wind speed within the Baltic Sea being smaller than those in the other areas (Figure C.2c), contributes further to smaller significant wave heights and hence smaller reductions in the roughness length and wind speeds in the Baltic Sea. The distribution

of the significant wave height in the Baltic Sea shows a peak at 0.4 m with 99 % of all significant wave heights below 4.2 m (Figure C.4b). Since the significant wave heights are small, the roughness length is short. Hence, the wind speed changes are small when small significant wave heights occur. In the North Sea, the significant wave heights are larger than those in the Baltic Sea (Figure C.4a). The North Sea is open to the Atlantic Ocean in the north and accesses the Atlantic in the west through the English Channel. Through these openings, especially that in the north, large swells can enter the North Sea. Furthermore, the fetch in the North Sea is larger than that in the Baltic Sea. Since large significant wave heights occur, the impacts of the coupling are larger in the North Sea than in the Baltic Sea. The largest impacts, however, occur in the areas that are truly exposed to the open ocean, such as the Norwegian Sea and the North Atlantic Ocean west of the British Isles. Significant wave heights up to 17.87 m in the reference ensemble and 13.53 m in the coupled ensemble occur. Furthermore, the mean significant wave heights in these areas are much larger at approximately 4 m compared with values of approximately 2 m and 1 m in the North and Baltic Seas, respectively. Since the Norwegian Sea and the North Atlantic Ocean are subject to the largest significant wave heights (Figure C.4), the impact of the coupling is the largest (Figure C.3). Due to the corresponding reductions in wind speed, the significant wave heights are reduced in the coupled ensemble in all four areas (Figure C.4).

The spreads of the distributions of the changes due to the coupling vary among the different areas. The Norwegian Sea and the North Atlantic Ocean west of the British Isles have the largest spreads with values of 1.11 m/s and 1.01 m/s respectively, since the significant wave heights in these areas similarly show the largest spreads. Small significant wave heights occur during phases with low wind speeds, but very large significant wave heights can be present during stormy periods, when waves are given sufficient time and long fetches to develop. In the North Sea, the spread of the distribution is 0.86 m/s, while that in the Baltic Sea is 0.71 m/s. These small spreads are due to the limited wave growth in these areas due to the fetch and water depth conditions. Thus, the largest significant wave heights in the Norwegian Sea and the North Atlantic Shelf cannot develop in the North and Baltic Seas. Therefore, the spreads of the significant wave height are smaller in the North and Baltic Seas, resulting in smaller distributions of changes in the wind speed. Therefore, the coupling has the largest impacts on the Norwegian Sea and the North Atlantic Ocean west of the British Isles, followed by the North Sea, while the smallest impact is found on the Baltic Sea.

The mean MSLP difference between cpl.nsn and ref.nsn tends towards lower pressures in the coupled ensemble than in the reference ensemble (Figure C.5). This trend is the largest in the North Sea and might be related to the geography of the North Sea, which is generally positioned between a low-pressure system moving through the area to the north and a high-pressure system moving over the continent but is more influenced by the reduction in the pressure over the continent (Figure C.2a). Since the general change in MSLP constitutes a reduction in the pressure gradient, both reduced and enhanced MSLPs can be found due to the coupling between the wave and atmospheric models in all

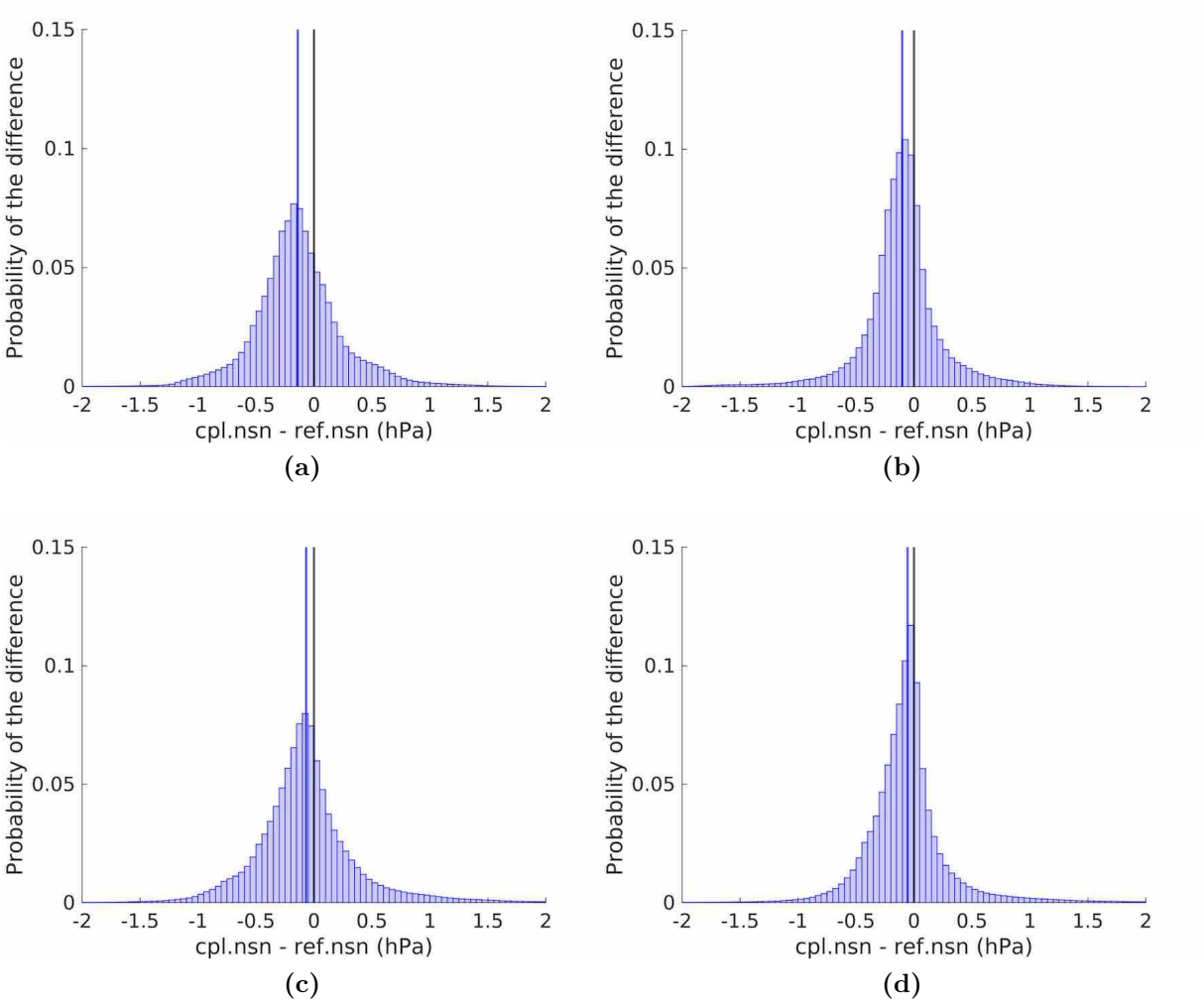

Figure C.5: Histogram of the MSLP difference between the coupled (cpl.nsn) and reference (ref.nsn) ensembles within the North Sea (a), the Baltic Sea (b), the southern Norwegian Sea (c) and the North Atlantic Ocean west of the British Isles (d). The blue line indicates the mean of the distribution, and the black indicates the zero line.

four areas. In particular, the Norwegian Sea and the North Atlantic Ocean are situated along the border between increasing and decreasing pressure (Figure C.2a). This is further reflected in the distribution of the MSLP differences in, where the mean is very close to zero and the distributions are spread similarly in positive and negative sectors (Figure C.5c and C.5d). The Baltic Sea is again the least influenced by the coupling (Figure C.5b) since the waves are smaller in this area (Figure C.4b), influencing the winds less (Figure C.3b).

C.3.1.2 Ensemble Spread

The standard deviation (Equation C.3) between the ensemble members is regarded as the spread of the ensemble, which is a measure for the internal variability of the system (Ho-Hagemann et al., 2020):

$$Sdt = \sqrt{\frac{1}{N-1}\sum_{i=1}^{N}(x_i - \overline{x})^2} \tag{C.3}$$

where $\{x_1, x_2, x_3, ..., x_N\}$ are the values of each ensemble member for a given variable, $\overline{x}$ represents the mean of the ensemble for the variable and N is the number of members of the ensemble, which is 10 in this study.

The probabilities of the standard deviation of the ensembles of the 10 m wind speed, MSLP and significant wave height are shown in Figure C.6. In general, the ensemble spread in cpl.nsn is smaller than that in ref.nsn, with larger probabilities for small standard deviations and smaller probabilities for larger standard deviations. This change is near the mean standard deviation of both ensembles (vertical lines).

The mean of the standard deviation of wind speed in ref.nsn is 0.37 m/s, and that in cpl.nsn is 0.35 m/s, which constitutes a reduction of 7.46 % (Table C.3). The reduction in the 99th percentile is 10.53 %, but the largest reduction is found in the maximum of the ensemble spread with 23.48 %. This shows that the spread in cpl.nsn is generally smaller than that in ref.nsn. Hence, due to the reduction in internal variability, the uncertainty in the coupled system is reduced compared to the reference model.

The MSLP spread in the ensembles is generally quite low (Figure C.6b) with a mean of approximately 0.14 hPa (Table C.3). The maximum spread is reduced by 9.14 % due to

the wave-atmosphere coupling. Therefore, although the internal MSLP variability of the ensembles is already very low, the maximum internal variability can still be reduced due to the coupling.

The variability of the significant wave height due to the wind speed variability is generally quite low at 5 cm in the reference ensemble and 3 cm in the coupled ensemble (Figure C.6c and Table C.3). The maximum spread, however, can be quite large (up to 2.68 m in the reference simulation). This spread is considerably reduced by 36.35 % to 1.71 m due to the coupling and the related reduction in the wind speed uncertainty within the atmospheric model (Figure C.6a and Table C.3).

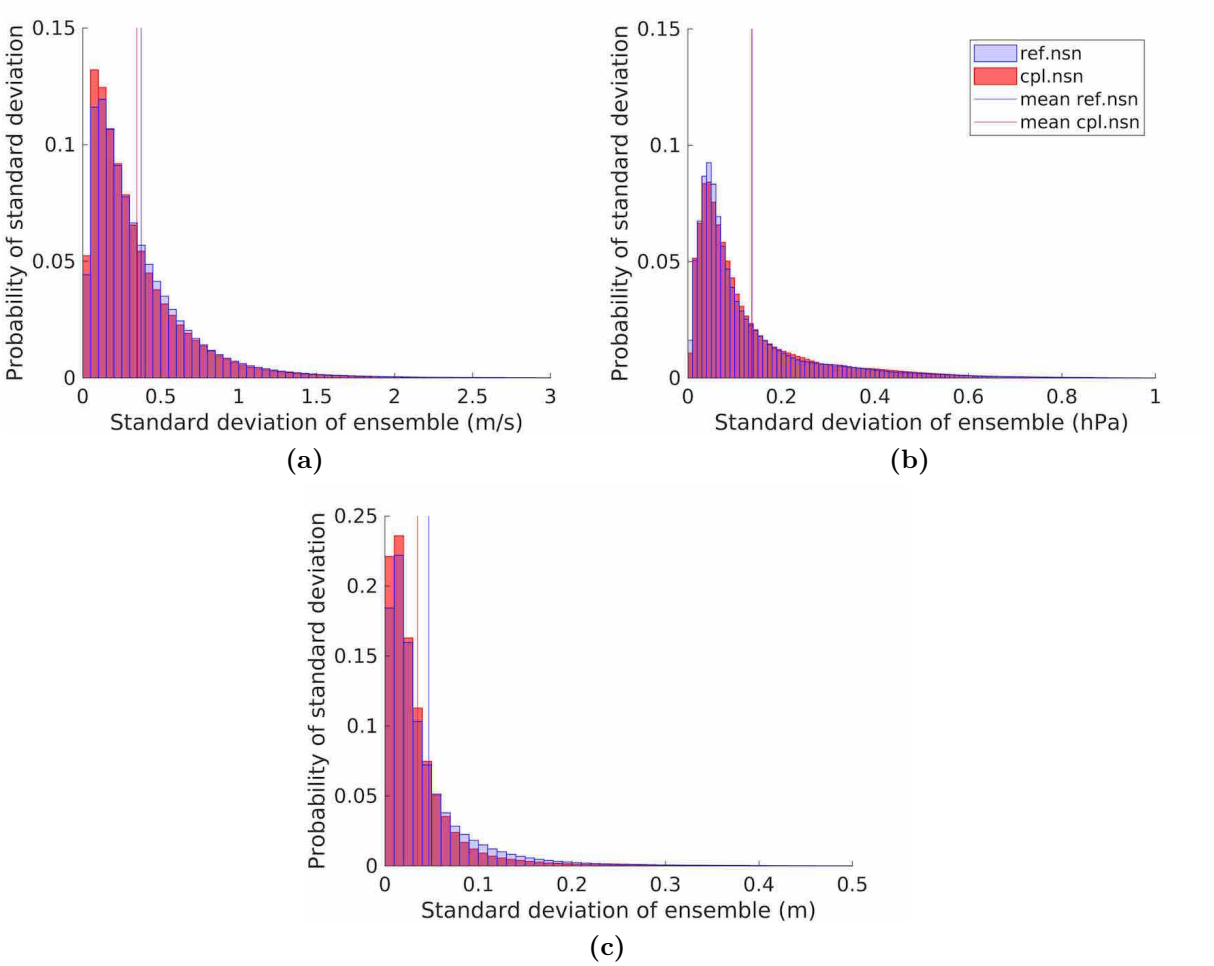

Figure C.6: Histogram of the standard deviation of the reference (ref.nsn) and coupled (cpl.nsn) ensembles within the North Sea for the wind speed (a), MSLP (b) and significant wave height (c).

In summary, coupling the wave model to the atmospheric model reduces the ensemble spread and therefore also the internal variability of the atmospheric model. In addition, the wave model profits from the reduction in wind speed variability with less variability of the significant wave height.

Table C.3: Evaluation of ensemble spread.

		Mean	**99th percentile**	**Maximum**
Wind speed	ref.nsn (m/s)	0.37	1.88	8.70
	cpl.nsn (m/s)	0.35	1.68	6.66
	Relative change (%)	-7.46	-10.53	-23.48
MSLP	ref.nsn (hPa)	0.14	0.80	4.63
	cpl.nsn (hPa)	0.14	0.71	4.21
	Relative change (%)	-0.58	-11.75	-9.14
Significant wave height	ref.nsn (m)	0.05	0.34	2.68
	cpl.nsn (m)	0.03	0.21	1.71
	Relative change (%)	-25.56	-39.14	-36.35

C.3.2 Temporal Evolution

After generally assessing the impacts of the wave-atmosphere coupling in comparison with the internal variability of the atmospheric model, a temporal analysis is performed. Figure C.7 presents the average wind speed, MSLP and significant wave height in the reference ensemble within the North Sea, which is the area the main analysis is conducted for. Furthermore, the absolute value of the mean differences between the coupled and reference ensembles are depicted along with the spread of the ensembles. This analysis is conducted in order to estimate under which conditions the spread of the ensembles and, therefore, the internal variability, as well as the effects of the coupling become large. Furthermore, this shows whether the ensemble spread or the effects of the coupling are larger and whether during events with high impacts by the coupling, the influence of the waves on the atmosphere is still larger than the internal variability of the atmospheric model. The analysis generally shows that the differences between cpl.nsn and ref.nsn are larger than the internal variability. Thus, the effects of the coupling can be clearly differentiated from the internal variability of the model. Furthermore, the internal variability is reduced in cpl.nsn compared to ref.nsn, especially when the internal variability is large.

A peak in difference between cpl.nsn and ref.nsn can be detected simultaneously with the

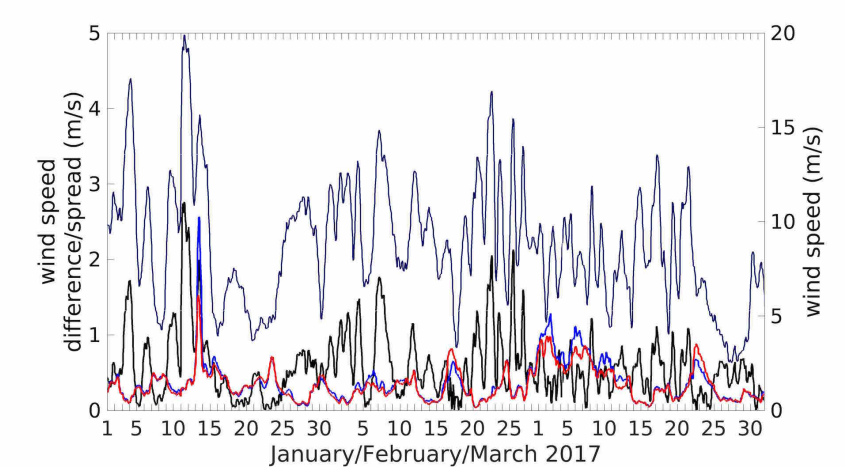

(a)

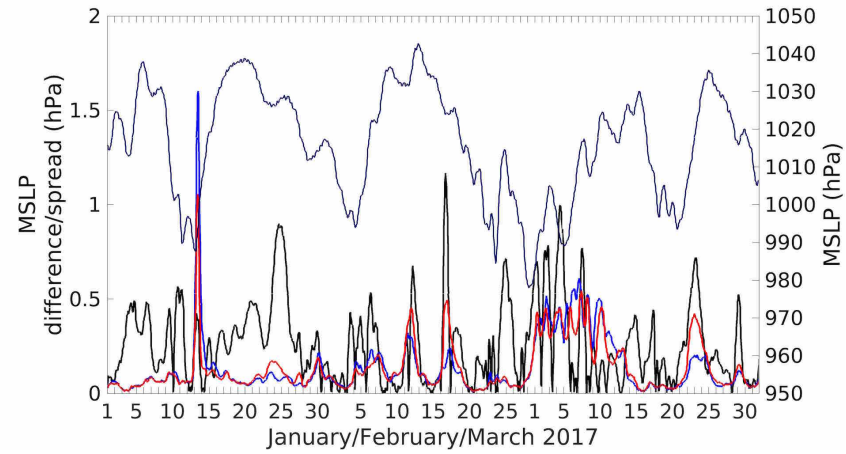

(b)

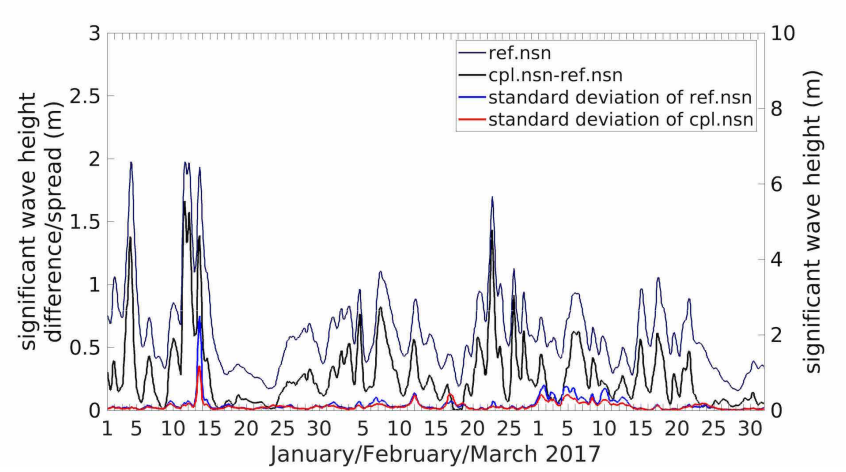

(c)

Figure C.7: Time series of the absolute differences in the ensemble means (black), standard deviations of the ensembles (red and blue) and values in the reference ensemble (ref.nsn, dark blue, right y-axis) in the North Sea for the wind speed (a), MSLP (b) and significant wave height (c).

peak wind speed in ref.nsn (Figure C.7a). This indicates that at higher wind speeds, the impact of the coupling between the two models is larger than that at lower wind speeds. At high wind speeds, the sea state needs more time to reach a fully developed state, and before that, the transfer of momentum and energy from the atmosphere to the waves is larger than when the sea state is already fully developed. Moreover, the roughness length is larger for young, developing waves than for old, mature waves, and thus, when the sea state is fully developed, the roughness length becomes smaller, and less energy is transferred from the atmosphere to the waves (Wu et al., 2017). The largest impacts of the coupling on the wind speed and significant wave height appear on 11 January, and the largest internal variability is identified two days later. This event is analysed in more detail in Section C.5.

During the majority of the simulation period, the difference between cpl.nsn and ref.nsn is larger than the internal variability (Figure C.7a), which corresponds to significant changes by the coupling approximately 70 % of the time (Figure C.2d). This is especially the case when the wind speed is high and when the differences between the coupled and reference ensembles are larger. Therefore, when the coupling has large impacts on the atmosphere by reducing the wind speed, the internal variability is still small, and the differences between the ensemble means can be differentiated from the internal variability of the atmospheric model and traced back as impacts of the coupling. Furthermore, events can occur during which the internal variability becomes larger than the differences between the ensemble means, and as a result, the ensembles cannot be differentiated from one another. Nevertheless, only sporadic events occurred during our study period, whereas the times when the differences between the ensemble means are larger than the ensemble spread are dominant. Furthermore, during events with large internal variability, the uncertainty is reduced in cpl.nsn compared to ref.nsn, which is in accordance with the results of Figure C.6.

Since the initial and boundary conditions and the wave model set-up are identical for all simulations, the variability of the wave model is attributable to the different winds in the atmospheric model initiated with different initial conditions. The variability in the wave model, however, is very small most of the time (Figure C.7c). Only in very few events is the variability of the significant wave height increased, which is due to an increase in the wind speed variability within the atmospheric model. Therefore, when the internal variability for wind speed is reduced due to the coupling, the variability of the significant wave height is reduced as well. The differences in the significant wave height between

cpl.nsn and ref.nsn follow the curve of the significant wave height in ref.nsn in the area. This indicates that the coupling impacts are larger for situations with large significant wave heights and smaller for situations with small significant wave heights. The impacts of the coupling in this case can be very clearly differentiated from the variability of the significant wave height, which is in accordance with the differences between ref.nsn and cpl.nsn being significant 93 % of the time (Figure C.2h).

Examining the MSLP time series reveals a similar scenario (Figure C.7b). Here, like for the wind speed and significant wave height, the differences between cpl.nsn and ref.nsn are larger than the internal variability of the ensembles most of the time and can be differentiated from one another, especially when large differences between the two ensembles are present, even though events can occur during which the internal variability and the ensemble difference have the same magnitude or the internal variability is larger than the differences. In addition, although events sometimes occur where the internal variability is increased in cpl.nsn compared to ref.nsn, during events with large internal variability of the MSLP, the uncertainty is smaller in cpl.nsn than in ref.nsn. Furthermore, the peaks of differences between cpl.nsn and ref.nsn are not always correlated with significant wave height peaks and hence changes in the roughness length (e.g., on 25 January 2017 and 30 March 2017). Therefore, the wave-atmosphere coupling can have impacts on the MSLP that are not directly linked to the change in the roughness length at that location and time, but are due to lasting effects of the coupling on the atmosphere. The findings for the North Sea exist in the other three study areas in a similar way (Figure C.S3, C.S4 and C.S5).

While the main effects of the coupling on the wind speed and the significant wave height are reductions, for the MSLP, increases are also common. The method used here takes the absolute value of the mean of the difference among the areas of interest. Therefore, increases and decreases cancel each other out, which constitutes a conservative approach to assessing the magnitudes of the differences between the ensembles. Another approach was tested in which the mean of the absolute differences among the areas and was found to differ only marginally from the approach used herein.

C.3.3 Comparison With Measurements

To investigate whether the wave-atmosphere coupling improves the realism of the observations, the results of the ensemble simulations are compared with wind speed and

significant wave height measurements. In this study, Sentinel-3A satellite measurements are used in conjunction with in situ GTS station measurements. The combination of satellite and in situ data is highly complementary since the satellite data have good spatial coverage and the in situ data possess good temporal coverage. The general agreement between the measurements and the ensemble means is good but can still be improved with the wave-atmosphere coupling (Figure C.8).

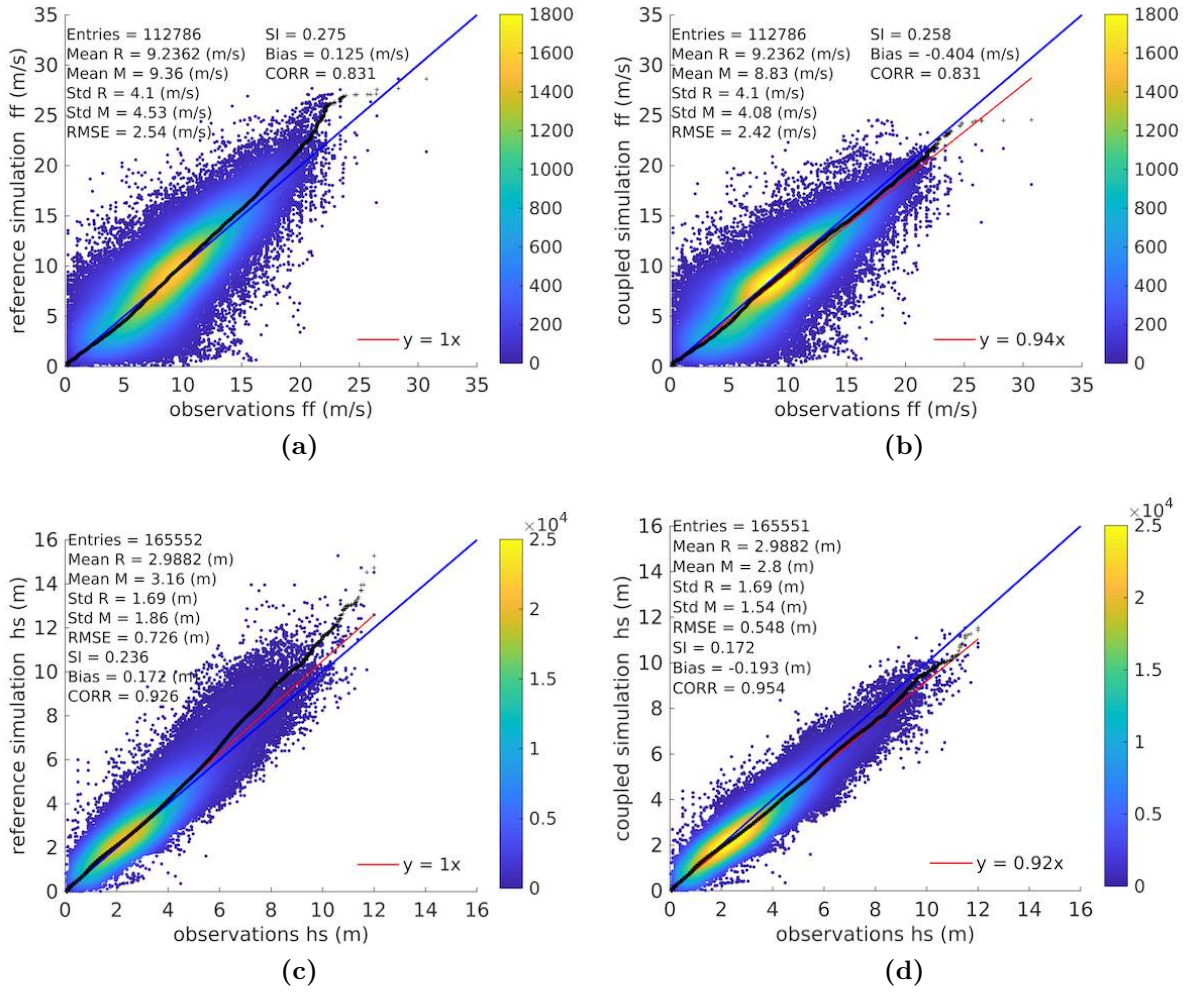

Figure C.8: Q-Q scatter plots for the measured (Sentinel-3A and GTS) (reference, R) and modelled (M) wind speeds (a,b) and significant wave heights (c,d) with the reference (ref.nsn) (a,c) and coupled (cpl.nsn) (b,d) ensemble model simulations. The Q-Q plot is shown as black crosses, the 45° reference line is denoted by the blue line, and the least-squares best-fit line is the red line. The equations for the statistical values are provided in the Supplementary Material.

Especially for wind speeds below 7 m/s, the results of both ensembles are very similar to the observations (Figure C.8a and C.8b). Beyond that, however, differences begin to show. As in the times series, the most obvious differences between cpl.nsn and ref.nsn can be detected in high wind speed areas. The wind speed in cpl.nsn is reduced compared to that in ref.nsn, which leads to better agreement with the observations. By taking the wave effects on the roughness length into account, the realism of the model simulations is enhanced. The parameterisation of the roughness length in the atmospheric model accounting for only the wind speed neglects the variety of wave states and development phases of the sea state at similar wind speeds, which the wave model can depict (Wu et al., 2017). This weakness of the atmospheric model becomes more apparent at higher wind speeds. Thus, the coupling leads to an improved realism of the atmospheric model. This weakness can likewise be detected in comparisons between the measurements and ensemble means of the significant wave height (Figure C.8c and C.8d). These differences begin to appear for significant wave heights above 2 m and are especially large for extreme significant wave heights. Although cpl.nsn tends to slightly underestimate large significant wave heights, the agreement between the measurements and cpl.nsn is better than the agreement between the observations and ref.nsn. Mainly the scatter index (SI, Equation C.S5) in significant wave height can be reduced in the coupled ensemble compared to the reference ensemble by 6.4 %, hence, increasing the correlation (CORR, Equation C.S7) by 2.8 % indicating, that the scatter in the comparison between observed and modelled significant wave height is decreased. Furthermore, the root-mean-square error (RMSE, Equation C.S4) is reduced in the coupled ensemble by 18 cm compared to the reference ensemble. This is to some degree also visible in the wind speed with a reduction of the SI of 1.7 % and RMSE of 0.12 m/s.

C.4 Sensitivity of Coupling to the Application of Spectral Nudging and Different Boundary Conditions in CCLM

C.4.1 Sensitivity to Spectral Nudging

In the atmospheric model, spectral nudging can be enabled to keep the large-scale atmospheric state close to the forcing data, while regional-scale details are permitted to develop conditioned by the large scales. This method is used for regional and local reconstructions or impact studies, where the representation of the exact weather situation

is vital. Furthermore, this method suppresses the internal variability of regional models (von Storch et al., 2000; Weisse and Feser, 2003; Schaaf et al., 2017). Therefore, simulations with spectral nudging are usually reliably closer to observations than those without spectral nudging. On the other hand, this approach might suppress the effects of the coupling (Ho-Hagemann et al., 2020). As shown in the previous Section C.3, the wave-atmosphere coupling has a positive effect on freely evolving regional models forced only at the lateral boundaries. In this section, it is investigated whether these effects can also be detected in simulations using spectral nudging in the atmospheric model. Hence, we perform a comparison between the effects of the coupling with and without spectral nudging enabled in the atmospheric model. This comparison is conducted mainly for the North Sea. The results show that the coupling has significant impacts on the atmosphere, resulting in better agreement with observations in simulations where spectral nudging is used, with similar impacts of the coupling on the atmosphere as in simulations without spectral nudging.

The wind speed differences in the ensembles with and without spectral nudging are very similar (Figure C.9a). The spread of the distribution is smaller for the ensemble with spectral nudging (0.73 m/s) than for the ensemble without spectral nudging (0.86 m/s). This demonstrates that the most extreme coupling effects are smaller in the simulation with spectral nudging, but the general effect is very similar to the effects in the simulation without spectral nudging. For the MSLP, however, this influence is more pronounced than for the other parameters (Figure C.9b). Since spectral nudging keeps the larger scales in position, the variability of the MSLP is kept low. Therefore, the coupling tends to reduce the MSLP rather than shift the pressure systems or reduce the pressure gradient.

The internal variability is reduced due to spectral nudging (Figure C.9c and C.9d) compared to the internal variability of the ensemble without spectral nudging (Figure C.6a and C.6b). This has been shown before in several studies (e.g., Weisse and Feser, 2003). The reduction in internal variability due to the coupling, which has been demonstrated in the previous section for simulations without spectral nudging (Section C.3.1.2), can still be detected in the simulations with spectral nudging (Figure C.9c and C.9d and Table C.S1). Therefore, the wave-atmosphere coupling reduces the internal variability even further, which supports the supposition that introducing the wave model reduces the model uncertainty of the atmospheric model.

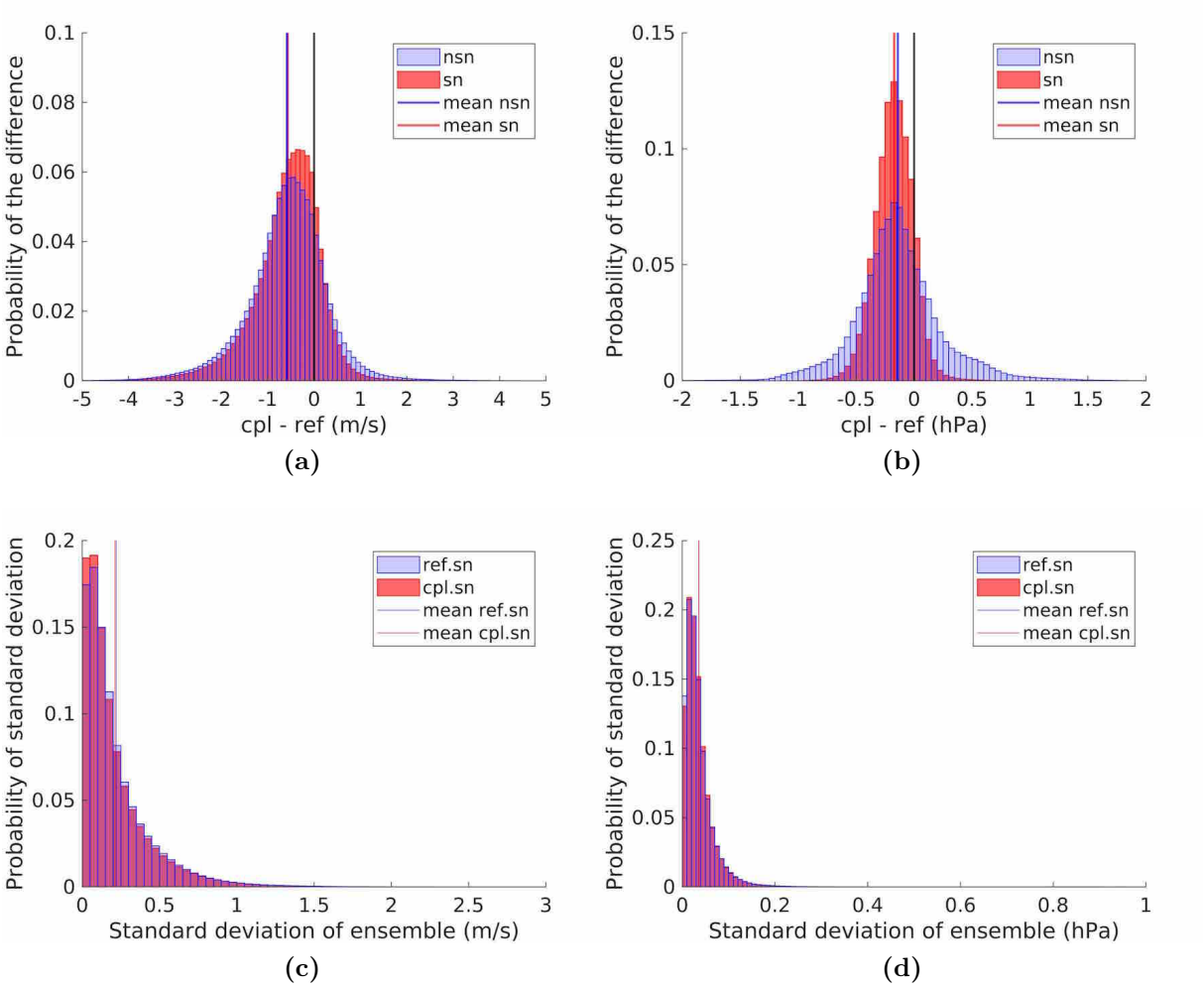

Figure C.9: Histogram of the differences between the coupled and reference ensembles in the wind speed (a) and MSLP (b) within the North Sea, as well as the standard deviation of the reference and coupled ensembles within the North Sea area for the wind speed (c) and MSLP (d).

Weisse and Feser (2003) found that the internal variability appears to be small in ensembles both with and without spectral nudging most of the time and is increased during some periods only in the ensemble without spectral nudging. We detect a similar effect upon examining the time series (Figure C.S2a, C.S2c and C.S2e). Nevertheless, we discover that the coupling effects on the wind speed (Figure C.S2a) and significant wave height (Figure C.S2e) are almost identical most of the time in simulations with and without spectral nudging. Therefore, although the large scales of the forcing data are kept in the regional model, the coupling of the wave model still influences the wind and wave fields

similar to the situation without spectral nudging. Furthermore, as in the simulations without spectral nudging, this coupling leads to better agreement with observations and especially reduces the overestimation of high wind speeds and significant wave heights (Figure C.S6). Hence, coupling the wave model to the atmospheric model enhances the realism of the model simulations also with spectral nudging enabled.

With regard to the impacts of the coupling on the MSLP, the application of spectral nudging in the atmospheric model has a larger impact (Figure C.9b and C.S2c). Here, the differences between the coupled and reference ensembles can be differentiated from each other. Most of the time, the impacts of the coupling are very similar, but during events with large differences between cpl.nsn and ref.nsn, these differences become smaller in the simulations with spectral nudging than in those without spectral nudging. Due to spectral nudging, the large-scale atmospheric state is kept close to the forcing data. Hence, the atmosphere has less freedom to develop, and therefore, the coupling impacts on the MSLP are smaller in the simulations with spectral nudging than in those without spectral nudging. Hence, spectral nudging has only a small impact on the effects of the wave-atmosphere coupling on the wind speed and significant wave height, while the effects of the coupling on the MSLP can be suppressed at times.

Furthermore, since the internal variability is reduced due to the inclusion of spectral nudging but the effects of the coupling remain almost identical, the percentage of time with significant changes due to the coupling is increased. The percentage of time that the MSLP is significantly changed is increased from 75.49 % in the ensemble without spectral nudging to 87.47 % in the ensemble with spectral nudging within the whole coupled model area. The increase in the percentage for the wind speed is approximately 4 % to 74.89 %, and that for the roughness length is approximately 2.5 % to 91.65 %. Additionally, in the higher parts of the atmosphere, the percentages of time with significant changes are similarly increased. The percentage of time with significant changes in the 850 hPa geopotential height increases by more than 10 % to 84.58 %, while that in the 500 hPa geopotential height increases by approximately 9 % to 79.03 % within the whole coupled area. Thus, in the ensemble simulations, where spectral nudging is used, the coupling has significant impacts on the atmosphere, resulting in better agreement with observations.

C.4.2 Sensitivity to Boundary Conditions

The boundary conditions for regional models are usually taken from global models to give realistic values at the lateral boundaries. Here, two different sets of reanalysis data are

used as the boundary forcing for the regional model. The boundary conditions can have large impacts on the results of regional model simulations (Déqué et al., 2007; Meißner, 2008; Kjellström et al., 2011; Keuler et al., 2016). Thus, in this study, the impacts of two different boundary conditions, namely, ERA5 and ERA-Interim, in the atmospheric model on the effects of the wave-atmosphere coupling are tested to assess whether the findings in Section C.3 are robust to different boundary conditions, which is found to be the case.

The general impact of the coupling between the atmospheric model and the wave model is very similar with both boundary conditions, as the distributions of the differences in the wind speed and MSLP are very similar for the ensembles with ERA5 and ERA-Interim boundary conditions (Figure C.10a and C.10b). Also the reduction in internal variability is still present with different boundary conditions (Figure C.10c and C.10d). Hence, the effects of the coupling are robust to different reanalysis data used as the boundary forcing (a more detailed analysis can be found in the Supplementary Material).

C.5 Case Study of an Extreme Event

The largest difference in the wind speed and significant wave height between cpl.nsn and ref.nsn is observed on 11 January 2017 (Figure C.7a), and the largest internal variability appears two days later. Therefore, this event is studied in more detail along with an analysis of the storm tracks of this low-pressure system.

The low-pressure system that passed over the North Sea during mid-January of 2017 formed as a secondary low in the Norwegian Sea. The secondary low was cut off from the main low-pressure system and made its way south across the North Sea, while the core of the main low-pressure system was filled and slowly moved eastwards (Figure C.S8, C.11 and C.12).

C.5.1 Differences in and Variability of the MSLP, Wind Speed, and Significant Wave Height

The largest difference in the wind speed between cpl.nsn and ref.nsn is observed on 11 January 2017 (Figure C.7a). At that time, the wind speed is approximately 20 m/s within

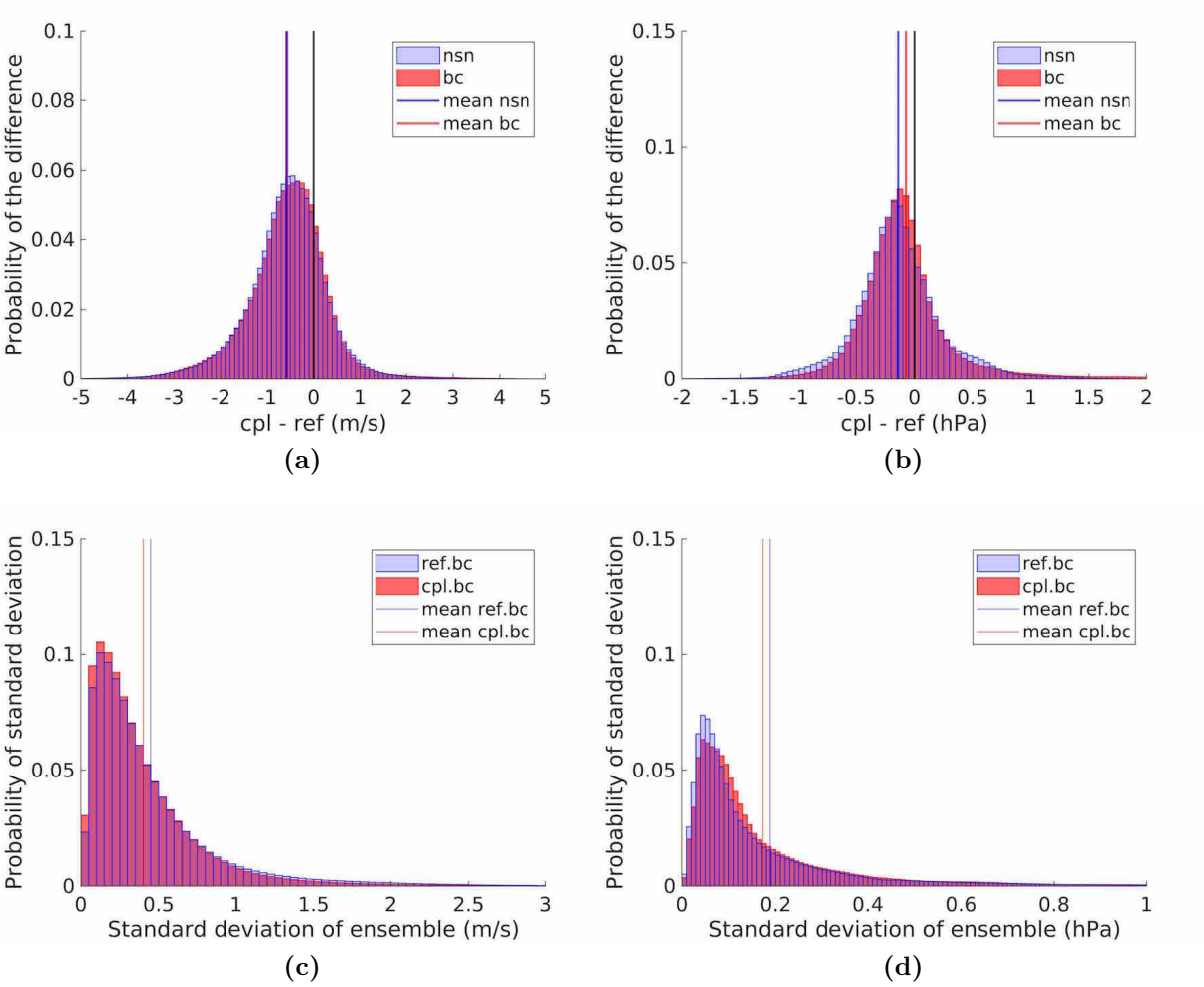

Figure C.10: Histogram of the differences between the coupled and reference ensembles in the wind speed (a) and MSLP (b) within the North Sea, as well as the standard deviation of the reference and coupled ensembles within the North Sea area for the wind speed (c) and MSLP (d).

the North and Baltic Seas. Since this wind speed is quite high, the reduction in the wind speed is also quite large, transferring energy from the atmosphere to the developing waves. The reduction in wind speed is fairly uniform. The internal variability is very small at that time and only slightly larger in ref.nsn than in cpl.nsn. This is very similar in the ensembles with spectral nudging and the changed boundary conditions (Figure C.S7). Due to the wave-atmosphere coupling, the pressure gradient is reduced at that time in all three ensembles. This reduction in the gradient is due to the enhanced surface roughness, which results in a larger ageostrophic wind component and leads to cross-isobar mass

transport from higher to lower pressures. This results in faster filling of the pressure system and hence a reduction in the pressure gradient. This finding is in accordance with previous studies (Lionello et al., 1998; Janssen et al., 2002; Wu et al., 2017). The reduction in the pressure gradient further adds to the reduction in the wind speed. The internal variability of the MSLP is very low in all ensembles, with slightly larger values in the reference ensembles than in the coupled ensembles (Figure C.S8). The reduction in wind speed ultimately leads to a reduced significant wave height. Although the amount of the wind speed reduction is fairly similar within the North and Baltic Seas and in the region between Iceland and Scotland, the decrease in the significant wave height is not uniform. The main attenuation of the significant wave height appears in the areas where the significant wave height peaks in the North Sea and the region between Iceland and Scotland. Since waves have the freedom to develop and are not limited by the fetch or water depth, the energy and momentum from the atmosphere can be converted into wave growth. Furthermore, the reduction in the significant wave height in the Baltic Sea is much smaller than the reductions in the other areas due to fetch limitations. The internal variability of the significant wave height is very low. This scenario is present in all three ensembles, with very slight variations in the magnitude of the difference between the coupled and reference ensembles (Figure C.S9).

The event with the largest internal variability during the study period is observed two days later (Figure C.7). At that time, the centre of the low-pressure system is located directly over the North Sea (Figure C.11) with a convergence zone extending from the centre of the low-pressure system to the British coast and a wind speed front embedded in that extending north-south over the North Sea (Figure C.S10). The overall changes in the MSLP in both ensembles without spectral nudging again reflect a reduction in the pressure gradient (Figure C.11a and C.11c), although other variations can also be detected. One of them is, that the location of this convergence zone differs among the ensembles. The internal variability is quite high in ref.nsn but is reduced in cpl.nsn (Figure C.S11d and C.S11g). Nevertheless, this large internal variability is concentrated in the centre of the secondary low in the North Sea, while the difference between ref.nsn and cpl.nsn spreads out considerably over the whole area. In the ensemble with the ERA-Interim boundary conditions, the internal variability is substantially diminished (Figure C.S11f and C.S11i). In the ensemble with spectral nudging, the internal variability of the MSLP is very low (Figure C.S11e and C.S11h), but the differences between cpl.sn and ref.sn are slightly different from those between the ensembles without spectral nudging. However, a shift in the location of the convergence zone can still be detected in the ensembles with spectral

nudging (Figure C.11b), but instead of a reduction in the pressure gradient, the pressure is reduced in the majority of the area. The differences when spectral nudging is enabled are smaller than those when spectral nudging is not enabled. This shows, that the changes in the MSLP are more sensitive towards the pressure field that is present, which differs due to the varying boundary conditions, and the spectral nudging.

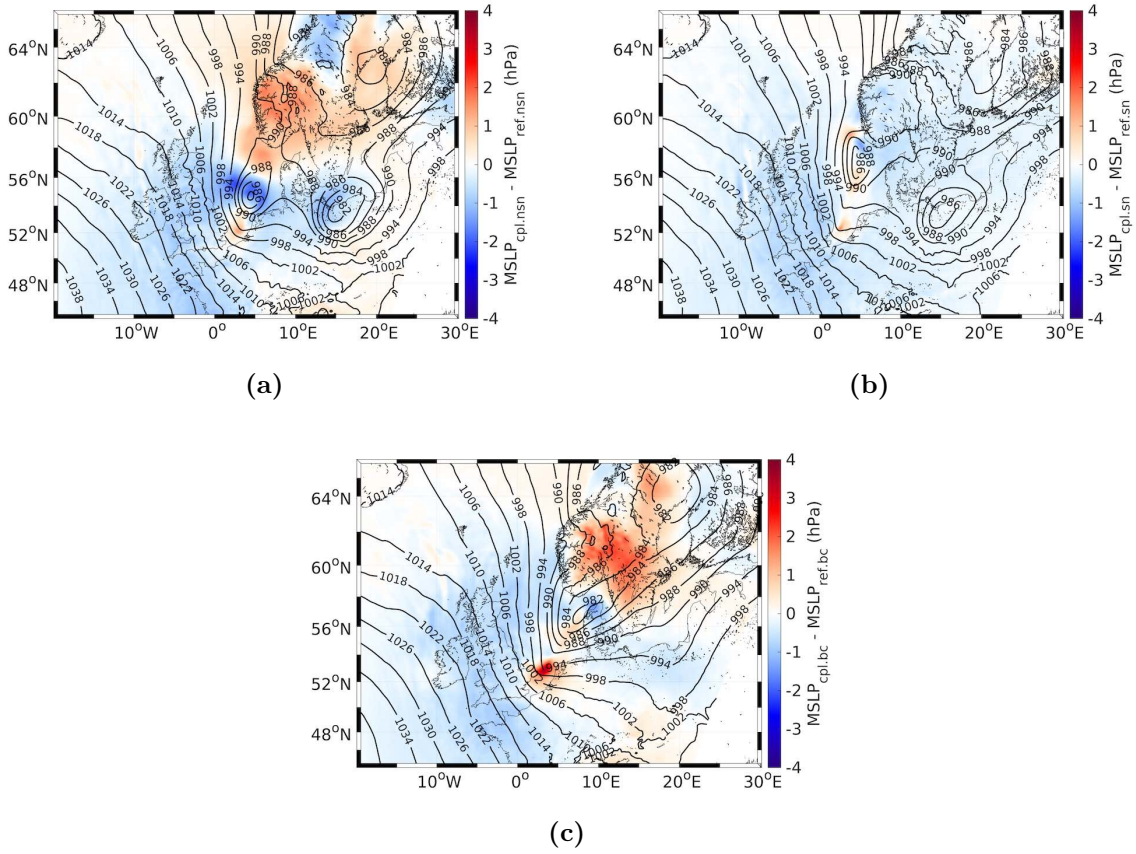

Figure C.11: MSLP in the reference simulation on 13 January 2017 at 12 UTC (contour plots) and the differences between the ensemble means of the reference and coupled ensembles both without (a) and with spectral nudging (b), as well as with the changed boundary conditions (c).

In wind speed a similar picture as in MSLP occurs, although the changes due to the coupling are more similar among the three ensembles (Figure C.S10). In all cases, the differences between the coupled and reference ensembles is a slight varying in the position of the front, and a wind speed reduction, especially behind the front. Since in all ensembles the coupling-induced differences are very similar, these differences can be attributed to the wave-atmosphere coupling. Especially in the simulations with spectral nudging, the

differences are much larger than the internal variability, which implies that the differences are the effect of the coupling between the two models. As in MSLP the internal variability can be reduced in the coupled simulations. The effect of the reduction in the wind speed is directly evident in the significant wave height (Figure C.S12). In the North Sea west of the front, the significant wave height is reduced according to the reduction in wind speed. This effect is very similar in all three ensembles. The weaker reduction in the significant wave height can be explained by the water depth on the Dogger Bank (Figure C.1). Since the waves can reach only a certain height before breaking, the reduction in the significant wave height is lower in that area than elsewhere. Furthermore, the internal variability of the wind speed is transferred straight into the wave model. Therefore, the uncertainty in the wave model is very similar to the uncertainty in the wind speed, although the changes in the significant wave height are always larger than the internal variability.

C.5.2 Variability of Storm Tracks

Additionally, the tracks of the secondary low across the North Sea are analysed (Figure C.12). A track is defined as the path of the minimum MSLP (for example, in Schrum et al., 2003; Wu et al., 2015; Rizza et al., 2018; Ho-Hagemann et al., 2020). The analysis in the present study shows that the variability of storm tracks can be reduced when the wave-atmosphere coupling is enabled.

The low forms as a secondary low of the low-pressure system situated off the Norwegian coast. In most ensemble members, the low circles around the centre of the main low before cutting off and making its way south across the North Sea (Figure C.12a). The uncertainty in the exact position of the centre of the low is most pronounced during the formation of the secondary low until it starts to move southwards. Furthermore, the distances from the tracks of individual ensemble members to the track of the ensemble mean are the largest during the formation stage (Figure C.12c). On 12 January at approximately noon, the low starts to makes its way south across the North Sea. In the area of the Norwegian Sea, the spread of cpl.nsn is reduced compared to ref.nsn, with the tracks becoming more confined farther to the west. The distances from the tracks to the mean ensemble track drop in cpl.nsn as soon as the low is formed and starts moving south on 12 January at noon. The distances remain small for the remainder of the time the low travels across the North Sea. In ref.nsn, however, the tracks spread over the whole North Sea, with larger distances to the mean track. This further illustrates that the coupling reduces the spread

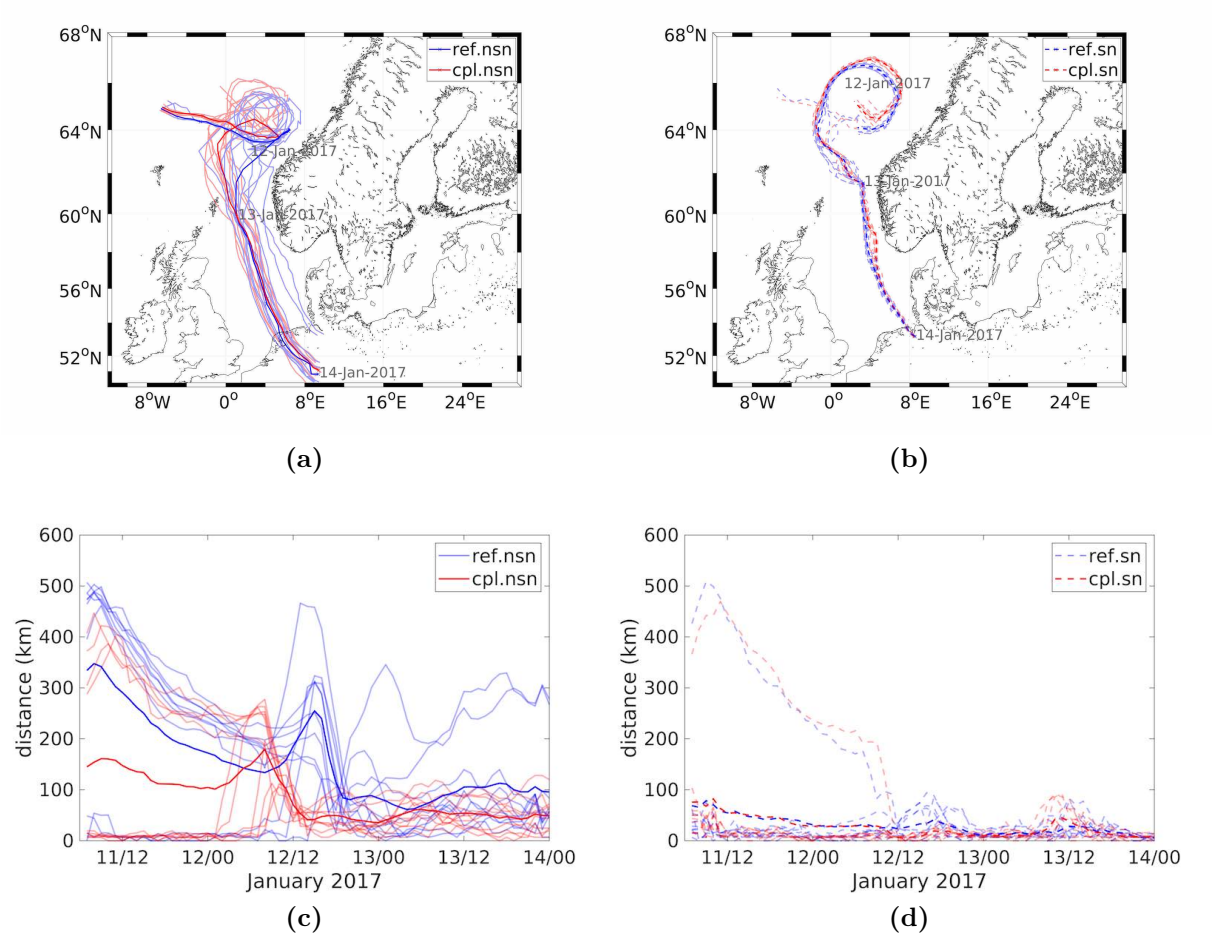

Figure C.12: Storm track of the secondary low from 11 January until 14 January 2017 in the simulations without (a) and with spectral nudging (b). Light lines indicate the tracks of individual ensemble members, while the thick lines show the ensemble mean tracks. The distances from the locations of the low of individual ensemble members to the track of the ensemble mean (light lines) and the mean distances of the ensemble members to the ensemble mean (thick lines) in the simulations without (c) and with spectral nudging (d) are also shown.

in the simulations.

For the simulations where spectral nudging is enabled, the tracks of one ensemble are very close together, which is eventually the goal of using spectral nudging. Nevertheless, variations between ref.sn and cpl.sn can be detected (Figure C.12b). One difference is the path of the low is during the formation stage, when the secondary low circles around the centre of the main low-pressure system. This is also the area with the largest uncertainty, as the distances from individual ensemble tracks to the track of the ensemble mean are

the largest (Figure C.12d) since one ensemble member in each ensemble takes a different track during the formation stage. Another difference in the tracks can be detected along the southern tip of Norway. In cpl.sn, the tracks are shifted farther eastwards compared to the tracks of ref.sn. This shift is present in most ensemble members, not only in the ensemble mean. In the Norwegian Sea, where ref.nsn shows large variations, ref.sn also exhibits some variations, albeit much smaller. During that time, the reduction in the variability of the storm track is also visible in the distances from the individual tracks to the ensemble mean. In general, though, the tracks are much closer together in the simulations with spectral nudging, as the distances from individual ensemble members to the mean track are much smaller than in the simulations without spectral nudging. This spread of the storm tracks observed in ref.sn is reduced in cpl.sn, where the path of the low is very similar among all ensemble members.

The above analysis shows that the variability of storm tracks is reduced due to the wave-atmosphere coupling, and spectral nudging reduces the variations in possible storm tracks more than the coupling. However, in simulations with spectral nudging, small changes in storm tracks generated by the coupling are still possible.

C.6 Summary, Conclusions, and Discussion

From this study on assessing the uncertainties in ensemble simulations with a wave-atmosphere coupled model relative to the impacts of the coupling, it can be concluded that the ensembles of the coupled system and the reference model differ significantly from one another during the majority of the study period but especially during extreme events. Furthermore, the model uncertainty and hence the internal variability can be reduced when using the coupled system compared with a stand-alone atmospheric model. These findings are still valid when using different boundary conditions or spectral nudging in the atmospheric model.

For most of the study period, the reference ensemble differs significantly from the coupled ensemble with regard to surface parameters such as the roughness length, 10 m wind speed, significant wave height and MSLP but also the geopotential heights at 850 hPa and 500 hPa, showing that the signals of waves are transported high into the atmosphere. These differences are especially large during extreme events, while the internal variability usually remains smaller than the impacts of the coupling, particularly in the wind speed

and significant wave height. Hence, we can conclude that the effects of the coupling and the internal variability of the atmospheric model in particular can be differentiated when large differences between the coupled and reference ensembles occur. Therefore, we can verify the significant impacts of the wave-atmosphere coupling on the atmosphere for the global ocean found by Janssen and Viterbo (1996) for our regional model set-up.

Moreover, the internal variability of the atmospheric model can be reduced by its coupling to the wave model. This effect can be detected particularly during events where the internal variability increases but is likewise present in the mean over the whole period. These findings are proven robust to the application of different sets of reanalysis data at the lateral boundaries of the atmospheric model.

In addition, one set of ensemble simulations is performed where spectral nudging is enabled in the atmospheric model to test the sensitivity of the coupled system to the implementation of spectral nudging in the atmospheric model. Spectral nudging seems to have almost no influence on the effects of the coupling on the wind speed and significant wave height during the analysed period. The differences in the MSLP, though, can deviate between the simulations without and with spectral nudging for short time periods and are in general smaller for simulations with spectral nudging than for simulations without spectral nudging. In addition, the internal variability is reduced even further due to the coupling.

From this study, it can be concluded that the wave-atmosphere coupling can be advantageous to the operational and climate modelling of waves and atmospheric components. This is especially important for all human activities on the ocean and close to the coast. For marine traffic and the installation and maintenance of offshore energy, precise forecasts are essential. By having significant impacts of the coupling approaching observational data, operational models can clearly benefit from the coupling of wave and atmospheric models, especially during events with high wind speeds. Furthermore, this coupling is also advantageous for regional climate studies. For coastal protection, harbour and offshore energy planning, projections with low uncertainties are needed. The analysis of this winter season showed that the coupling of wave and atmospheric models reduces their uncertainties, and therefore, regional climate studies can profit from this coupling. Since the impacts of the coupling are significant in simulations using spectral nudging in the atmospheric model, in order to keep the large scales closer to the forcing data, for a better local or regional reconstruction, the coupling is recommended to use, especially

for the reconstruction of extreme events, where realistic simulation results are desired. With the coupling of the wave model to the atmospheric model, the realism in the atmospheric model is increased and the model uncertainty decreased since the roughness of ocean surfaces depends on the sea state and the development phase of the waves and cannot be sufficiently represented by functions of wind speed only (Wu et al., 2017). This enhanced realism leads to better agreement with observations in the simulations using spectral nudging, as well as in simulations where no spectral nudging is used.

This study highlights the importance of the wave-atmosphere coupling, especially during extreme events, which are greatly important for guaranteeing safety at sea, and thereby emphasises the importance of utilising coupled atmosphere-wave models for weather prediction. Another topic to assess in future research is how the impact of this coupling behaves during other seasons of the year. The focus of this study is on the winter months, when the largest impacts of the coupling can be expected due to high storm activity (Janssen et al., 2002; Wahle et al., 2017; Wu et al., 2017; Wiese et al., 2019; Varlas et al., 2020). Furthermore, assessing the model uncertainty stemming from the structure of the model, like grid resolution and altering the model parameters within their range of uncertainty would add to the understanding of uncertainties in the atmospheric model. In the last couple of years, regional climate models have transitioned from stand-alone atmospheric or ocean models to coupled ocean-atmosphere models, thereby adding value to regional climate projections (Schrum, 2017). However, these coupled models rarely incorporate wave models (Schrum, 2017). Therefore, a logical next step for future research would be to integrate a wave model into a coupled ocean-atmosphere model. The benefits of coupling waves with oceanic components have already been shown (Breivik et al., 2015; Staneva et al., 2016a,b). Furthermore, the exchange of heat and mass between the ocean and atmosphere are controlled by the waves (Cavaleri et al., 2012b). Hence, the effects of the waves on these fluxes needs to be investigated in fully coupled atmosphere-waves-ocean systems, since they are highly dependent on all three components of the system. Moreover, Ho-Hagemann et al. (2020) have shown the stabilising effect of the ocean on the atmosphere. Hence, the effects of coupling all three together on the uncertainty of the system is a point worth to investigate, when using fully coupled models including atmosphere, waves and ocean. With each component added to the coupled system, the depicted processes come closer to the ones occurring in the real earth system, since this interacts on all scales transporting and exchanging energy and momentum. Still, there are approximations in the description of the coupling and other processes within the models, which need further analysis. Therefore, future research on the added value of coupling

all three components would be beneficial, as indicated by research on hurricanes (Chen et al., 2007; Warner et al., 2010; Olabarrieta et al., 2012; Zambon et al., 2014; Pant and Prakash, 2020) and offshore energy (Wu et al., 2020). However, further research is needed to assess the interactions among all three components during extratropical storms. The study by Wu et al. (2019) makes for a good starting point for research in this field.

Data Availability Statement

The datasets presented in this article are not readily available because the observational and reanalyses data needs to be requested. The model output can be made available upon request to the corresponding author. Publicly available datasets used in this study can be found from: the ECMWF dataserver (https://apps.ecmwf.int/datasets/) for ERA-Interim data, https://cds.climate.copernicus.eu/cdsapp#!/search?type=application for ERA5 data, https://sentinels.copernicus.eu/documents/247904/1848151/Sentinel-3_Altimetry_Data_Access_and_Products.pdf for Sentinel-3A data.

Author Contributions

AW and JS conceived the work. AW set up the COSMO-CLM, performed all the coupled and reference model simulations, conducted the analyses, and wrote the paper. HTMH-H provided the assistance with the set-up of the COSMO-CLM regional climate model and the initialisation of the ensembles. SG and WK implemented the coupling in CCLM and WAM and provided technical support with the model system. CS and JS provided guidance on the overall direction of the work. All authors reviewed the manuscript.

Funding

This publication has received funding from the European Union's H2020 Programme for Research, Technological Development and Demonstration under grant agreement no. H2020-EO-2016-730030-CEASELESS. This work is a contribution to the Excellence Cluster of Universität Hamburg, funded by the DFG under Germany's Excellence Strategy EXC 2037 "Climate, Climatic Change, and Society" Project 390683824. The work described in this article is a contribution to the project "Advanced Earth System Modelling

Capacity (ESM)", financed through the Initiative and Networking Fund of the Helmholtz Association and to the Helmholtz initiative REKLIM

Acknowledgements

The authors would like to thank Jean-Raymond Bidlot from ECMWF for providing the in situ observations, Luciana Fenoglio-Marc from the University of Bonn for making the Sentinel-3A altimeter data available, Arno Behrens for providing the boundary conditions for the wave model and Ronny Petrik for technical support with CCLM.

Conflict of Interest

The authors declare that the research was conducted in the absence of any commercial or financial relationships that could be construed as a potential conflict of interest.

Supplementary Material

The Supplementary Material for this article can be found online at:
https://www.frontiersin.org/articles/10.3389/fmars.2020.596843/full#supplementary-material

Further Analysis to the Sensitivity to Boundary Conditions

The general impact of the coupling between the atmospheric model and the wave model is very similar with both boundary conditions (Figure C.10a and C.10b). The distributions of the differences in the wind speed and MSLP are very similar for the ensembles with ERA5 and ERA-Interim boundary conditions. The mean wind speed reduction in both ensembles is approximately 0.57 m/s. The standard deviation is 0.86 m/s in the ensemble with ERA5 boundary conditions, while the standard deviation is 0.90 m/s in the ensemble using ERA-Interim boundary conditions.

The mean MSLP difference varies slightly between the two different boundary conditions, with mean differences of -0.14 hPa using ERA5 boundary conditions and -0.07 hPa using ERA-Interim conditions. In addition, the standard deviation is slightly smaller

(0.39 hPa) for the ensemble using ERA5 boundary conditions than that (0.47 hPa) using ERA-Interim conditions, but the overall agreement between the two distributions is quite good.

Furthermore, the above discovery of the reduced internal variability due to the coupling is still valid with different boundary conditions (Figure C.10c and C.10d). The reduction in the standard deviation of the wind speed in the ensemble members is 10.95 %. Moreover, the mean ensemble spread for the MSLP is reduced by 7.89 %.

By comparing the temporal evolution characteristics of the differences between cpl.bc and ref.bc with those of the differences between cpl.nsn and ref.nsn during the study period, it becomes increasingly evident that the impacts on the wind speed are very similar in both ensembles (Figure C.S2b). Therefore, the differences in the significant wave height are also very alike (Figure C.S2f). For the MSLP differences between the ensembles, variations begin to appear (Figure C.S2d) with neither a prevailing reduction nor a predominant enhancement in the differences between cpl.bc and ref.bc relative to the differences between cpl.nsn and ref.nsn. Therefore, the MSLP differences are more sensitive to the boundary conditions than the wind speed differences. Since the distributions of the differences between cpl.bc and ref.bc and between cpl.nsn and ref.nsn are very similar (Figure C.10b), the general impacts of the coupling are similar but are altered in the time series since the solutions for the local pressure fields can differ due to the different boundary conditions, and the changes in the MSLP due to the coupling are more sensitive to the boundary conditions.

This analysis of the sensitivity of the coupling to boundary conditions shows that the general impact of the coupling is very similar between the ensembles with different boundary conditions. Moreover, the conclusions drawn for the ensemble with ERA5 boundary conditions are still valid for the simulations with ERA-Interim boundary conditions. Hence, the effects of the coupling are robust to different reanalysis data used as the boundary forcing.

Supplementary Tables and Figures

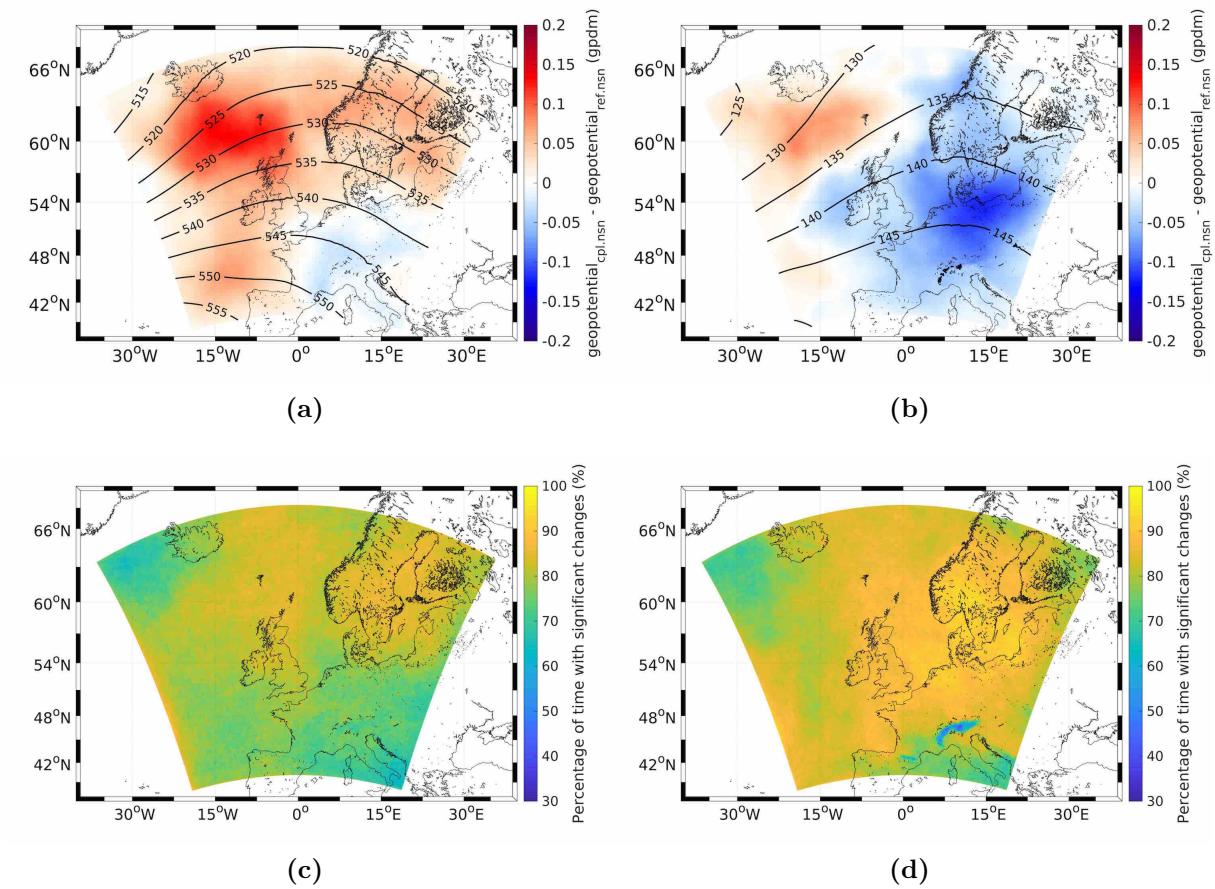

Figure C.S1: Mean over three months in geopotential in 500 hPa (a) and 850 hPa (c). The contour plot shows the values of the reference simulation and the colour plot shows the difference of the reference and coupled ensembles for the ensembles without spectral nudging. The percentage of time with significant differences between coupled and reference ensemble in geopotential in 500 hPa (b) and 850 hPa (d).

Table C.S1: Evaluation of ensemble spread in simulations with spectral nudging enabled.

		mean	**99th percentile**	**maximum**
wind speed	ref.sn (m/s)	0.22	1.09	7.73
	cpl.sn (m/s)	0.21	1.06	5.92
	relative change (%)	-3.78	-1.95	-23.39
MSLP	ref.sn (hPa)	0.04	0.16	1.19
	cpl.sn (hPa)	0.04	0.16	0.89
	relative change (%)	-0.20	-1.26	-24.94

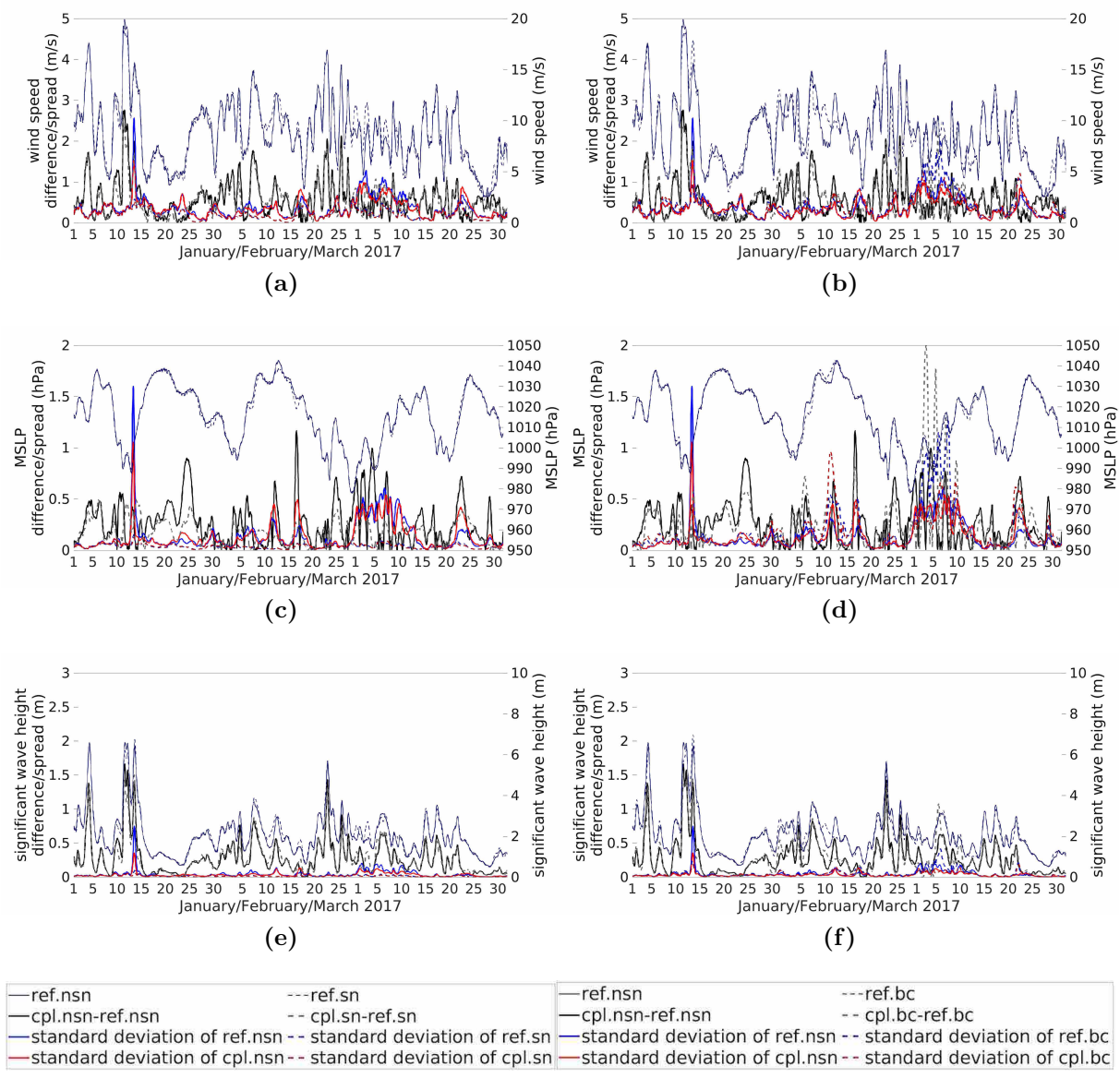

Figure C.S2: Time series of the absolute differences of the ensemble means (black), standard deviation of the ensembles (red and blue) and values in the reference ensemble (dark blue) in the North Sea area in wind speed (a,b), MSLP (c,d) and significant wave height (e,f). The solid line denote the ensemble without spectral nudging. The dashed lines denote the ensemble simulation with the application of spectral nudging within CCLM (a,c,e) and the ensemble with different boundary conditions (b,d,f).

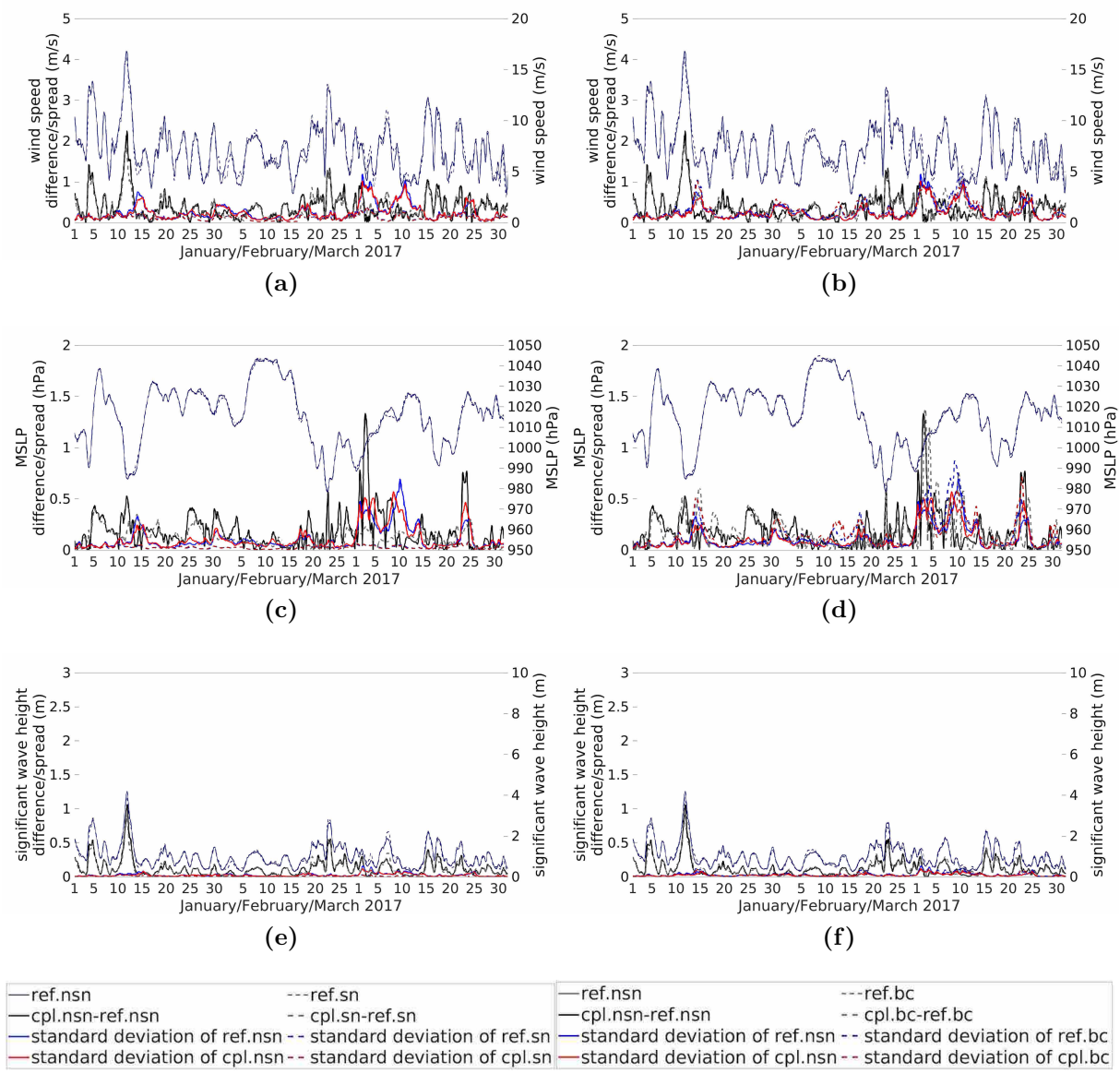

Figure C.S3: Time series of the absolute differences of the ensemble means (black), standard deviation of the ensembles (red and blue) and values in the reference ensemble (dark blue) in the Baltic Sea area in wind speed (a,b), MSLP (c,d) and significant wave height (e,f). The solid line denote the ensemble without spectral nudging. The dashed lines denote the ensemble simulation with the application of spectral nudging within CCLM (a,c,e) and the ensemble with different boundary conditions (b,d,f).

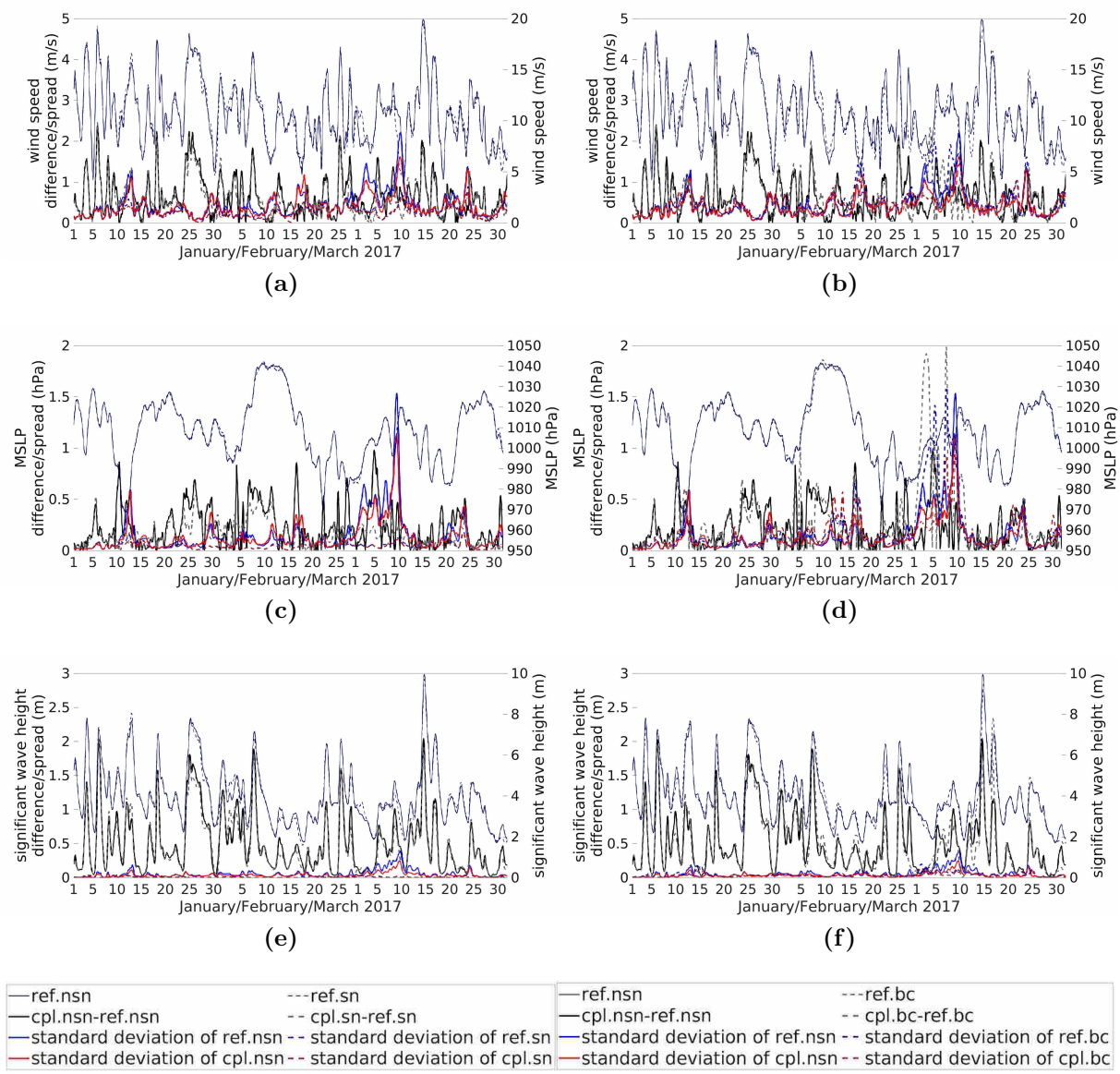

Figure C.S4: Time series of the absolute differences of the ensemble means (black), standard deviation of the ensembles (red and blue) and values in the reference ensemble (dark blue) in the Norwegian Sea area in wind speed (a,b), MSLP (c,d) and significant wave height (e,f). The solid line denote the ensemble without spectral nudging. The dashed lines denote the ensemble simulation with the application of spectral nudging within CCLM (a,c,e) and the ensemble with different boundary conditions (b,d,f).

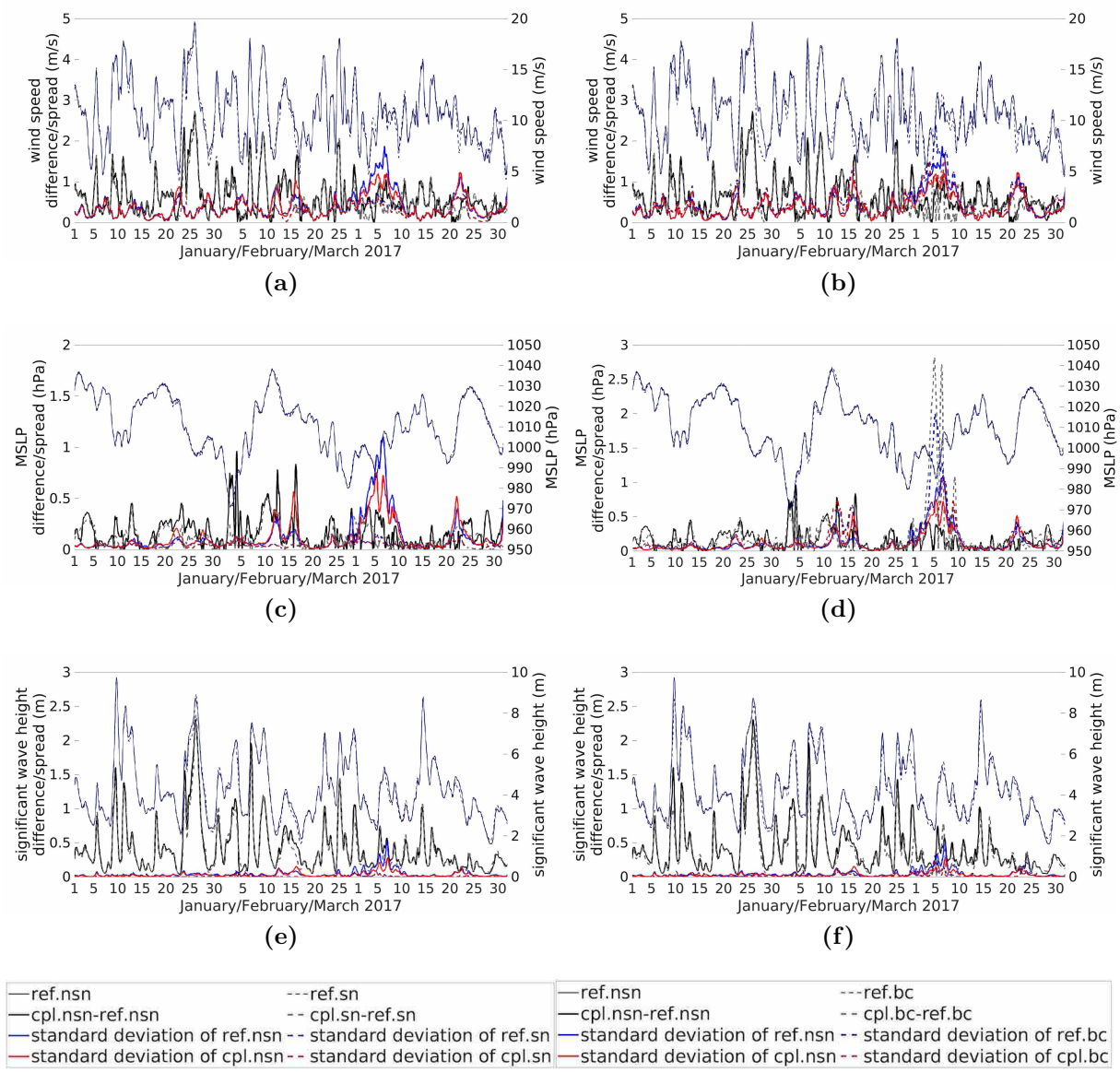

Figure C.S5: Time series of the absolute differences of the ensemble means (black), standard deviation of the ensembles (red and blue) and values in the reference ensemble (dark blue) in the area west of the British Islands in wind speed (a,b), MSLP (c,d) and significant wave height (e,f). The solid line denote the ensemble without spectral nudging. The dashed lines denote the ensemble simulation with the application of spectral nudging within CCLM (a,c,e) and the ensemble with different boundary conditions (b,d,f).

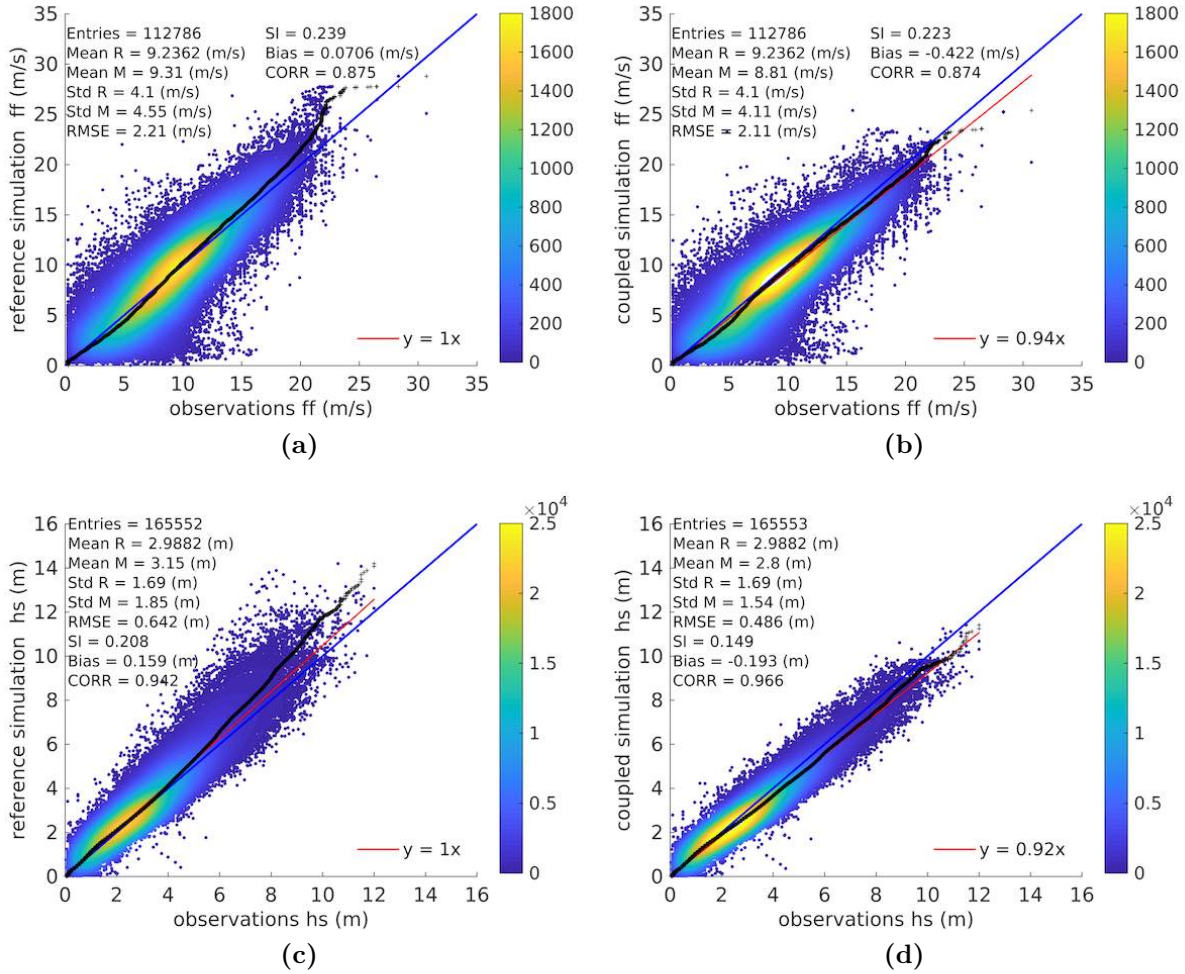

Figure C.S6: Q-Q scatter plots for the measured (Sentinel-3A and GTS) and modelled wind speeds (a,b) and significant wave heights (c,d) with the reference (ref.sn) (a,c) and coupled (cpl.sn) (b,d) model simulations. The Q-Q plot is shown as black crosses, the 45° reference line is denoted by the blue line, and the least-squares best-fit line is the red line.

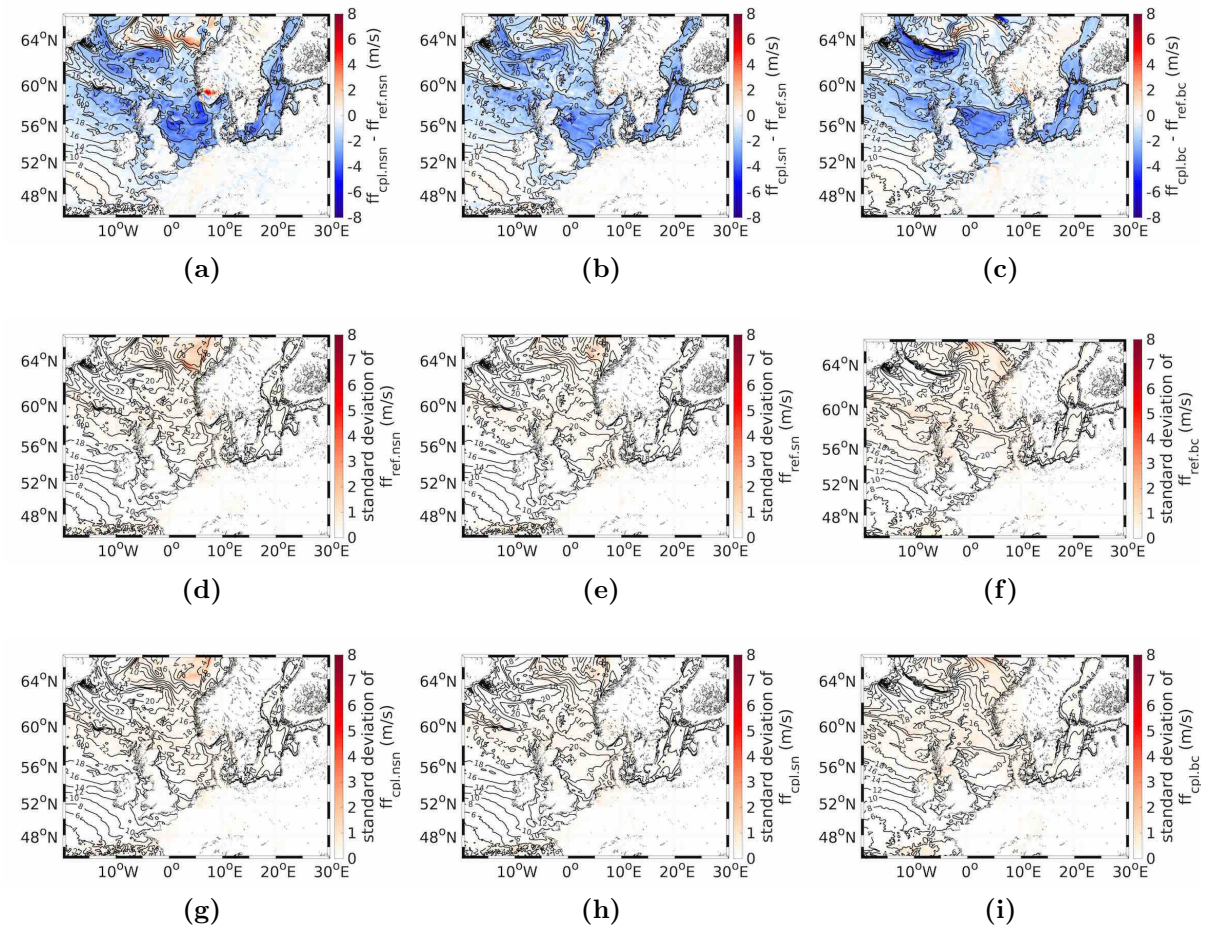

Figure C.S7: Wind speed in the reference simulation on 11.01.2017 12 UTC (contour plot in a-i). The difference between the ensemble means of the reference and the coupled ensemble (a-c), the standard deviation of the reference ensemble (d-f) and the coupled ensemble (g-i) for the ensembles without (a,d,g) and with spectral nudging (b,e,h), as well as with changed boundary conditions (c,f,i).

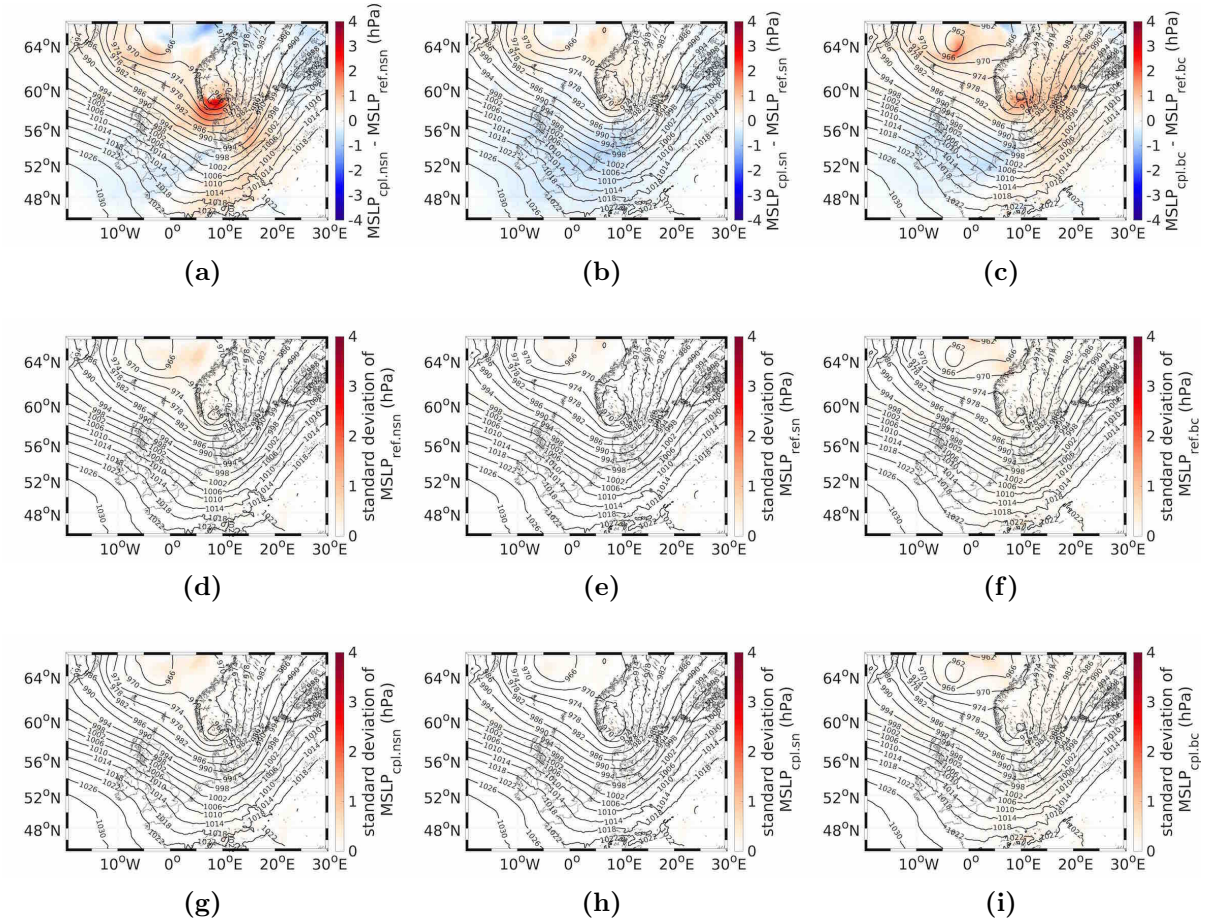

Figure C.S8: MSLP in the reference simulation on 11.01.2017 12 UTC (contour plot in a-i). The difference between the ensemble means of the reference and the coupled ensemble (a-c), the standard deviation of the reference ensemble (d-f) and the coupled ensemble (g-i) for the ensembles without (a,d,g) and with spectral nudging (b,e,h), as well as with changed boundary conditions (c,f,i).

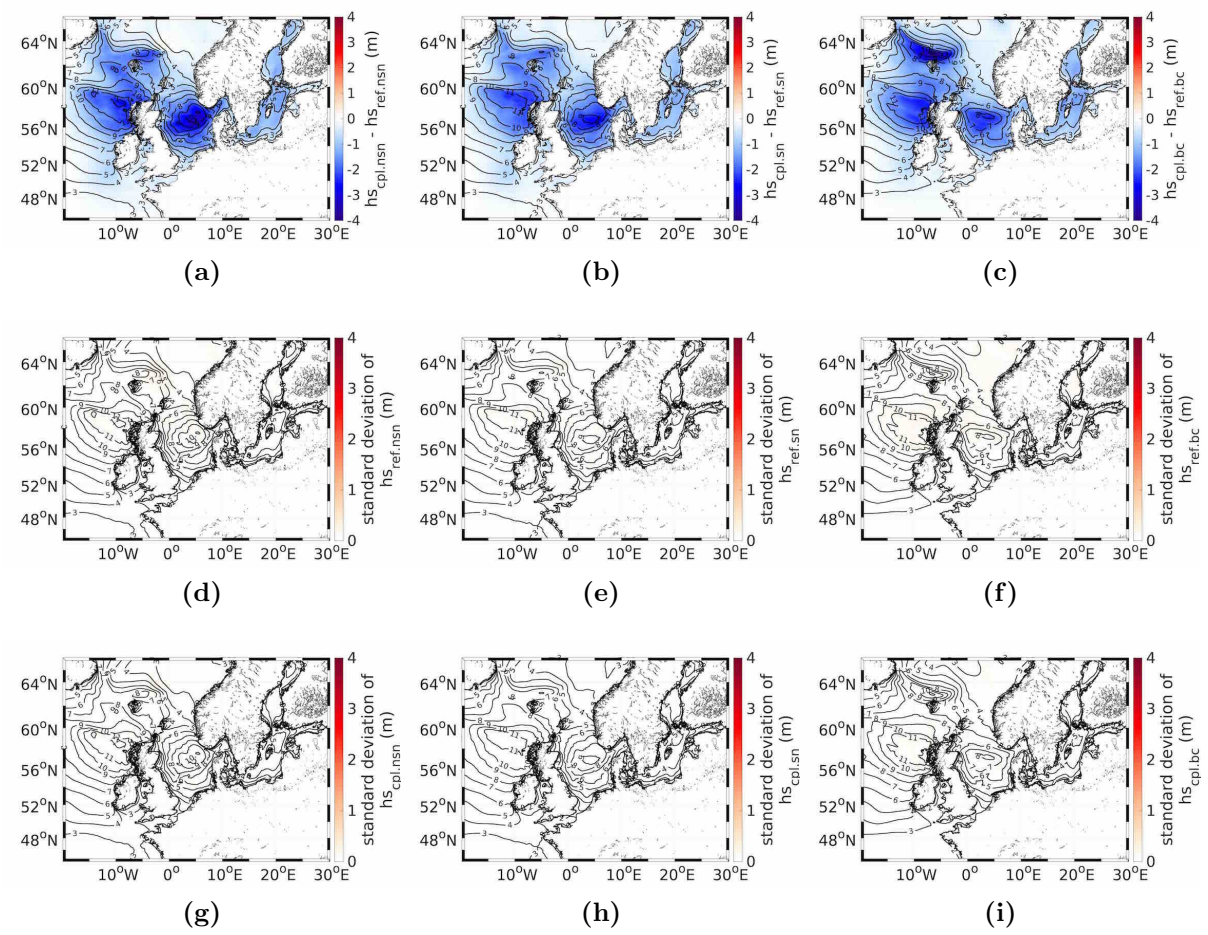

Figure C.S9: Significant wave height in the reference simulation on 11.01.2017 12 UTC (contour plot in a-i). The difference between the ensemble means of the reference and the coupled ensemble (a-c), the standard deviation of the reference ensemble (d-f) and the coupled ensemble (g-i) for the ensembles without (a,d,g) and with spectral nudging (b,e,h), as well as with changed boundary conditions (c,f,i).

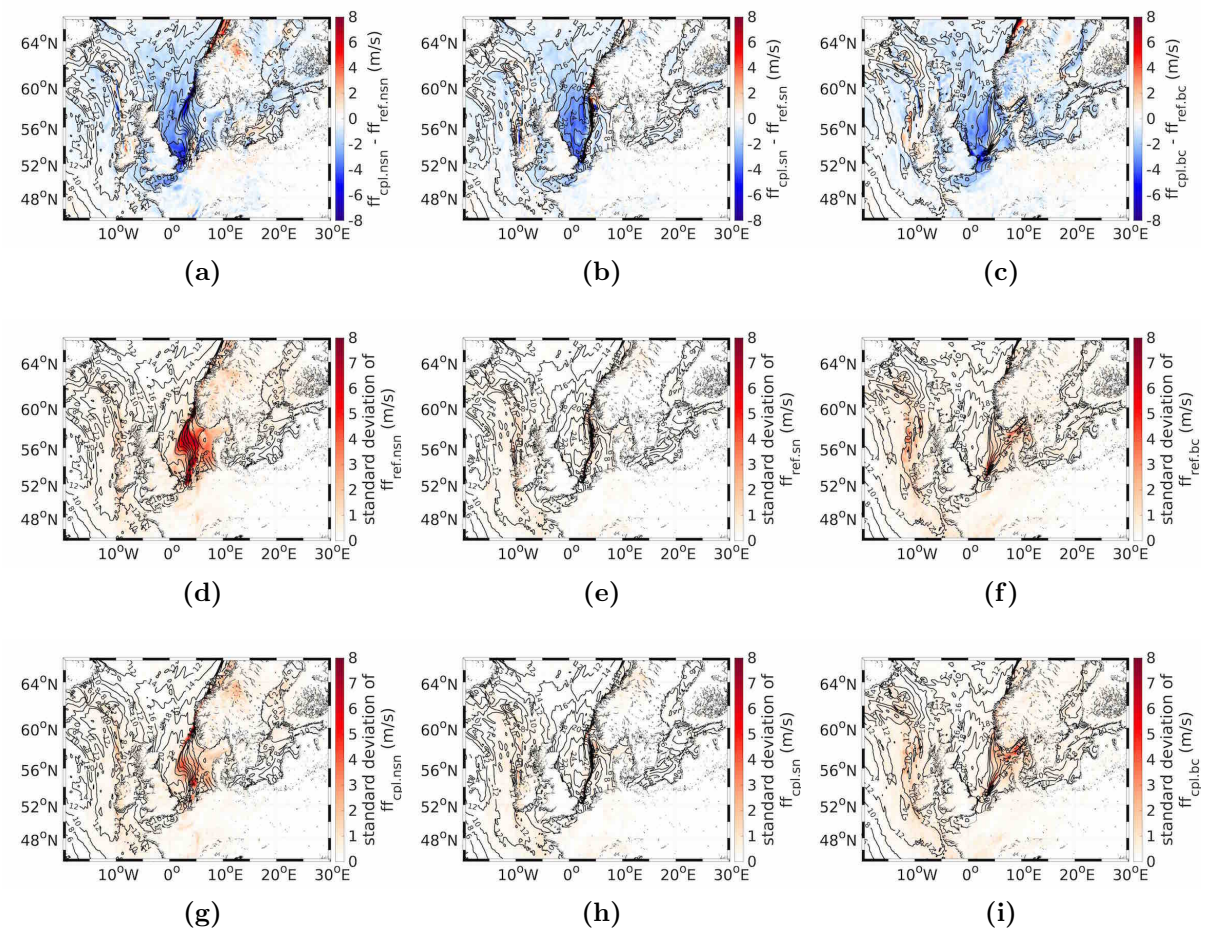

Figure C.S10: Windspeed in the reference simulation on 13.01.2017 12 UTC (contour plot in a-i). The difference between the ensemble means of the reference and the coupled ensemble (a-c), the standard deviation of the reference ensemble (d-f) and the coupled ensemble (g-i) for the ensembles without (a,d,g) and with spectral nudging (b,e,h), as well as with changed boundary conditions (c,f,i).

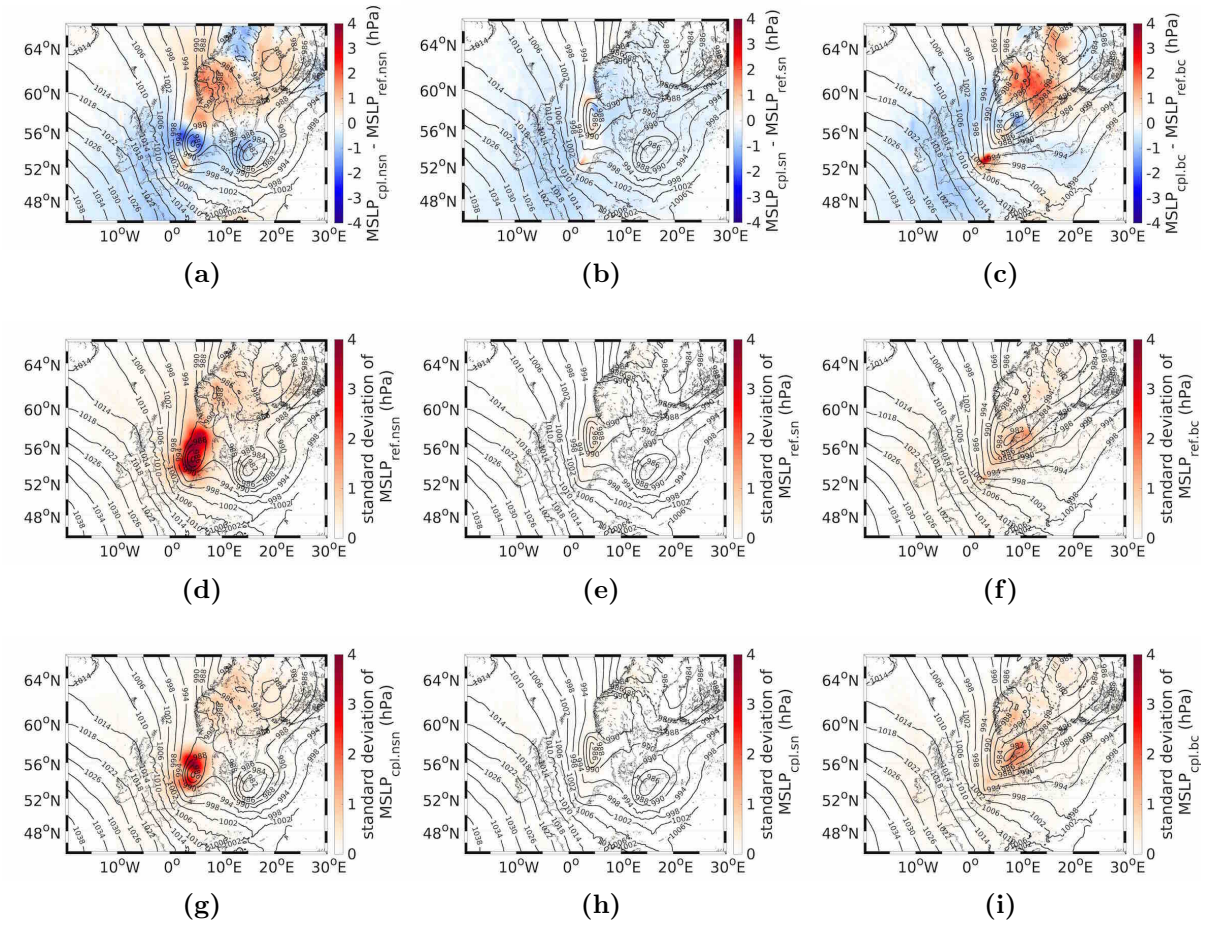

Figure C.S11: MSLP in the reference simulation on 13.01.2017 12 UTC (contour plot in a-i). The difference between the ensemble means of the reference and the coupled ensemble (a-c), the standard deviation of the reference ensemble (d-f) and the coupled ensemble (g-i) for the ensembles without (a,d,g) and with spectral nudging (b,e,h), as well as with changed boundary conditions (c,f,i).

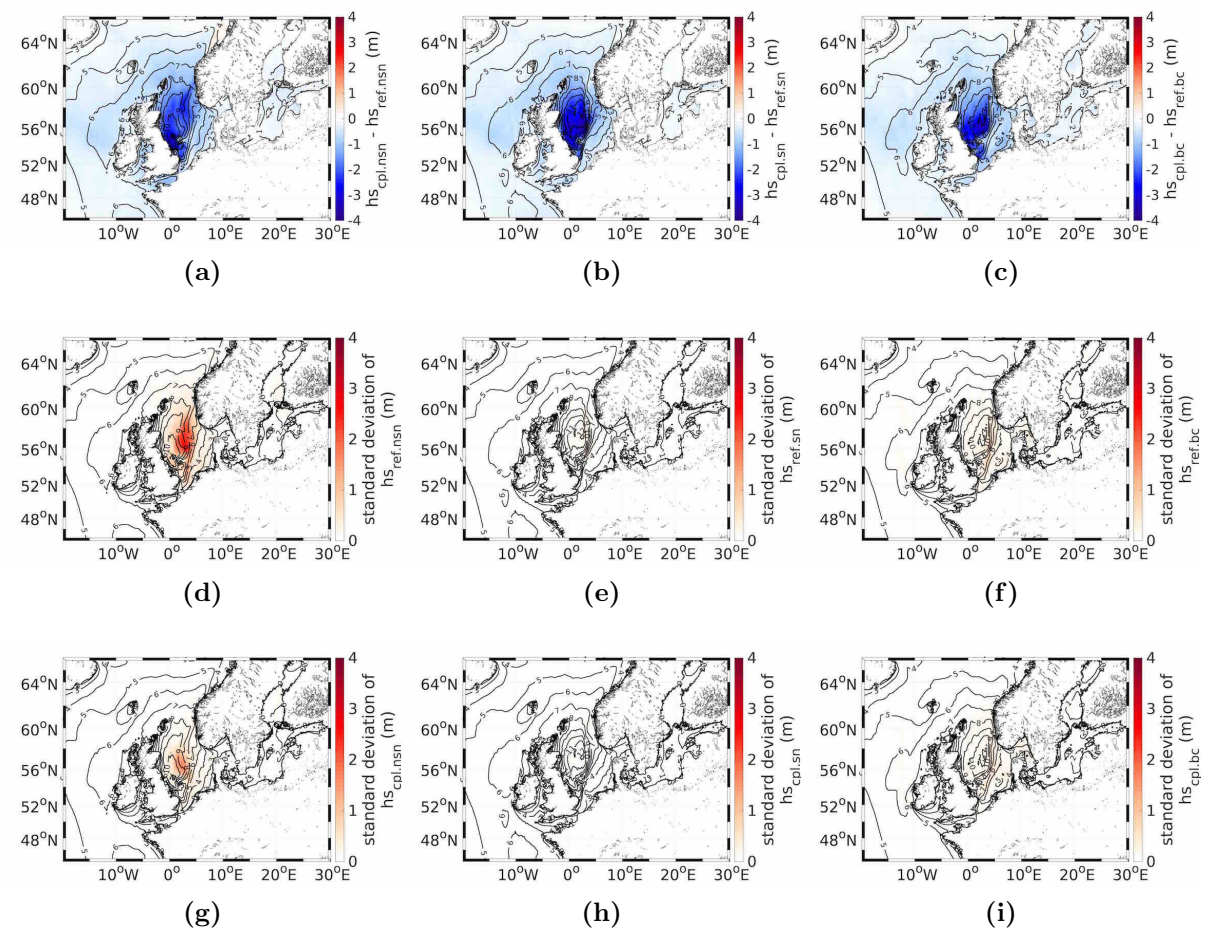

Figure C.S12: Significant wave height in the reference simulation on 13.01.2017 12 UTC (contour plot in a-i). The difference between the ensemble means of the reference and the coupled ensemble (a-c), the standard deviation of the reference ensemble (d-f) and the coupled ensemble (g-i) for the ensembles without (a,d,g) and with spectral nudging (b,e,h), as well as with changed boundary conditions (c,f,i).

Equations to Determine Statistical Values

Mean Value:

$$\overline{R} = \frac{1}{N} \sum_{i=1}^{N} R_i \tag{C.S1}$$

Errors:

$$E = M - R \tag{C.S2}$$

Standard deviation of the errors:

$$s_E = \sqrt{\frac{1}{N-1} \sum_{i=1}^{N} \left(E_i - \overline{E}\right)^2} \tag{C.S3}$$

Root Mean Square Error:

$$RMSE = \sqrt{\frac{1}{N} \sum_{i=1}^{N} \left(M_i - R_i\right)^2} \tag{C.S4}$$

Scatter Index:

$$SI = \frac{s_E}{\overline{R}} \tag{C.S5}$$

Bias:

$$bias = \overline{E} \tag{C.S6}$$

Correlation:

$$CORR = \frac{1}{N-1} \sum_{i=1}^{N} \left(\frac{M_i - \overline{M}}{s_M}\right) \left(\frac{R_i - \overline{R}}{s_R}\right) \tag{C.S7}$$

List of Figures

List of Tables

References

Alexandru, A., de Elia, R., and Laprise, R.: Internal Variability in Regional Climate Downscaling at the Seasonal Scale, Monthly Weather Review, 135, 3221–3238, https://doi.org/10.1175/MWR3456.1, 2007.

Alexandru, A., de Elia, R., Laprise, R., Separovic, L., and Biner, S.: Sensitivity Study of Regional Climate Model Simulations to Large-Scale Nudging Parameters, Monthly Weather Review, 137, 1666–1686, https://doi.org/10.1175/2008MWR2620.1, 2009.

Aouf, L., Hauser, D., Tison, C., and Chapron, B.: On the Assimilation of Multi-Source of Directional Wave Spectra from Sentinel-1A and 1B, and CFOSAT in the Wave Model MFWAM: Toward an Operational Use in CMEMS-MFC, in: IGARSS 2018-2018 IEEE International Geoscience and Remote Sensing Symposium, 22-27 July 2018, Valencia, Spain, pp. 5663–5666, IEEE, https://doi.org/10.1109/IGARSS.2018.8517731, 2018.

Appendini, C. M., Torres-Freyermuth, A., Oropeza, F., Salles, P., López, J., and Mendoza, E. T.: Wave modeling performance in the Gulf of Mexico and Western Caribbean: Wind reanalyses assessment, Applied Ocean Research, 39, 20–30, https://doi.org/10.1016/j.apor.2012.09.004, 2013.

Ardhuin, F. and Orfila, A.: Wind Waves, in: New Frontiers in Operational Oceanography, E. Chassignet, A. Pascual, J. Tintoré, and J. Verron, Eds., GODAE OceanView, pp. 393–422, https://doi.org/10.17125/gov2018.ch14, 2018.

Avgouleas, K. and Sclavounos, P. D.: Fuel-Efficient Ship Routing, Nausivios Chora, 5, 39–72, 2014.

Babanin, A. V., Onorato, M., and Qiao, F.: Surface waves and wave-coupled effects in lower atmosphere and upper ocean, Journal of Geophysical Research: Oceans, 117, https://doi.org/10.1029/2012JC007932, 2012.

Bao, J.-W., Wilczak, J. M., Choi, J.-K., and Kantha, L. H.: Numerical Simulations of Air–Sea Interaction under High Wind Conditions Using a Coupled Model: A Study of Hurricane Development, Monthly Weather Review, 128, 2190–2210, 2000.

Beneviste, J. and Vignudelli, S.: Challenges in Coastal Satellite Radar Altemitry, Eos Trans. AGU, 90, 225, https://doi.org/10.1029/2009EO260007, 2009.

Berrisford, P., Dee, D., Fielding, K., Fuentes, M., Kållberg, P., Kobayashi, S., and Uppala, S.: The ERA-Interim archive, ERA report series, ECMWF, Reading, UK, `https://www.ecmwf.int/sites/default/files/elibrary/2011/8174-era-interim-archive-version-20.pdf`, last accessed: 01.March 2018, 2009.

Bidlot, J.-R. and Holt, M. W.: Verification of operational global and regional wave forecasting systems against measurements from moored buoys, JCOMM Technical Report No. 30, WMO & IOC, Geneva, Switzerland, 2006.

Bidlot, J.-R., Holmes, D. J., Wittmann, P. A., Lalbeharry, R., and Chen, H. S.: Intercomparison of the Performance of Operational Ocean Wave Forecasting Systems with Buoy Data, Weather and Forecasting, 17, 287–310, 2002.

Björnsson, H. and Venegas, S. A.: A Manual for EOF and SVD Analyses of Climatic Data, CCGCR Report, 97, 112–134, 1997.

Bolaños-Sanchez, R., Sanchez-Arcilla, A., and Cateura, J.: Evaluation of two atmospheric models for wind–wave modelling in the NW Mediterranean, Journal of Marine Systems, 65, 336–353, https://doi.org/10.1016/j.jmarsys.2005.09.014, 2007.

Bonaduce, A., Staneva, J., Behrens, A., Bidlot, J.-R., and Wilcke, R. A. I.: Wave Climate Change in the North Sea and Baltic Sea, Journal of Marine Science and Engineering, 7, 166, https://doi.org/10.3390/jmse7060166, 2019.

Breivik, Ø. and Allen, A. A.: An operational search and rescue model for the Norwegian Sea and the North Sea, Journal of Marine Systems, 69, 99–113, https://doi.org/10.1016/j.jmarsys.2007.02.010, 2008.

Breivik, Ø., Allen, A. A., Maisondieu, C., and Olagnon, M.: Advances in search and rescue at sea, Ocean Dynamics, 63, 83–88, https://doi.org/10.1007/s10236-012-0581-1, 2013.

Breivik, Ø., Mogensen, K., Bidlot, J.-R., Balmaseda, M. A., and Janssen, P. A. E. M.: Surface wave effects in the NEMO ocean model: Forced and coupled experiments, Journal of Geophysical Research: Oceans, 120, 2973–2992, https://doi.org/10.1002/2014JC010565, 2015.

Buckley, M. P. and Veron, F.: The turbulent airflow over wind generated surface waves, European Journal of Mechanics-B/Fluids, 73, 132–143, https://doi.org/10.1016/j.euromechflu.2018.04.003, 2019.

Cavaleri, L.: Wave Modeling - Missing the Peaks, Journal of Physical Oceanography, 39, 2757–2778, https://doi.org/10.1175/2009JPO4067.1, 2009.

Cavaleri, L. and Bertotti, L.: In Search of the Correct Wind and Wave Fields in a Minor Basin, Monthly Weather Review, 125, 1964–1975, 1997.

Cavaleri, L. and Bertotti, L.: The characteristics of wind and wave fields modelled with different resolutions, Quarterly Journal of the Royal Meteorological Society, 129, 1647–1662, https://doi.org/10.1256/qj.01.68, 2003a.

Cavaleri, L. and Bertotti, L.: The improvement of modelled wind and wave fields with increasing resolution, ECMWF Technical Memorandum No.408, ECMWF, Reading, England, 2003b.

Cavaleri, L. and Bertotti, L.: Accuracy of the modelled wind and wave fields in enclosed seas, Tellus A: Dynamic Meteorology and Oceanography, 56, 167–175, https://doi.org/10.3402/tellusa.v56i2.14398, 2004.

Cavaleri, L. and Bertotti, L.: The improvement of modelled wind and wave fields with increasing resolution, Ocean Engineering, 33, 553–565, https://doi.org/10.1016/j.oceaneng.2005.07.004, 2006.

Cavaleri, L., Alves, J.-H. G. M., Ardhuin, F., Babanin, A., Banner, M., Belibassakis, K., Benoit, M., Donelan, M., Groeneweg, J., Herbers, T. H. C., Hwang, P., Janssen, P. A. E. M., Janssen, T., Lavrenov, I. V., Magne, R., Monbaliu, J., Onorato, M., Polnikov, V., Resio, D., Rogers, W. E., Sheremet, A., McKee Smith, J., Tolman, H. L., van Vledder, G., Wolf, J., and Young, I.: Wave modelling - The state of the art, Progress in Oceanography, 75, 603–674, https://doi.org/10.1016/j.pocean.2007.05.005, 2007.

Cavaleri, L., Fox-Kemper, B., and Hemer, M.: Wind Waves in the Coupled Climate System, Bulletin of the American Meteorological Society, 93, 1651–1661, https://doi.org/10.1175/Bams-d-11-00170.1, 2012a.

Cavaleri, L., Roland, A., Dutour Sikiric, M., Bertotti, L., and Torrisi, L.: On the coupling of COSMO to WAM, in: Proceedings of the ECMWF Workshop on Ocean Waves, 25-27 June 2012, ECMWF, Reading, England, pp. 41–58, 2012b.

Charnock, H.: Wind stress on a water surface, Quarterly Journal of the Royal Meteorological Society, 81, 639–640, https://doi.org/10.1002/qj.49708135027, 1955.

Chelton, D. B. and Freilich, M. H.: Scatterometer-Based Assessment of 10-m Wind Analyses from the Operational ECMWF and NCEP Numerical Weather Prediction Models, Monthly Weather Review, 133, 409–429, https://doi.org/10.1175/MWR-2861.1, 2005.

Chen, S. S., Price, J. F., Zhao, W., Donelan, M. A., and Walsh, E. J.: The CBLAST-Hurricane Program and the Next-Generation Fully Coupled Atmosphere–Wave–Ocean Models for Hurricane Research and Prediction, Bulletin of the American Meteorological Society, 88, 311–318, https://doi.org/10.1175/BAMS-88-3-311, 2007.

Chen, S. S., Zhao, W., Donelan, M. A., and Tolman, H. L.: Directional Wind–Wave Coupling in Fully Coupled Atmosphere–Wave–Ocean Models: Results from CBLAST-Hurricane, Journal of the Atmospheric Sciences, 70, 3198–3215, https://doi.org/10.1175/JAS-D-12-0157.1, 2013.

Cipollini, P., Benviste, J., Bouffard, J., Emery, W., Fenoglio-Marc, L., Gommenginger, C., Griffin, D., Høyer, J., Kurapov, A., Madsen, K., Mercier, F., Miller, L., Pascual, A., Ravichandran, M., Shillington, F., Snaith, H., Strub, P. T., Vandemark, D., Vignudelli, S., Wilkin, J., Woodworth, P., and Zavala-Garay, J.: The Role of Altimetry in Coastal Observing Systems, in: Proceedings of OceanObs'09: Sustained Ocean Observations and Information for Society, 21-25 September 2009, Venice, Italy, 2, 181–191, https://doi.org/10.5270/OceanObs09.cwp.16, 2010.

CLM-Community: `https://www.clm-community.eu/`, last accessed: 06.February 2019, 2019.

Copernicus Climate Change Service (C3S): ERA5: Fifth generation of ECMWF atmospheric reanalyses of the global climate, `https://cds.climate.copernicus.eu/cdsapp#!/home`, last accessed: 16.July 2020, 2017.

COSMO: `http://www.cosmo-model.org/`, last accessed: 06.February 2019, 2019.

CryoSat-2 RDSAR: satellite data, available at:, `http://rads.tudelft.nl/rads/rads.shtml`, last accessed: 5.December 2018, 2018.

CryoSat-2 SAR: satellite data, available at:, `https://gpod.eo.esa.int`, last accessed: 16.November 2018, 2018.

Cutululis, N. A., Detlefsen, N. K., and Sørensen, P. E.: Offshore wind power prediction in critical weather conditions, in: 10th International Workshop on Large-Scale Integration

of Wind Power into Power Systems as well as on Transmission Networks for Offshore Wind Farms, 25-26 October 2011, Aarhus, Denmark, Energynautics GmbH, 2011.

de León, S. P. and Soares, C. G.: Sensitivity of wave model predictions to wind fields in the Western Mediterranean sea, Coastal Engineering, 55, 920–929, https://doi.org/10.1016/j.coastaleng.2008.02.023, 2008.

de León, S. P., Orfila, A., Gómez-Pujol, L., Renault, L., Vizoso, G., and Tintoré, J.: Assessment of wind models around the Balearic Islands for operational wave forecast, Applied Ocean Research, 34, 1–9, https://doi.org/10.1016/j.apor.2011.09.001, 2012.

Dee, D. P., Uppala, S. M., Simmons, A. J., Berrisford, P., Poli, P., Kobayashi, S., Andrae, U., Balmaseda, M. A., Balsamo, G., Bauer, P., Bechtold, P., Beljaars, A. C. M., van de Berg, L., Bidlot, J., Bormann, N., Delsol, C., Dragani, R., Fuentes, M., Geer, A. J., Haimberger, L., Healy, S. B., Hersbach, H., Hólm, E. V., Isaksen, L., Kållberg, P., Köhler, M., Matricardi, M., McNally, A. P., Monge-Sanz, B. M., Morcrette, J.-J., Park, B.-K., Peubey, C., de Rosnay, P., Tavolato, C., Thépaut, J.-N., and Vitart, F.: The ERA-Interim reanalysis: configuration and performance of the data assimilation system, Quarterly Journal of the Royal Meteorological Society, 137, 553–597, https://doi.org/10.1002/qj.828, 2011.

Déqué, M., Rowell, D. P., Lüthi, D., Giorgi, F., Christensen, J. H., Rockel, B., Jacob, D., Kjellström, E., de Castro, M., and van den Hurk, B.: An intercomparison of regional climate simulations for Europe: assessing uncertainties in model projections, Climatic Change, 81, 53–70, https://doi.org/10.1007/s10584-006-9228-x, 2007.

Dinardo, S., Fenoglio-Marc, L., Becker, M., Scharroo, R., Fernandes, M. J., Staneva, J., Grayek, S., and Benveniste, J.: A RIP-based SAR retracker and its application in North East Atlantic with Sentinel-3, Advances in Space Research, https://doi.org/10.1016/j.asr.2020.06.004, 2020.

Dobrynin, M., Murawsky, J., and Yang, S.: Evolution of the global wind wave climate in CMIP5 experiments, Geophysical Research Letters, 39, https://doi.org/10.1029/2012GL052843, 2012.

Doms, G. and Baldauf, M.: A Description of the Nonhydrostatic Regional COSMO-Model Part I: Dynamics and Numerics, Deutscher Wetterdienst, Offenbach, Germany, https://doi.org/10.5676/DWD_pub/nwv/cosmo-doc_5.00_I, 2013.

Doms, G., Förstner, J., Heise, E., Herzog, H.-J., Mironov, D., Raschendorfer, M., Reinhardt, T., Ritter, B., Schrodin, R., Schulz, J.-P., and Vogel, G.: A Description of the Nonhydrostatic Regional COSMO-Model Part II: Physical Parameterizations, Deutscher Wetterdienst, Offenbach, Germany, https://doi.org/10.5676/DWD_pub/nwv/cosmo-doc_5.00_II, 2013.

Donelan, M. A.: On the Decrease of the Oceanic Drag Coefficient in High Winds, Journal of Geophysical Research: Oceans, 123, 1485–1501, https://doi.org/10.1002/2017JC013394, 2018.

Donelan, M. A., Dobson, F. W., Smith, S. D., and Anderson, R. J.: On the Dependence of Sea Surface Roughness on Wave Development, Journal of Physical Oceanography, 23, 2143–2149, 1993.

Doyle, J. D.: Coupled ocean wave/atmosphere mesoscale model simulations of cyclogenesis, Tellus A, 47, 766–778, 1995.

Du, J., Bolaños, R., and Larsén, X. G.: The use of a wave boundary layer model in SWAN, Journal of Geophysical Research: Oceans, 122, 42–62, https://doi.org/10.1002/2016JC012104, 2017.

Du, J., Bolaños, R., Larsén, X. G., and Kelly, M.: Wave boundary layer model in SWAN revisited, Ocean Science, 15, 361–377, https://doi.org/10.5194/os-15-361-2019, 2019.

DWD: Seegangsvorhersage, `https://www.dwd.de/DE/forschung/wettervorhersage/num_modellierung/03_umweltvorhersage/seegangvorhersage.html`, last accessed: 23.June 2020, 2020.

ECMWF: ECMWF/WWRP Workshop Model Uncertainty, 11-15 April 2016, ECMWF, Reading, UK, `https://www.ecmwf.int/sites/default/files/elibrary/2016/16551-ecmwfwwrp-workshop-model-uncertainty-proceedings.pdf`, last accessed: 30.September 2020, 2016.

ECMWF: IFS documentation, `https://www.ecmwf.int/en/forecasts/documentation-and-support/changes-ecmwf-model/ifs-documentation`, last accessed: 05.July 2018, 2017a.

ECMWF: ERA5 data documentation, `https://software.ecmwf.int/wiki/display/CKB/ERA5+data+documentation#ERA5datadocumentation-Spatialgrid`, last accessed: 01.March 2018, 2017b.

ECMWF: Part VII: ECMWF Wave Model, No. 7 in IFS Documentation CY46R1, ECMWF, Reading, England, https://doi.org/10.21957/21g1hoiuo, 2019.

ECMWF: Quantifying forecast uncertainty, `https://www.ecmwf.int/en/research/modelling-and-prediction/quantifying-forecast-uncertainty`, last accessed: 12.August 2020, 2020.

Ehrendorfer, M.: Predicting the uncertainty of numerical weather forecasts: a review, Meteorologische Zeitschrift, 6, 147–183, https://doi.org/10.1127/metz/6/1997/147, 1997.

ERA5: wind forcing data, available at:, `https://cds.climate.copernicus.eu/cdsapp#!/search?type=dataset`, last accessed: 30.November 2018, 2018.

ESA: Sentinel-3: Data Access and Products, `https://sentinels.copernicus.eu/documents/247904/1848151/Sentinel-3_Altimetry_Data_Access_and_Products.pdf`, last accessed: 05.February 2019, 2015.

Feng, H., Vandemark, D., Quilfen, Y., Chapron, B., and Beckley, B.: Assessment of wind-forcing impact on a global wind-wave model using the TOPEX altimeter, Ocean Engineering, 33, 1431–1461, https://doi.org/10.1016/j.oceaneng.2005.10.015, 2006.

Fenoglio-Marc, L., Dinardo, S., Scharroo, R., Roland, A., Dutour Sikiric, M., Lucas, B., Becker, M., Beneviste, J., and Weiss, R.: The German Bight: A validation of CryoSat-2 altimeter data in SAR mode, Advances In Space Research, 55, 2641–2656, https://doi.org/10.1016/j.asr.2015.02.014, 2015.

Feser, F., Weisse, R., and von Storch, H.: Multi-decadal Atmospheric Modeling for Europe Yields Multi-purpose Data, Eos Trans. AGU, 82, 305–310, https://doi.org/10.1029/01EO00176, 2001.

Gautier, C. and Caires, S.: Operational Wave Forecasts in the Southern North Sea, in: E-proceedings of the 36th IAHR World Congress, 28 June-3 July 2015, The Hague, the Netherlands, 1, pp. 2–5, 2015.

Geyer, B.: High-resolution atmospheric reconstruction for Europe 1948-2012: coastDat2, Earth System Science Data, 6, 147–164, https://doi.org/10.5194/essd-6-147-2014, 2014.

Gintautas, T., Sørensen, J. D., and Vatne, S. R.: Towards a risk-based decision support for offshore wind turbine installation and operation & maintenance, Energy Procedia, 94, 207–217, https://doi.org/10.1016/j.egypro.2016.09.225, 2016.

Günther, H., Rosenthal, W., Stawarz, M., Carretero, J. C., Gomez, M., Lozano, I., Serrano, O., and Reistad, M.: The wave climate of the Northeast Atlantic over the period 1955-1994: the WASA wave hindcast, GKSS-Forschungszentrum Geesthacht GmbH, Geesthacht, Germany, 1997.

Hasselmann, D., Bösenberg, J., Dunckel, M., Richter, K., Grünewald, M., and Carlson, H.: Measurements of Wave-Induced Pressure over Surface Gravity Waves, in: Phillips O.M., Hasselmann K. (eds) Wave Dynamics and Radio Probing of the Ocean Surface, pp. 353–368, Springer, Boston, MA., https://doi.org/10.1007/978-1-4684-8980-4_25, 1986.

Hasselmann, K.: On the non-linear energy transfer in a gravity-wave spectrum Part 1. General theory, Journal of Fluid Mechanics, 12, 481–500, https://doi.org/10.1017/S0022112062000373, 1962.

Hasselmann, K., Barnett, T. P., Bouws, E., Carlson, H., Cartwright, D. E., Enke, K., Ewing, J. A., Gienapp, H., Hasselmann, D. E., Kruseman, P., Meerburg, A., Müller, P., Olbers, D. J., Richter, K., Sell, W., and Walden, H.: Measurements of Wind-Wave Growth and Swell Decay during the Joint North Sea Wave Project (JONSWAP), Ergänzungsheft zur Deutschen Hydrographischen Zeitschrift, Reihe A, Nr. 12, 1973.

Hersbach, H. and Dee, D.: ERA5 reanalysis is in production, ECMWF Newsletter No. 147, ECMWF, Reading, England, `https://software.ecmwf.int/wiki/display/CKB/What+is+ERA5?preview=/58140637/58140636/16299-newsletter-no147-spring-2016_p7.pdf`, last accessed: 16.November 2018, 2016.

Hersbach, H., Bell, B., Berrisford, P., Hirahara, S., Horányi, A., Muñoz-Sabater, J., Nicolas, J., Peubey, C., Radu, R., Schepers, D., Simmons, A., Soci, C., Abdalla, S., Abellan, X., Balsamo, G., Bechtold, P., Biavati, G., Bidlot, J., Bonavita, M., De Chiara, G., Dahlgren, P., Dee, D., Diamantakis, M., Dragani, R., Flemming, J., Forbes, R., Fuentes, M., Geer, A., Haimberger, L., Healy, S., Hogan, R. J., Hólm, E., Janisková, M., Keeley, S., Laloyaux, P., Lopez, P., Lupu, C., Radnoti, G., de Rosnay, P., Rozum, I., Vamborg, F., Villaume, S., and Thépaut, J.-N.: The ERA5 global reanalysis, Quarterly Journal of the Royal Meteorological Society, 146, 1999–2049, https://doi.org/10.1002/qj.3803, 2020.

Ho-Hagemann, H. T. M., Rockel, B., Kapitza, H., Geyer, B., and Meyer, E.: COSTRICE

- an atmosphere - ocean - sea ice model coupled system using OASIS3, HZG Report 2013-5, Helmholtz-Zentrum Geesthacht, Geesthacht, Germany, 2013.

Ho-Hagemann, H. T. M., Hagemann, S., and Rockel, B.: On the role of soil moisture in the generation of heavy rainfall during the Oder flood event in July 1997, Tellus A: Dynamic Meteorology and Oceanography, 67, 28 661, https://doi.org/10.3402/tellusa.v67.28661, 2015.

Ho-Hagemann, H. T. M., Gröger, M., Rockel, B., Zahn, M., Geyer, B., and Meier, H. E. M.: Effects of air-sea coupling over the North Sea and the Baltic Sea on simulated summer precipitation over Central Europe, Climate Dynamics, 49, 3851–3876, https://doi.org/10.1007/s00382-017-3546-8, 2017.

Ho-Hagemann, H. T. M., Hagemann, S., Grayek, S., Petrik, R., Rockel, B., Staneva, J., Feser, F., and Schrum, C.: Internal Model Variability of the Regional Coupled System Model GCOAST-AHOI, Atmosphere, 11, 227, https://doi.org/10.3390/atmos11030227, 2020.

HZG: coastDat-3_COSMO-CLM_ERAi. World Data Center for Climate (WDCC) at DKRZ, `https://cera-www.dkrz.de/WDCC/ui/cerasearch/entry?acronym=coastDat-3_COSMO-CLM_ERAi`, last accessed: 13.March 2018, 2017.

Janssen, P.: The Interaction of Ocean Waves and Wind, Cambridge University Press, pp. 301–318, 2004.

Janssen, P. A. E. M.: Wave-Induced Stress and the Drag of Air Flow over Sea Waves, Journal of Physical Oceanography, 19, 745–754, 1989.

Janssen, P. A. E. M.: Quasi-linear Theory of Wind-Wave Generation Applied to Wave Forecasting, Journal of Physical Oceanography, 21, 1631–1642, 1991.

Janssen, P. A. E. M.: Experimental Evidence of the Effect of Surface Waves on the Airflow, Journal of Physical Oceanography, 22, 1600–1604, 1992.

Janssen, P. A. E. M. and Bidlot, J.-R.: Progress in Operational Wave Forecasting, Procedia IUTAM, 26, 14–29, https://doi.org/10.1016/j.piutam.2018.03.003, 2018.

Janssen, P. A. E. M. and Viterbo, P.: Ocean Waves and the Atmospheric Climate, Journal of Climate, 9, 1269–1287, 1996.

Janssen, P. A. E. M., Hansen, B., and Bidlot, J.-R.: Verification of the ECMWF Wave Forecasting System against Buoy and Altimeter Data, Weather and Forecasting, 12, 763–784, 1997.

Janssen, P. A. E. M., Doyle, J. D., Bidlot, J., Hansen, B., Isaksen, L., and Viterbo, P.: Impact and feedback of ocean waves on the atmosphere, Advances in Fluid Mechanics, 33, 155–198, 2002.

Jason-2: satellite data, available at:, `ftp://avisoftp.cnes.fr`, last accessed: 16.November 2018, 2018.

Katsafados, P., Papadopoulos, A., Korres, G., and Varlas, G.: A fully coupled atmosphere-ocean wave modeling system for the Mediterranean Sea: interactions and sensitivity to the resolved scales and mechanisms, Geoscientific Model Development, 9, 161–173, https://doi.org/10.5194/gmd-9-161-2016, 2016.

Kelemen, F. D., Primo, C., Feldmann, H., and Ahrens, B.: Added Value of Atmosphere-Ocean Coupling in a Century-Long Regional Climate Simulation, Atmosphere, 10, 537, https://doi.org/10.3390/atmos10090537, 2019.

Keuler, K., Radtke, K., Kotlarski, S., and Lüthi, D.: Regional climate change over Europe in COSMO-CLM: Influence of emission scenario and driving global model, Meteorologische Zeitschrift, 25, 121–136, https://doi.org/10.1127/metz/2016/0662, 2016.

Kjellström, E., Nikulin, G., Hansson, U., Strandberg, G., and Ullerstig, A.: 21st century changes in the European climate: uncertainties derived from an ensemble of regional climate model simulations, Tellus A: Dynamic Meteorology and Oceanography, 63, 24–40, https://doi.org/10.1111/j.1600-0870.2010.00475.x, 2011.

Komen, G. J.: Forecasting Wind-driven Ocean Waves, in: Pinardi N., Woods J. (eds) Ocean Forecasting, pp. 267–279, Springer, Berlin, Heidelberg, https://doi.org/10.1007/978-3-662-22648-3_14, 2002.

Komen, G. J., Cavaleri, L., Donelan, M., Hasselmann, K., Hasselmann, S., and Janssen, P. A. E. M.: Dynamics and Modelling of Ocean Waves, Cambridge University Press, 1994.

Laprise, R., Kornic, D., Rapaić, M., Šeparović, L., Leduc, M., Nikiema, O., Di Luca, A., Diaconescu, E., Alexandru, A., Lucas-Picher, P., de Elía, R., Caya, D., and Biner, S.: Considerations of Domain Size and Large-Scale Driving for Nested Regional Climate

Models: Impact on Internal Variability and Ability at Developing Small-Scale Details, in: Climate Change, eds. A. Berger, F. Mesinger, and D. Sijacki, pp. 181–199, Springer, Vienna, https://doi.org/10.1007/978-3-7091-0973-1_14, 2012.

Larsén, X. G., Du, J., Bolaños, R., Imberger, M., Kelly, M. C., Badger, M., and Larsen, S.: Estimation of offshore extreme wind from wind-wave coupled modeling, Wind Energy, 22, 1043–1057, https://doi.org/10.1002/we.2339, 2019.

Li, D., Staneva, J., Grayek, S., Behrens, A., Feng, J., and Yin, B.: Skill Assessment of an Atmosphere–Wave Regional Coupled Model over the East China Sea with a Focus on Typhoons, Atmosphere, 11, 252, https://doi.org/10.3390/atmos11030252, 2020.

Lionello, P., Günther, H., and Janssen, P. A. E. M.: Assimilation of Altimeter Data in a Global Third-Generation Wave Model, Journal of Geophysical Research: Oceans, 97, 14 453–14 474, https://doi.org/10.1029/92JC01055, 1992.

Lionello, P., Malguzzi, P., and Buzzi, A.: Coupling between the Atmospheric Circulation and the Ocean Wave Field: An Idealized Case, Journal of Physical Oceanography, 28, 161–177, 1998.

Lucas-Picher, P., Caya, D., de Elía, R., and Laprise, R.: Investigation of regional climate models' internal variability with a ten-member ensemble of 10-year simulations over a large domain, Climate Dynamics, 31, 927–940, https://doi.org/10.1007/s00382-008-0384-8, 2008.

Meißner, C.: High-Resolution Sensitivity Studies with the Regional Climate Model COSMO-CLM, Ph.D. thesis, Universität (TH) Karlsruhe, Karlsruhe, Germany, 2008.

Meissner, C., Schädler, G., Panitz, H.-J., Feldmann, H., and Kottmeier, C.: High-resolution sensitivity studies with the regional climate model COSMO-CLM, Meteorologische Zeitschrift, 18, 543–557, https://doi.org/10.1127/0941-2948/2009/0400, 2009.

Moon, I.-J., Hara, T., Ginis, I., Belcher, S. E., and Tolman, H. L.: Effect of Surface Waves on Air–Sea Momentum Exchange. Part I: Effect of Mature and Growing Seas, Journal of the Atmospheric Sciences, 61, 2321–2333, 2004.

Murphy, J. M., Sexton, D. M. H., Barnett, D. N., Jones, G. S., Webb, M. J., Collins, M., and Stainforth, D. A.: Quantification of modelling uncertainties in a large ensemble of climate change simulations, Nature, 430, 768–772, https://doi.org/10.1038/nature02771, 2004.

Nose, T., Webb, A., Waseda, T., Inoue, J., and Sato, K.: Predictability of storm wave heights in the ice-free Beaufort Sea, Ocean Dynamics, 68, 1383–1402, https://doi.org/10.1007/s10236-018-1194-0, 2018.

Olabarrieta, M., Warner, J. C., Armstrong, B., Zambon, J. B., and He, R.: Ocean–atmosphere dynamics during Hurricane Ida and Nor'Ida: An application of the coupled ocean–atmosphere–wave–sediment transport (COAWST) modeling system, Ocean Modelling, 43-44, 112–137, https://doi.org/10.1016/j.ocemod.2011.12.008, 2012.

Pacheco, M. B. and Guedes Soares, C.: Ship weather routing based on seakeeping performance, in: Advancements in Marine Structures, Guedes Soares & Das (eds), pp. 71–78, Taylor & Francis Group, London, 2007.

Pant, V. and Prakash, K. R.: Response of Air–Sea Fluxes and Oceanic Features to the Coupling of Ocean–Atmosphere–Wave During the Passage of a Tropical Cyclone, Pure and Applied Geophysics, 177, 3999–4023, https://doi.org/10.1007/s00024-020-02441-z, 2020.

Perrie, W. and Zhang, Y.: A regional climate model coupled to ocean waves: Synoptic to multimonthly simulations, Journal of Geophysical Research: Atmospheres, 106, 17 753–17 771, https://doi.org/10.1029/2001JD900207, 2001.

Phillips, O. M.: The equilibrium range in the spectrum of wind-generated waves, Journal of Fluid Mechanics, 4, 426–434, https://doi.org/10.1017/S0022112058000550, 1958.

Quante, M. and Colijn, F.: North Sea Region Climate Change Assessment, Springer Nature, pp. xxxix–xlv,409,457, https://doi.org/10.1007/978-3-319-39745-0, 2016.

Reinert, D., Prill, F., Frank, H., Denhard, M., and Zängl, G.: Database Reference Manual for ICON and ICON-EPS, Deutscher Wetterdienst, Offenbach am Main, Germany, `https://isabel.dwd.de/DWD/forschung/nwv/fepub/icon_database_main.pdf`, last accessed: 16.November 2018, 2018.

Reistad, M., Breivik, Ø., Haakenstad, H., Aarnes, O. J., Furevik, B. R., and Bidlot, J.-R.: A high-resolution hindcast of wind and waves for the North Sea, the Norwegian Sea, and the Barents Sea, Journal of Geophysical Research: Oceans, 116, https://doi.org/10.1029/2010JC006402, 2011.

Rizza, U., Canepa, E., Ricchi, A., Bonaldo, D., Carniel, S., Morichetti, M., Passerini, G., Santiloni, L., Scremin Puhales, F., and Miglietta, M. M.: Influence of Wave State

and Sea Spray on the Roughness Length: Feedback on Medicanes, Atmosphere, 9, 301, https://doi.org/10.3390/atmos9080301, 2018.

Rockel, B., Will, A., and Hense, A.: The Regional Climate Model COSMO-CLM (CCLM), Meteorologische Zeitschrift, 17, 347–348, https://doi.org/10.1127/0941-2948/2008/0309, 2008.

Romeiser, R.: Global Validation of the Wave Model WAM Over a One-Year Period Using Geosat Wave Height Data, Journal of Geophysical Research: Oceans, 98, 4713–4726, https://doi.org/10.1029/92JC02258, 1993.

Rummukainen, M.: Annex 3: Uncertainties in Climate Change Projections, in: M. Quante and F. Colijn (eds.) North Sea Region Climate Change Assessment, pp. 505–513, https://doi.org/10.1007/978-3-319-39745-0, 2016.

Rutgersson, A., Sætra, Ø., Semedo, A., Carlsson, B., and Kumar, R.: Impact of surface waves in a Regional Climate Model, Meteorologische Zeitschrift, 19, 247–257, https://doi.org/10.1127/0941-2948/2010/0456, 2010.

Sanchez-Gomez, E. and Somot, S.: Impact of the internal variability on the cyclone tracks simulated by a regional climate model over the Med-CORDEX domain, Climate Dynamics, 51, 1005–1021, https://doi.org/10.1007/s00382-016-3394-y, 2018.

Schaaf, B., von Storch, H., and Feser, F.: Does Spectral Nudging Have an Effect on Dynamical Downscaling Applied in Small Regional Model Domains?, Monthly Weather Review, 145, 4303–4311, https://doi.org/10.1175/MWR-D-17-0087.1, 2017.

Schlembach, F., Passaro, M., Quartly, G. D., Kurekin, A., Nencioli, F., Dodet, G., Piollé, J.-F., Ardhuin, F., Bidlot, J., Schwatke, C., Seitz, F., Cipollini, P., and Donlon, C.: Round Robin Assessment of Radar Altimeter Low Resolution Mode and Delay-Doppler Retracking Algorithms for Significant Wave Height, Remote Sensing, 12, 1254, https://doi.org/10.3390/rs12081254, 2020.

Schrum, C.: Regional Climate Modeling and Air-Sea Coupling, in: Oxford Research Encyclopedia of Climate Science, https://doi.org/10.1093/acrefore/9780190228620.013.3, 2017.

Schrum, C., Hübner, U., Jacob, D., and Podzun, R.: A coupled atmosphere/ice/ocean model for the North Sea and the Baltic Sea, Climate Dynamics, 21, 131–151, https://doi.org/10.1007/s00382-003-0322-8, 2003.

Schulz-Stellenfleth, J. and Stanev, E. V.: Statistical assessment of ocean observing networks – A study of water level measurements in the German Bight, Ocean Modelling, 33, 270–282, https://doi.org/10.1016/j.ocemod.2010.03.001, 2010.

Schulz-Stellenfleth, J. and Staneva, J.: A multi-collocation method for coastal zone observations with applications to Sentinel-3A altimeter wave height data, Ocean Science, 15, 249–268, https://doi.org/10.5194/os-15-249-2019, 2019.

Sieck, K.: Internal Variability in the Regional Climate Model REMO, Ph.D. thesis, Universität Hamburg, Hamburg, Germany, 2013.

Signell, R. P., Carniel, S., Cavaleri, L., Chiggiato, J., Doyle, J. D., Pullen, J., and Sclavo, M.: Assessment of wind quality for oceanographic modelling in semi-enclosed basins, Journal of Marine Systems, 53, 217–233, https://doi.org/10.1016/j.jmarsys.2004.03.006, 2005.

Snyder, R. L., Dobson, F. W., Elliott, J. A., and Long, R. B.: Array measurements of atmospheric pressure fluctuations above surface gravity waves, Journal of Fluid Mechanics, 102, 1–59, https://doi.org/10.1017/S0022112081002528, 1981.

SOLAS: SOLAS Chapter V: Safety of Navigation, `https://assets.publishing.service.gov.uk/government/uploads/system/uploads/attachment_data/file/343175/solas_v_on_safety_of_navigation.pdf`, last accessed: 10.July 2020, 1974, as amended.

Staneva, J., Behrens, A., and Groll, N.: Recent Advances in Wave Modelling for the North Sea and German Bight, Die Küste, 81. Karlsruhe: Bundesanstalt für Wasserbau, pp. 233–254, 2014.

Staneva, J., Wahle, K., Günther, H., and Stanev, E.: Coupling of wave and circulation models in coastal-ocean predicting systems: a case study for the German Bight, Ocean Science, 12, 797–806, https://doi.org/10.5194/os-12-797-2016, 2016a.

Staneva, J., Wahle, K., Koch, W., Behrens, A., Fenoglio-Marc, L., and Stanev, E. V.: Coastal flooding: impact of waves on storm surge during extremes – a case study for the German Bight, Natural Hazards and Earth System Sciences, 16, 2373–2389, https://doi.org/10.5194/nhess-16-2373-2016, 2016b.

Staneva, J., Alari, V., Breivik, Ø., Bidlot, J.-R., and Mogensen, K.: Effects of wave-induced forcing on a circulation model of the North Sea, Ocean Dynamics, 67, 81–101, https://doi.org/10.1007/s10236-016-1009-0, 2017.

Stopa, J. E.: Wind forcing calibration and wave hindcast comparison using multiple reanalysis and merged satellite wind datasets, Ocean Modelling, 127, 55–69, https://doi.org/10.1016/j.ocemod.2018.04.008, 2018.

Sverdrup, H. U. and Munk, W. H.: Wind, Sea and Swell: Theory of Relations for Forecasting, 601, U.S. Hydrographic Office, 1947.

Teixeira, J. C., Abreu, M. P., and Soares, C. G.: Uncertainty of Ocean Wave Hindcasts Due to Wind Modeling, Journal of Offshore Mechanics and Arctic Engineering, 117, 294–297, https://doi.org/10.1115/1.2827237, 1995.

Thomas, T. J. and Dwarakish, G. S.: Numerical wave modelling – A review, Aquatic Procedia, 4, 443–448, https://doi.org/10.1016/j.aqpro.2015.02.059, 2015.

TRR181: Energy Transfers in Atmosphere and Ocean, `https://www.trr-energytransfers.de/`, last accessed: 28.August 2020, 2020.

TRR181:M6: Energy Transfers in Atmosphere and Ocean: M6 Techniques for Atmosphere-Ocean Wave Coupling, `https://www.trr-energytransfers.de/research/area-m/m6/`, last accessed: 28.August 2020, 2020.

Valcke, S., Craig, T., and Coquart, L.: OASIS3-MCT User Guide, OASIS3-MCT 3.0, Technical Report TR/CMGC/15/38, CERFACS/CNRS SUC URA No1875, CERFACS, Toulouse, France, 2015.

Van Pham, T., Brauch, J., Dieterich, C., Frueh, B., and Ahrens, B.: New coupled atmosphere-ocean-ice system COSMO-CLM/NEMO: assessing air temperature sensitivity over the North and Baltic Seas, Oceanologia, 56, 167–189, https://doi.org/10.5697/oc.56-2.167, 2014.

Van Vledder, G. P. and Akpınar, A.: Wave model predictions in the Black Sea: Sensitivity to wind fields, Applied Ocean Research, 53, 161–178, https://doi.org/10.1016/j.apor.2015.08.006, 2015.

Varlas, G., Katsafados, P., Papadopoulos, A., and Korres, G.: Implementation of a two-way coupled atmosphere-ocean wave modeling system for assessing air-sea interaction

over the Mediterranean Sea, Atmospheric Research, 208, 201–217, https://doi.org/10.1016/j.atmosres.2017.08.019, 2018.

Varlas, G., Spyrou, C., Papadopoulos, A., Korres, G., and Katsafados, P.: One-year assessment of the CHAOS two-way coupled atmosphere-ocean wave modelling system over the Mediterranean and Black Seas, Mediterranean Marine Science, 21, 372–385, https://doi.org/10.12681/mms.21344, 2020.

Vignudelli, S., Kostianoy, A., Cipollini, P., and Benveniste, J.: Coastal Altimetry, Springer, Berlin, Heidelberg, pp. vi,1–18,61–102, https://doi.org/10.1007/978-3-642-12796-0, 2011.

von Storch, H., Langenberg, H., and Feser, F.: A Spectral Nudging Technique for Dynamical Downscaling Purposes, Monthly Weather Review, 128, 3664–3673, 2000.

Wahle, K., Staneva, J., Koch, W., Fenoglio-Marc, L., Ho-Hagemann, H. T. M., and Stanev, E. V.: An atmosphere-wave regional coupled model: improving predictions of wave heights and surface winds in the southern North Sea, Ocean Science, 13, 289–301, https://doi.org/10.5194/os-13-289-2017, 2017.

WAM: WAM model code, available at:, `http://mywave.github.io/WAM/`, last accessed: 30.November 2018, 2018.

WAMDI Group: The WAM Model - A Third Generation Ocean Wave Prediction Model, Journal of Physical Oceanography, 18, 1775–1810, 1988.

Warner, J. C., Armstrong, B., He, R., and Zambon, J. B.: Development of a Coupled Ocean–Atmosphere–Wave–Sediment Transport (COAWST) Modeling System, Ocean Modelling, 35, 230–244, https://doi.org/10.1016/j.ocemod.2010.07.010, 2010.

Weisse, R. and Feser, F.: Evaluation of a method to reduce uncertainty in wind hindcasts performed with regional atmosphere models, Coastal Engineering, 48, 211–225, https://doi.org/10.1016/S0378-3839(03)00027-9, 2003.

Weisse, R. and Schneggenburger, C.: The Effect of Different Sea-State-Dependent Roughness Parameterizations on the Sensitivity of the Atmospheric Circulation in a Regional Model, Monthly Weather Review, 130, 1593–1600, 2002.

Weisse, R., Heyen, H., and von Storch, H.: Sensitivity of a Regional Atmospheric Model to a Sea State-Dependent Roughness and the Need for Ensemble Calculations, Monthly Weather Review, 128, 3631–3642, 2000.

Weisse, R., Günther, H., and Feser, F.: A 40-year high-resolution wind and wave hindcast for the Southern North Sea, in: 7th International Workshop on Wave Hindcasting and Forecasting, 21-25 October 2002, Banff, Alberta, Canada, pp. 97–104, 2002.

Weisse, R., von Storch, H., Callies, U., Chrastansky, A., Feser, F., Grabemann, I., Günther, H., Pluess, A., Stoye, T., Tellkamp, J., Winterfeldt, J., and Woth, K.: Regional Meteorological–Marine Reanalyses and Climate Change Projections: Results for Northern Europe and Potential for Coastal and Offshore Applications, Bulletin of the American Meteorological Society, 90, 849–860, https://doi.org/10.1175/2008BAMS2713.1, 2009.

Wiese, A., Staneva, J., Schulz-Stellenfleth, J., Behrens, A., Fenoglio-Marc, L., and Bidlot, J.-R.: Synergy of wind wave model simulations and satellite observations during extreme events, Ocean Science, 14, 1503–1521, https://doi.org/10.5194/os-14-1503-2018, 2018.

Wiese, A., Stanev, E., Koch, W., Behrens, A., Geyer, B., and Staneva, J.: The Impact of the Two-Way Coupling between Wind Wave and Atmospheric Models on the Lower Atmosphere over the North Sea, Atmosphere, 10, 386, https://doi.org/10.3390/atmos10070386, 2019.

Wiese, A., Staneva, J., Ho-Hagemann, H. T. M., Grayek, S., Koch, W., and Schrum, C.: Internal Model Variability of Ensemble Simulations With a Regional Coupled Wave-Atmosphere Model GCOAST, Frontiers in Marine Science, 7, 596 843, https://doi.org/10.3389/fmars.2020.596843, 2020.

Will, A., Akhtar, N., Brauch, J., Breil, M., Davin, E. L., Ho-Hagemann, H. T. M., Maisonnave, E., Thürkow, M., and Weiher, S.: The COSMO-CLM 4.8 regional climate model coupled to regional ocean, land surface and global earth system models using OASIS3-MCT: description and performance, Geoscientific Model Development, 10, 1549–1586, https://doi.org/10.5194/gmd-10-1549-2017, 2017.

Wu, L., Rutgersson, A., Sahlée, E., and Larsén, X. G.: The impact of waves and sea spray on modelling storm track and development, Tellus A: Dynamic Meteorology and Oceanography, 67, 27 967, https://doi.org/10.3402/tellusa.v67.27967, 2015.

Wu, L., Sproson, D., Sahlée, E., and Rutgersson, A.: Surface Wave Impact When Simulating Midlatitude Storm Development, Journal of Atmospheric and Oceanic Technology, 34, 233–248, https://doi.org/10.1175/JTECH-D-16-0070.1, 2017.

Wu, L., Breivik, Ø., and Rutgersson, A.: Ocean-Wave-Atmosphere Interaction Processes in a Fully Coupled Modeling System, Journal of Advances in Modeling Earth Systems, 11, 3852–3874, https://doi.org/10.1029/2019MS001761, 2019.

Wu, L., Shao, M., and Sahlée, E.: Impact of Air–Wave–Sea Coupling on the Simulation of Offshore Wind and Wave Energy Potentials, Atmosphere, 11, 327, https://doi.org/10.3390/atmos11040327, 2020.

Zambon, J. B., He, R., and Warner, J. C.: Investigation of hurricane Ivan using the coupled ocean–atmosphere–wave–sediment transport (COAWST) model, Ocean Dynamics, 64, 1535–1554, https://doi.org/10.1007/s10236-014-0777-7, 2014.

Acknowledgements

First and foremost I would like to thank my supervisors Dr. Joanna Staneva and Prof. Dr. Corinna Schrum. Thank you Joanna, for your guidance, encouragement and support to progress with my thesis during my work. Especially being able to attend so many conferences and workshops as well as a summer school is not a given and I am very thankful for having had the opportunity to present and discuss my work on an international level. Thank you Corinna, for your support, constructive discussions and motivation during my PhD-project.

I am thankful to the members of the KSD group during my PhD-time for the scientific exchange and the friendly working environment. Especially I would like to thank Dr. Arno Behrens, Gerhard Gayer, Dr. Sebastian Grayek, Dr. Heinz Günther, Wolfgang Koch, Dr. Oliver Krüger, Dr. Johannes Schulz-Stellenfleth and Prof. Dr. Emil Stanev for their technical support, sharing their knowledge and patiently answering all kind of technical and scientific questions. Gerhard Gayer provided the matlab script to produce the style of the scatter plots and Dr. Johannes Schultz-Stellenfleth provided the matlab script for the EOF analysis.

I would also like to thank Dr. Beate Geyer, Dr. Ha Thi Minh Ho-Hagemann, Dr. Ronny Petrik and Dr. Burkhardt Rockel for their support with and discussions about the atmospheric model CCLM.

I am grateful for the financial support I received from the European Union's H2020 Programme for Research, Technological Development and Demonstration under grant agreement no. H2020-EO-2016-730030-CEASELESS and HZG. I am particularly thankful for the support I received from the members of the project. I would like to thank Dr. Jean-Raymond Bidlot for the discussions and supplying suggestions regarding the wave and atmospheric modelling and Dr. Luigi Cavaleri for the encouraging conversations. Thank you to the RAM group at the Technical University of Denmark for welcoming me during my stay. Especially the discussions with Dr. Jana Fischereit about the wave model code and the physics behind it improved my understanding of the wave model. Thanks to Dr. Xiaoli Larsén and Dr. Joanna Staneva for making that possible.

Thank you to Dr. Jean-Raymond Bidlot and PD Dr. Lucianna Fenoglio-Marc for providing observational data that have been used as a reference for model outputs. Also I

would like to thank the ECMWF, DWD, HZG, CLM-Community, Aviso, RADS, ESA and Copernicus for making data used within this study available.

Thanks to the colleagues at HZG, scientist at conferences and project meetings or reviewing the papers within this thesis for asking critical questions about my work helping me progress and improve it.

I would like to thank Dr. Arno Behrens and Dr. Ulla Seidel-Wiese for proof-reading parts of my thesis.

Finally, a massive thank you to my parents and family for always supporting me throughout the years. Thank you very much for introducing me to the sport of sailing at an early age. Since then I have sailed around large parts of the area studied in this thesis. Experiencing the different faces the ocean surface can show, has always been very fascinating to me and taught me how important knowledge about wind and waves and a good forecast are.

Eidesstattliche Versicherung

Hiermit versichere ich an Eides statt, dass ich die vorliegende Dissertation mit dem Titel: „Assessing and Reducing the Uncertainty in Regional Wave and Coupled Wave-Atmosphere Models during Extreme Events“ selbstständig verfasst und keine anderen als die angegebenen Hilfsmittel - insbesondere keine im Quellenverzeichnis nicht benannten Internet-Quellen - benutzt habe. Alle Stellen, die wörtlich oder sinngemäß aus Veröffentlichungen entnommen wurden, sind als solche kenntlich gemacht. Ich versichere weiterhin, dass ich die Dissertation oder Teile davon vorher weder im In- noch im Ausland in einem anderen Prüfungsverfahren eingereicht habe und die eingereichte schriftliche Fassung der auf dem elektronischen Speichermedium entspricht.

Hamburg, den 12. Oktober 2020